UNIVERSITY OF CAPE TOWN

FACULTY OF ENGINEERING AND BUILT ENVIRONMENT

DEPARTMENT OF CIVIL ENGINEERING

A Comparative Study on Shear Strength Testing of Single and Multi-layer Interfaces using Large Direct Shear Apparatus

Author: **Shade Muluti**

Supervisor: **A/Prof. Denis Kalumba**
Co-Supervisor: **Dr. Laxmee Sobhee-Beetul**

A thesis submitted in partial fulfilment of the requirement for the award of the degree of Master of Science in Civil Engineering Specialising in Geotechnical Engineering at the University of Cape Town.

[May 2021]

DECLARATION

1. Plagiarism is to use another's work and pretend that it's one's own. I know that plagiarism is wrong.

2. I have used the UCT Harvard convention for citation and referencing. Each significant contribution to, and quotation in, this thesis project from the work(s) of other people have been attributed and has been cited and referenced.

3. This report is my work.

4. I have not allowed or will not allow anyone, to copy my work with the intention of passing it off as his or her own work.

Signature: Signed by candidate Date: 07th May 2021

Student Name: Shade Muluti

DEDICATION

TO

My beloved God-fearing grandmother, **CATHERINE MUSHOKOBANJI SIKANDA**, her constant love, wisdom, and support laid down the foundations for the person I am today.

KU

“Bo Kuku waka ba ba lateha ni ku saba Mulimu, Bo **CATHERINE MUSHOKOBANJI SIKANDA**, lilato la bona la kamita, zibo ni tuso libile mutomo wa Mutu ye ni li yena kacenu.”

ACKNOWLEDGEMENTS

There are several individuals, institutions, and organisations without whom this dream would not have been possible, but I am heavily indebted to some.

First and foremost, I would like to thank my heavenly father, GOD ALMIGHTY, for his fruitful help in completing this thesis. My sincerest gratitude goes to my supervisor, A/Prof. Denis Kalumba and co-supervisor, Dr. Laxmee Sobhee-Beetul, whose attention to detail and positive criticism was highly appreciated. Their knowledge, noble guidance and unreserved commitment were key in the completion of this dissertation.

I am extremely grateful to both Dr. Petrina Johannes, the Dean of the Faculty of Engineering & Information Technology and, Dr.-Ing. Joachim Lengricht, the Head of Department of Civil Engineering & Environmental Engineering at the University of Namibia. I am truly thankful to them for providing me with the opportunity to pursue my masters at an esteemed institution such as the University of Cape Town (UCT).

I acknowledge the robust financial support from UNAM and the German Federal Ministry for Economic Cooperation and Development, through its implementing agency Deutsche Gesellschaft für lnternationale Zusammenarbeit and the Project “Transport, Mobility and Logistics”. I am tremendously grateful for making it possible for me to pursue this Master of Science degree. Special gratitude goes to Prof. Dr. Heinrich Semar, Mr. Ernst-Benedikt Riehle, Mr. Moritz Lange and Susanne Raukamp. I would also like to acknowledge the financial contribution from the CG Clarkson Educational Trust.

On the technical side, I wish to recognise Mr. Peter Hardie from AKS Lining Systems (Pty) Ltd and Mr. Deon Stipp from Kaytech Engineered Fabrics, for generously donating and transporting the geosynthetics materials used in this research to the UCT Geotechnical Engineering Laboratory

If the assistance of Mr Noor Hassen, Mr. Tahir Mukaddam, and Mr. Elvino Witbooi of the Civil Engineering Laboratory, and Mr. Charles Nicholas and Mr. Swayiza 'Siya' Masimthembe of the Civil Engineering Workshop had been withdrawn, the laboratory testing carried out in this work would have been deprived of technical support. Special recognition for their continuous support and resources during my laboratory work.

My experience in Cape Town would be incomplete without the fun times and support of my friends and colleagues. Much appreciation to Daniel, Charles, Lunga, Mutsa, Emilia, Victoria, Samuel, Sima, Jaziitha, Shalongo, and Faridah for making my stay in Cape Town a very memorable one.

Mr. Beaven Sikanda, his tough love, mentorship, guidance, support and wisdom as my uncle and father figure can never be undervalued. Special thanks also to my best friends, Olavi, Sean, Joviita, and Grant for always being readily available whenever I needed assistance.

Finally, my gratitude goes to my mother, Joyce Sikanda, siblings, relatives, and acquaintances for their countless efforts, support, and encouragement during my entire stay in Cape Town.

ABSTRACT

Geotechnical structures such as composite liner systems in landfills consist of multiple interfaces, which include a broad range of geosynthetics in conjunction with soil, rocks and any other related materials. This results in the introduction of many interface planes into the structure, which can potentially create instability especially along the slope and ultimately result in failure. To date, many laboratories use single interface testing instead of multi-layer interface testing to determine geosynthetic shear design characteristic values that are used in the design of structures such as landfill liners. A topic of discussion remains the preferred interface testing configuration and only a few studies have substantiated and quantified the significance of varying the different interface shear testing configurations. This study, therefore, aimed to evaluate and compare the effects of the use of the two interface test configurations on the shear strength of soil/geosynthetic and geosynthetic/geosynthetic interfaces. Furthermore, it was intended to identify the test configuration that provides the most critical shear strength results, while also understanding the fundamental mechanisms responsible for the shear strength observed.

In this study, three geosynthetics were used: geotextile (GTX), geomembrane (GMB) and geosynthetic clay liner (GCL), which generally constitute the critical interface components of a lining system in a modern South African landfill liner. Two soils were utilised as a part of the materials required for the investigation and they were: river sand and red clay. The laboratory tests were conducted under saturated conditions in accordance with the ASTM D5321 and ASTM D6243 standards, using a 305 mm x 305 mm large direct shear box. The tests were carried out over a range of applied normal pressures of 50, 100, 200 and 400 kPa. A constant shear rate of 1.0 mm/min was used in the interface tests that did not involve GCLs or clay specimens and therefore no excess pore pressure was anticipated at the interface. On the other hand, for all other interface tests involving either clay or GCLs samples, a shearing rate of 0.1 mm/min was utilized.

The results showed that nonlinear behaviour of the shear stress versus shear displacement responses was exhibited in both the single and multi-layer interface tests, regardless of the normal stress applied. However, it was noted that with an increase in normal stress applied, the deviation in mobilized shear stress between the two test configurations increased, with single interface tests yielding higher shear stress values compared to multi-layer interface tests. In single interface tests, the high shear stresses could be related to the clamping that confined each of the test specimens during shearing to one end of the shear block. On the other hand, only the top and bottom test specimens were clamped in multi-layer interface tests, thus allowing failure to have occurred at the weakest of the available interfaces.

Moreover, for single interface tests, peak strengths were generally 9% lower for the range of normal stresses considered, whereas Large Displacement (LD) strengths were generally 24 % lower for the single interface tests, compared to the peak and LD strength values for multi-layer interface tests. This was particularly observed at low normal stresses between 50 and 200 kPa, and it could probably have been caused by the rigid clamping of the geosynthetics which results in some tensile strains in the geosynthetics. In addition, it was observed in multi-layer interface tests that a transfer of shear stresses within the system could have occurred, which could have

led to higher overall shear resistance of the composite. As a result, single interface tests yielded a conservative estimate of the peak and LD shear strengths for the tested interfaces compared to multi-layer interface tests. This may be attributed to higher displacement along with the critical interface in single interface tests than in multi-layer interface tests. To allow the investigator to observe the displacement, as well as the possible transfer of shear stresses within the system during the shearing of the various geosynthetics, it was recommended that real-time monitoring of the displacement mobilization should be carried out in multi-layer interface tests during shearing.

TABLE OF CONTENTS

LIST OF FIGURES

LIST OF TABLES

ABBREVIATIONS

ASTM	-	American Society for Testing and Materials
BS	-	British Standard
CBR	-	California Bearing Ratio
CCL	-	Compacted Clay Liner
CMD	-	Counter Machine Direction
CPE	-	Chlorinated Polyethylene
DEA	-	Department of Environmental Affairs
DSA	-	Direct Shear Apparatus
FLS	-	Foundation Layer Soil
GC	-	Geocomposite
GCL	-	Geosynthetic Clay Liner
GHS	-	Globally Harmonised System
GMB	-	Geomembrane
GSI	-	Geosynthetic Institute
GTX	-	Geotextile
HDPE	-	High Density Polyvinylchloride
IPA	-	Inclined Plane Apparatus
ISO	-	International Organization for Standardization
LD	-	Large Displacement
LDPE	-	Low Density Polyvinylchloride
LDSA	-	Large Direct Shear Apparatus
LL	-	Liquid Limit
MARV	-	Minimum Average Roll Value
MD	-	Machine Direction
MDD	-	Maximum Dry Density
MEs	-	Microsoft Excel software
MSW	-	Municipal Solid Waste
OMC	-	Optimum Moisture Content
PD	-	Percentage Difference
PI	-	Plasticity Index
PL	-	Plastic Limit
POA	-	Pull-Out Apparatus
PP	-	Polypropylene
PVC	-	Polyvinylchloride
RSA	-	Ring Shear Apparatus
SANS	-	South African National Standard
SL	-	Shrinkage Limit
USA	-	United States of America
USCS	-	Unified Soil Classification System
UV	-	Ultraviolet

NOMENCLATURE

$\emptyset_p$	degrees (°)	Peak Friction angle
$\emptyset_r$	degrees (°)	Residual Friction angle
Δ_s	mm	Shear displacement
C_c	-	Coefficient of curvature
C_u	-	Coefficient of uniformity
G_s	-	Specific Gravity
K_0	-	Initial slope of R-D curve
K_{si}	-	Initial Shear Modulus
K_{st}	-	Tangent Shear Modulus
P_1 & P_1^t	percent (%)	70 percent of strength
P_2 & P_2^t	percent (%)	95 percent of strength
P_a	kPa	Atmospheric Pressure
R_f	-	Failure ratio
c_p	kN/m^2	Peak cohesion
c_r	kN/m^2	Residual cohesion
t_{100}	hours	Time for 100 per cent primary consolidation
u^p	-	Plastic Shear displacement
u_r^p	-	Plastic shear displacement at residual strength
γ_w	kN/m^3	Unit weight of water
σ_n	kN/m^2	Normal or Confining Pressure
τ_f/τ_p	kN/m^2	Peak interface Shear strength
τ_{pr}	kN/m^2	Post-peak shear strength
τ_r	kN/m^2	Residual shear strength
τ_{ult}	kN/m^2	Ultimate shear strength
$\emptyset$	degrees (°)	Friction angle of soil
A	m^2	Cross-sectional area.
D	-	Displacement ratio
F	-	Tangential (Shear) Force
K	-	Dimensionless shear coefficient
N	-	Normal load (stress)
R	-	Strain-softening factor
a & b	-	Hyperbolic parameters
n	-	Modulus exponent
z	-	Coefficient (dimensionless)
c_α	-	Adhesion of the interface
δ	degrees (°)	Friction angle of soil/geosynthetic interface
τ	kN/m^2	Shear strength

1 INTRODUCTION

1.1 Background

Geosynthetics have become a well-established material in geotechnical and environmental engineering. This is due to sustainability and reliability as well as providing an economical solution to challenges rising from design, (Guler, 2017; Koffler et al., 2008; Palmeira et al., 2008). Geosynthetics, which can be defined as a broad range of synthetic planar products manufactured from polymeric material, can be utilized as an integral part of engineering structures and systems in conjunction with soil, rocks and any other related materials, (Shukla & Yin, 2006). Currently, the most widely used geosynthetics in engineering include: geotextiles (GTXs), geogrids, geonets, geomembranes (GMBs), geosynthetic clay liners (GCLs), geofoams, geocells, geopipes, geotubes, and geocomposites, (Guler, 2017; Koerner, 2005; Shukla, 2016; Zhao & Karim, 2018).

In South Africa, geosynthetics are mostly employed in solid waste containment systems as a combination of each other, protecting the contamination of both surface and groundwater, (Bouazza et al., 2002; Sikwanda et al., 2019). However, the use of multiple liners in landfills results in many interface planes being introduced into the structure, potentially creating slope instability issues which can lead to failure, (Zhao & Karim, 2018). Therefore, it is of most importance to use appropriate geosynthetic interface and/or internal shear strength in the theoretical design and construction of landfills, (Sikwanda, 2018). In **Figure 1-1**, a typical example of a landfill with significant geosynthetic utilization and the various interfaces is shown.

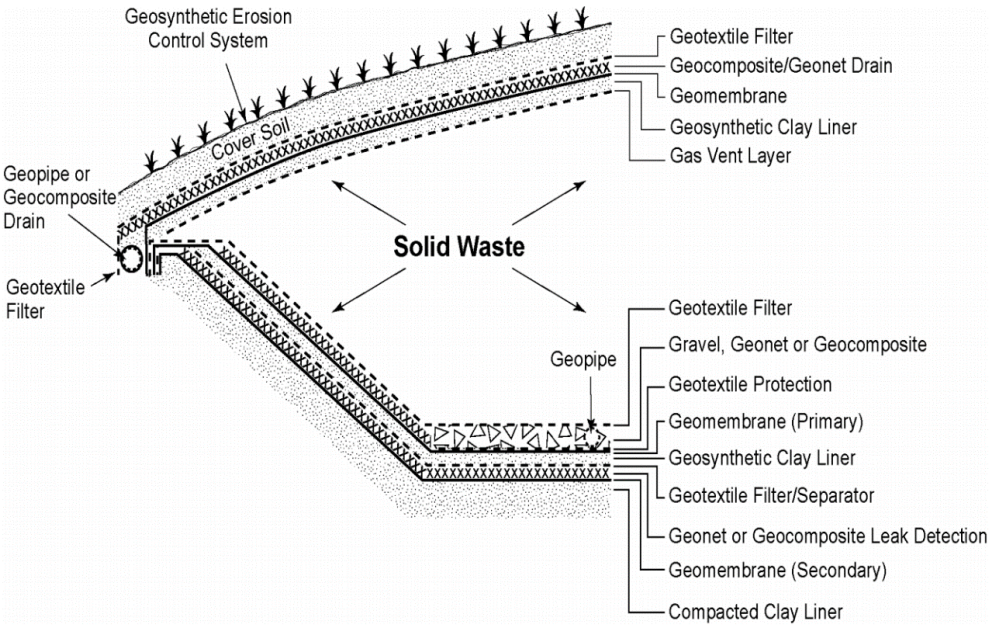

Figure 1-1 Solid waste containment system with high geosynthetic utilization and the various interfaces. (Ng & Ramsey (2012)).

The geosynthetics interface and internal shear strength can be determined from laboratory tests using direct shear, ring-shear, inclined plane and pull-out apparatus, (Evangelou & Markou, 2018; Moraci et al., 2014). However, the direct shear is a commonly used device in most laboratories in South Africa and around the world, (Lings & Dietz, 2004). This is because the equipment is considered to be user-friendly yet effective. To date, there are two types of direct shear apparatus: small and large. A small direct shear box is generally 100 mm long, 100 mm wide and 30 mm high, while a large direct shear box is generally 300 mm in length, 300 m in width and 100 m in height. In this study, the comparison of shear strength testing of single and multiple geosynthetic interfaces was conducted using a large direct shear apparatus.

According to Shenthan et al. (2019), determining the interface shear strength on a large direct shear device can be achieved by using two approaches: (a) single-interface shear tests, and (b) multi-layer interface shear tests. Single interface tests are conducted by shearing two materials, (i.e. soil/geosynthetic), in contact at a time. This test is carried out for all the individual interfaces involved in a landfill configuration. Conversely, multi-layer interfaces tests in a sandwich configuration comprising of all interfaces considered in the landfill liner. The weakest interface can then be interpreted from the combination of shear strength envelopes, (Khilnani et al., 2017; Shenthan et al., 2019).

Great effort has been made by researchers, i.e. (Eid et al., 1999; Fox & Kim, 2008; Jones & Dixon, 1998), to study the geosynthetic interface through single interface tests. There is, however, limited publications on determining the geosynthetic interface utilizing multi-layer interface shear testing, i.e. (Evangelou & Markou, 2018; Sikwanda et al., 2019; Stark et al., 2015).

1.2 Research Justification

Many researchers have done studies on the shear behaviour of geosynthetic materials and interfaces, focusing primarily on single interface tests, i.e. (Bacas et al., 2015, 2011; Buthelezi et al., 2016; Chai & Saito, 2016; Kalumba & Scheele, 1999). Landfill liners, however, consist of multiple interfaces, and single interface shear tests have been found to overestimate or underestimate the shear strength of some geosynthetic interfaces, (Stark et al., 2015). This is a disadvantage and it can lead to slope instability and substantial remedial costs, (Stark & Choi, 2004). Furthermore, since a composite liner system has many interfaces that would require testing, performing several single interface tests would require a substantial amount of cost and time to fully understand the shear strength characteristics of the entire liner system, (Sikwanda et al., 2019).

In single interface testing, the failure surface is forced to occur along a specific geosynthetic interface that may not represent the actual field condition, since the shear movement of a composite liner system occurs on more than one interface plane, (Khilnani et al., 2017). In multi-layer interface testing, however, there is a possibility of capturing all these limitations, (Stark et al., 2011). When carrying out multi-layer interfaces testing, interfaces are tested simultaneously,

thus failure will be allowed to occur along the weakest interface as anticipated in the field, (Stark & Choi, 2004). This can provide designers with a better simulation of field conditions.

It was anticipated that the results obtained from this research would provide useful and practical application for both researchers and practitioners who use these geosynthetic materials in the field. This would assist them in their decision-making process concerning the selection of geosynthetic material for site-specific condition and result in more efficient geosynthetics system designs.

1.3 Research Objectives

The main objective of this study was to evaluate, using a large direct shear device, the effects of using different testing configurations, single and multi-layer interface, on the shear strength at soil/geosynthetic and geosynthetic/geosynthetic interfaces. It was desirable to compare results obtained from single interface testing with those obtained from multi-layer interface tests in terms of interface shear strength parameters, under different loading conditions. It was anticipated that the study would outline some clarification about the compatibility of single and multi-layer interface tests in determining the critical interface, by comparing the shear strength parameters obtained from both single and multi-layer interface test configurations.

The following methodology was completed to achieve the outlined objectives:

- A review of previous literature and the resultant current state of knowledge concerning interface shear behaviour of single and multiple geosynthetic interfaces.
- Conducting a series of large direct shear tests using the most applicable standards with geosynthetics from a South African-based geosynthetics manufacturing company.
- Development of combination peak and large displacement (LD) strength envelopes from selected shear strength parameters quantified from large direct shear device tests.
- Interpretation and comparison of results from single and multi-layer interface tests, and
- Finally, conclusions and recommendations were drawn from the results obtained.

1.4 Scope of the Study

This research focused mainly on assessing and comparing the influence of interface shear strength parameters, obtained from both single and multi-layer interface shear testing, on the performance of geosynthetic composite liner systems. A modern landfill liner consisting of the clay/geotextile, geotextile/geomembrane, geomembrane/GCL and GCL/river sand interfaces was utilized to achieve this objective. A 305 mm x 305 mm large direct shear device was used to carry out the tests following the ASTM D 5321 and ASTM D 6243 standards. Therefore, the results obtained in this study were limited to the conditions considered herein. Although theory, methodology and analysis might be similar irrespective of geographical location, this research was aimed at testing materials obtainable in South Africa, and that included the use of locally produced geosynthetic materials.

1.5 Thesis Overview

This research was undertaken to explore multi-layer interface tests in relation to single interface tests. Chapter 1, therefore, provided the context of the study with the background, justification, objectives and scope outlined to contextualize the problem being investigated. The relevant literature on previous studies and other research-related areas of interest was presented in Chapter 2. The methodology adopted, the testing standards followed, as well as the research materials used in this investigation were defined in Chapter 3. Chapter 4 presented a comparison of single and multi-layer interface experimental data of the large direct shear tests and a detailed analysis of the output parameters (i.e. interface friction angle and apparent adhesion). Finally, in Chapter 5, the conclusions of this study were drawn based on the findings, and recommendations were made.

2 LITERATURE REVIEW

2.1 Introduction

In this chapter, a review of the literature on geosynthetics and their applications in landfills, interface shear testing and previous studies on both single and multi-layer interface testing being presented. A theoretical background to the current research on the shear behaviour of typical geosynthetic interfaces used in composite liner systems of landfills is discussed. Also, a brief review of the literature on modelling of interface shear behaviour for both soil-geosynthetic and geosynthetic-geosynthetic interfaces is provided. This chapter is concluded by providing a summary of the discussion of the findings.

2.2 Geosynthetics in Landfills

2.2.1 Overview

The introduction of modern landfill lining systems resulted from a growing awareness of the need to contain waste as well as to protect public health and the environment. The innovative designs of landfill liners were made possible by improved geotechnical expertise and inventions of the polymer industries towards the end of the 20th century. This section explores the history of these polymers in the form of geosynthetics, the way they evolved and their current impact on South African waste management solutions. In line with the South African standards, a generic landfill lining system will be provided to show how geosynthetics have been integrated into the design over the years.

2.2.2 Landfills

Landfilling is one of the oldest and most effective options for waste disposal in most countries, including South Africa. It is relatively economical and offers an environmentally appropriate form of disposal of solid residual waste, (Shukla, 2016). Landfills have been revolutionized from just being open dumps to becoming modern engineered waste containment facilities that make use of controlled methods for disposal of waste. Leachate, however, is generated from the liquid squeezed out of the waste and the water that infiltrates into the landfill and percolates through the waste. Hence, the design of a landfill consists of an envelope that is constructed to encapsulate the waste and prevent leachate from escaping into the environment, (Barlaz, 2016; Fowmes et al., 2007). The leachate generated was previously allowed to percolate into the environment through the landfill base, and the unsaturated soil beneath the landfill was expected to purify the leachate. However, due to the potential of environmental risks and contamination of groundwater, geosynthetics were introduced as relatively impermeable layers to prevent pollution of the ground, (Orebowale, 2006). These polymer products are placed above and below the waste to minimize the exposure of leachate and harmful gases that are produced by the waste in the landfill.

2.2.2.1 Waste Types and Classification

In South Africa, standards and regulations have been developed and they require that all waste be disposed of under the authority of a permit issued in terms of section 20 of the Environment Conversation Act (Act No. 73 of 1989), based on the risk posed by the waste to the environment, (Department of Environmental Affairs, 2013). Before the waste can be disposed of into the landfill, it must be classified (within 180 days of generation) in accordance with the Globally Harmonised System (GHS) of Classification and Labelling of Chemicals, as specified in the SANS 10234:2008 (South African National Standard, 2008). Waste listed in Annexure 1 (**Table 2-1**) of the Waste Management Regulations do not require classification in terms of SANS 10234. Once the waste is classified, the physical and biological properties of the waste material and the potential hazards associated with landfill waste disposal are determined. This is done in compliance with the Norms and Standards for waste assessment for landfill disposal. Upon determination of these chemical elements, the waste type is rated based on predetermined risk level limit values depending on the risk posed by the waste, as can be seen in **Table 2-2**.

2.2.2.2 Landfill Types and Geometry

Landfills can be classified according to their size, type of waste and the climatic environment. This, in turn, can affect the type and amount of contaminants produced throughout the life of the landfill facility, (Deparment of Water Affairs and Forestry, 1998). The landfill type directly constrains the performance requirements, and hence the design of the lining system. Once a decision has been made as to how effectively the contaminants must be handled, a lining system can be constructed according to these requirements, (Stark, 1999).

There are essentially two types of landfills: (1) Municipal Solid Waste (MSW) and (2) Hazardous waste Landfills. Commercial and household waste is disposed of at MSW landfills, also known as sanitary landfills, which is the most common type of landfill, (Shukla & Yin, 2006). This landfill's geometric configurations usually include area fill, trench fill, above and below ground fill, and valley fill, as can be seen in **Figure 2-1**. The area-filled type of landfill is used where the ground is not suitable for excavation, due mainly to the existence of a high groundwater table. The trench fill is typically only used for small quantities of wastes. It is highly dependent on the depth of the natural clay layer and the groundwater table, which, in turn, determines the excavation's waste capacity. The above and below landfill types can be viewed as a combination of area and trench fill configurations. The valley-filled type of landfill, on the other hand can store solid waste between hills, creating a valley, (Buthelezi, 2017).

Table 2-1 Examples of general and hazardous waste. (Department of Environmental Affairs, 2013)

General Waste	Hazardous Waste
Domestic waste	Asbestos Waste
Business waste not containing hazardous waste or chemicals	PCB waste or PCB containing waste
Uncontaminated buildings and demolition waste	Expired, spoilt or unusable hazardous products
Waste tyres	General waste (excluding domestic waste) which contains hazardous waste or hazardous chemicals
Garden waste	
Post consumer packaging	Mixed hazardous chemical waste from analytical or academic laboratories in containers less than 100 litres
Non-infectious animal carcasses	
Uncontaminated, excavated earth	Health care risk waste

Table 2-2 Waste risk level, type and disposal requirements in South Africa. (adapted from Department of Environmental Affairs, 2013)

Waste Risk Level	Listed waste types	Disposal Requirements
Type 0:	N/A	Disposal **not allowed**. The waste must be treated first and then re-tested to determine the risk profile for disposal.
Type 1:	Asbestos Waste, expired, spoilt or unusable hazardous products, PCBs, general waste, excluding domestic waste, which contains hazardous waste or hazardous chemicals.	**Class A** or **Hh/HH**
Type 2:	Domestic waste, business waste not containing hazardous waste or hazardous chemicals, non-infectious animal carcasses, and garden waste.	**Class B** or **GLB+**
Type 3:	Post-consumer packaging and Waste tyres.	**Class C** or **GLB+**
Type 4:	Building and demolition waste not containing hazardous waste or hazardous chemicals, excavated earth material not containing hazardous waste or hazardous chemicals.	**Class D** or **GSB-**

2.2.3 Containment barrier systems

Landfill types, however, are no longer treated in terms of general and hazardous landfills but are now more risk-based, (Department of Environmental Affairs, 2013). The waste disposal requirements and specifications to landfilling ensure that disposed waste meets the type/class of landfill allocated. Different standard containment barrier criteria are allocated according to the risk posed by the waste. The varying design criteria for landfill containment barriers are classified into class A, B, C, and D based on the waste risk level, as indicated in **Figure 2-2**.

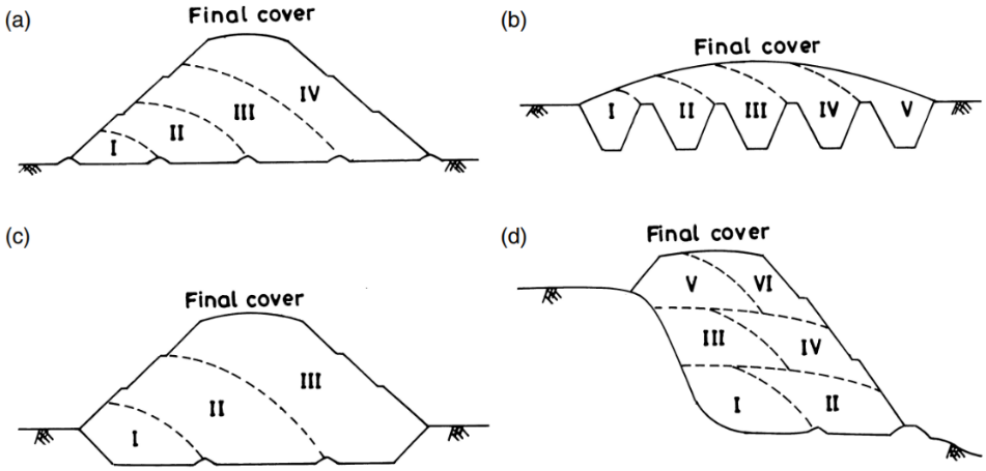

Figure 2-1 Examples of MSW landfill geometric configurations: (a) area fill; (b) trench fill; (c) above and below ground fill; (d) valley fill. (Shukla & Yin, 2006)

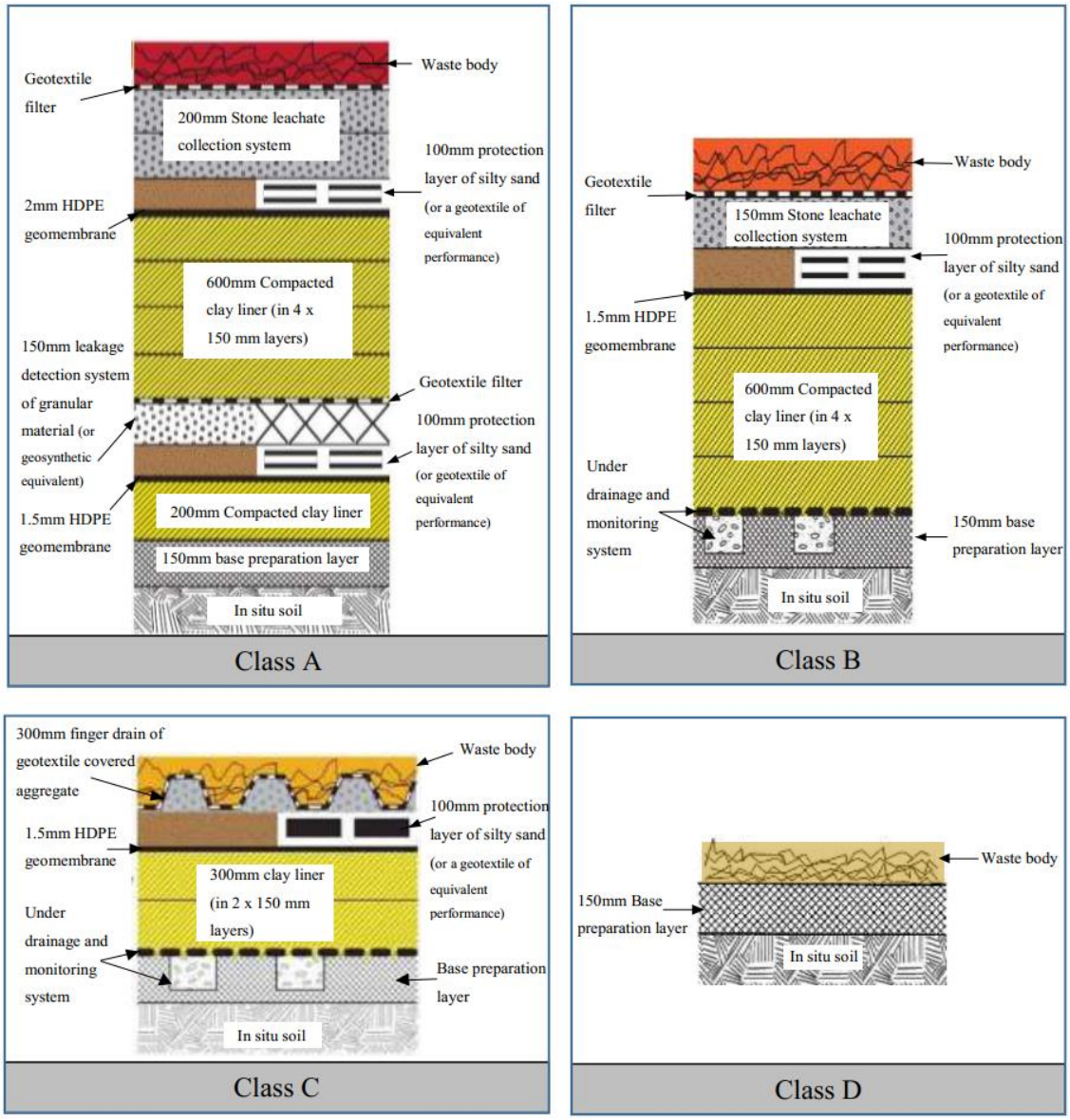

Figure 2-2 Various classes of containment barriers of landfills. (after Buthelezi, 2017))

Municipal solid waste (MSW) landfill facilities are generally designed with a barrier system that consists of a liner, leachate collection and cover system. These three elements or systems are used in conjunction with each other to form the waste containment barrier system, as can be seen in **Figure 2-3**, (Ng & Ramsey, 2012). The liner system, which is placed on the landfill's bottom and side slopes, acts as a barrier against leachate transport and thus prevents contamination of the surrounding soil and groundwater. This makes it the single most significant component out of all three components of a landfill, (Shukla, 2016). A typical liner system of an MSW landfill is made up of three main liner components, i.e. (i) basal/bottom, (ii) side slope and (iii) capping liners, (Sikwanda, 2018). If a liner uses as a combination of a geomembrane layer and an underlying low-permeability soil layer (clayey soil) placed in good hydraulic contact, then the combined system is referred to as a composite liner system (**Figure 2-4**).

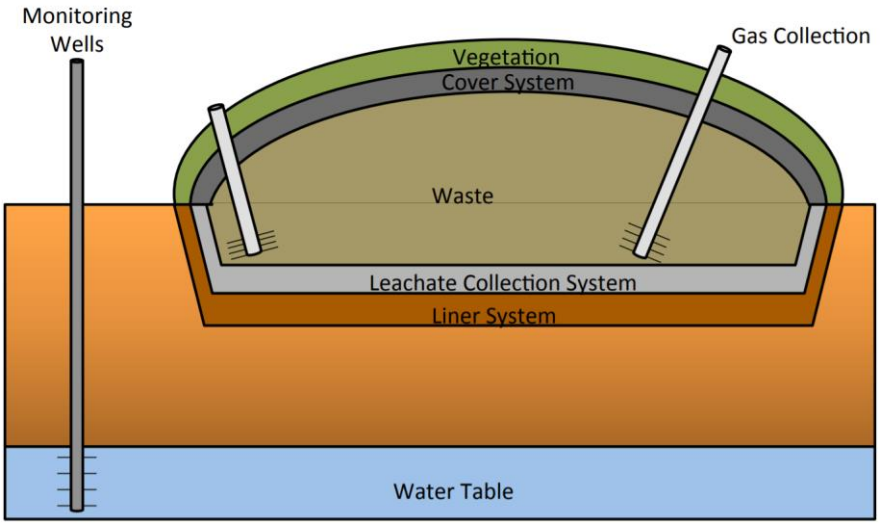

Figure 2-3 A typical modern municipal solid waste (MSW) landfill design with a composite liner, leachate collection and cover system (Barlaz, 2016).

The term "liner" refers to only the low-permeability barrier that impedes the flow of fluids towards the ground. Liner systems are placed above and below the waste and consist of either single or double liners. Single liners consist of one layer of barrier system and are used for MSW, while double liners consist of two layers of barrier system with a leak detection/drainage layer system in between, (Chrysovergis, 2012). Conversely, the term "lining system" refers to the combination of the low-permeability barriers and drainage layers in a containment facility. They are designed for the containment, collection and removal of leachate generated within a landfill, preventing the contamination of ground and surface water. The containment integrity of these lining systems can be relied on over the long term due to the advancements in the technology involved in the design, (Akgün, 1997; Meegoda et al., 2016).

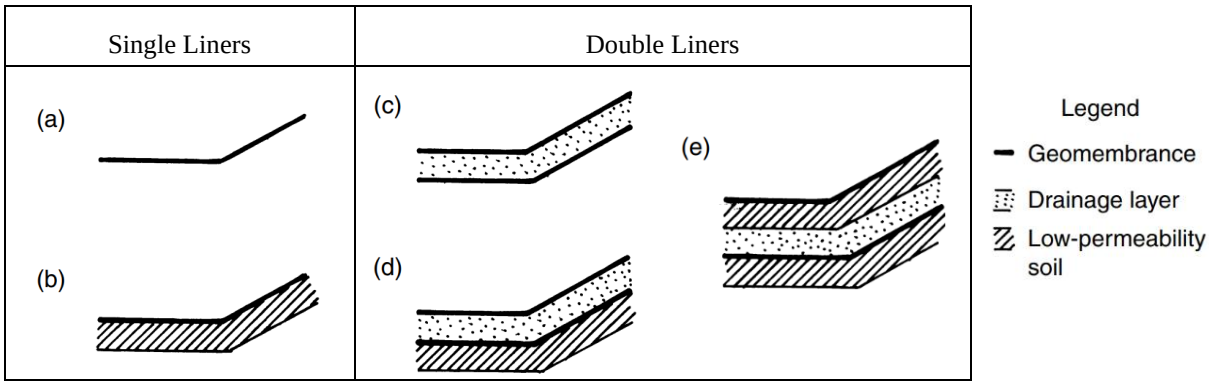

Figure 2-4 Examples of lining systems: (a) single geomembrane liner; (b) single composite liner; (c) double geomembrane liner; (d) double liner with geomembrane top (or primary) liner and composite bottom (or secondary) liner; (e) double composite liner. (Shukla & Yin, 2006)

The composite liner system is the most frequently used standard liner system for MSW landfills, (Ng & Ramsey, 2012). It consists of one or more geomembrane (GMB) overlying a natural soil barrier, such as Compacted Clay Liner (CCL) or Geosynthetic Clay Liner (GCL). These two materials, i.e. GMB and clays, are utilized together due to their respective advantages such as hydraulic and physical properties, and durability. The GMB serves as the primary resistance to the flow and diffusion of contaminants. Alternatively, the clay component acts as a supplementary liner for the reduction of possible leakages through any holes or defects in the GMB that may result from poor construction quality or vandalism during construction, (Ng & Ramsey, 2012; Rowe, 1998).

The bottom liner system is the engineered containment system below the waste which is constructed prior to the placement of the waste. It consists of a double composite liner system made up of a primary and secondary liner system. The primary liner system consists of a GMB/GCL composite liner, whereas the secondary liner system is made up of a GMB/CCL composite liner. Overlying the primary bottom liner system is the leachate collection system, which is generally made up of gravel with a network of perforated pipes. Similarly, the side slope liner commonly adopts a geocomposite drainage sheet overlain by a geotextile filter, (Chrysovergis, 2012; Ng & Ramsey, 2012). **Figure 1-1**, from Section 1 illustrated the usage of the most commonly used examples of geosynthetics in landfill applications. These geosynthetics are briefly discussed in the next section.

2.3 Overview of Geosynthetics

2.3.1 Introduction

There has been an increasing interest by civil engineers in geosynthetics and understanding their correct usage, (Guler, 2017). These materials offer alternative solutions to many geotechnical engineering-related problems, thus significant advances have been made in understanding their applications in different areas of geotechnical engineering. The term “geosynthetics” has two parts; the prefix ‘geo’, referring to an end user associated with civil engineering works that involve earth/ground/soil/rock, and the suffix ‘synthetics’, referring to the fact that the materials are almost exclusively made from man-made products, (Koerner, 2005). The prevalent application of geosynthetics in modern landfills was triggered by their economic and technical advantages over traditional materials previously used. Examples of advantages of incorporating geosynthetics in landfill construction include superior hydraulic efficiency, good compliance with differential settlements of underlying soil or waste and ease of installation.

2.3.2 Functions of geosynthetics

According to Shukla (2016), geosynthetics are available in a wide range of compositions and therefore have a wide variety of applications and conditions under which they can be used. Major types of geosynthetics are employed in landfill engineering to perform various primary functions namely; separation, reinforcement, drainage, filtration, hydraulic/gas barrier and protection. These primary functions may also serve as secondary functions for complementing each other in other geotechnical applications. In the case of a landfill lining system all functions are necessary

and geosynthetics are therefore integral to the operation of a modern lining system, (Bouazza et al., 2002; Zhao & Karim, 2018). A summary of geosynthetics conventionally used in a landfill and their functions is provided in **Table 2-3**.

Table 2-3 Functions of geosynthetics in modern landfill design. (adapted from Zhao & Karim, 2018)

Function	Description	Geosynthetic Type
Seperation	Placed between two different materials to maintain or improve the integrity and functioning of both materials.	Non-woven geotextile; woven geotextile; geocells; geocomposite
Reinforcement	Provides tensile strength in materials that lacks sufficient tensile capacity.	Woven geotextile; geogrids; geocells; geocomposite
Filtration	Allows water or gas flow across it while retaining the fine particles on its upstream side	Non-woven geotextile; woven geotextile; geocomposite
Drainage	Transmits flow within the plane of their structure	Non-woven geotextile; geopipe; geocomposite; geonet
Hydraulic/Gas Barrier	Relatively impervious material to contain liquids or gasses	Non-woven geotextile; geomembrane; geosynthetic clay liner; geocomposite; geonet
Protection	Provides a cushion above/below to prevent damage by punctures during placement of overlying materials.	Non-woven geotextile; geosynthetic clay liner; geocomposite

2.3.3 Types of Geosynthetics

The most commonly used examples of geosynthetics in landfill applications include geotextiles (GTXs), geomembranes (GMBs), geosynthetic clay liners (GCLs), geopipes and geogrids, while geosynthetics such as geonets, geofoams, geocells, geotubes and geocomposites are used to a lesser extent. This study, however, only focused on the GMBs, GTXs and GCLs as the main interest of the research work as discussed below.

2.3.3.1 Geotextiles

Geotextiles are planar, polymeric and permeable products formed from flexible sheets, and they have been the most frequently utilized type of geosynthetic over the years, (Shukla, 2016). There exists a variety of geotextiles that have been produced throughout the years for continuous utilization in different applications. Based on the manufacturing process, there are four (4) categories of geotextiles namely; woven, non-woven, knitted and stitched geotextiles, as illustrated in **Figure 2-5**. The most frequently utilized family of geotextiles, however, are woven, non-woven and knitted geotextiles.

There has been extensive use of geotextiles in various geotechnical engineering applications. Their functions in different applications have ranged from soil separation, filtration, drainage, soil reinforcement, protection and erosion control, (ASTM D4439, 2017). GTXs are used as an alternative to conventional granular soil layers in landfills, resulting in decreased weight and a reduction in landfill settlement, (Zhao & Karim, 2018). In addition, they act as a cushion to prevent puncture damage to the geomembrane liner by augmenting and replacing conventional protective soil layers for geomembrane liners and function as a filter in the leachate collection system. Thus, with a higher mass per unit area, geotextiles provide better puncture resistance than conventional protective soil layers, (Kiptoo et al., 2018).

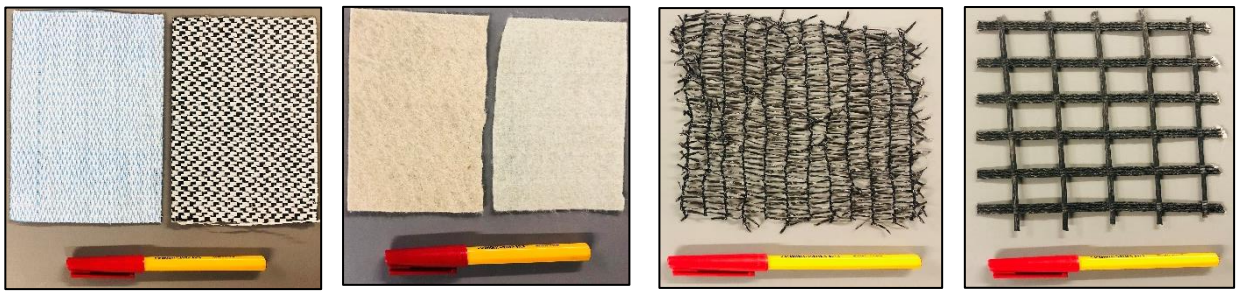

(a) (b) (c) (d)

Figure 2-5 Typical geotextiles: (a) woven geotextile; (b) non-woven geotextile; (c) knitted geotextile; (d) stitched geotextile.

2.3.3.2 Geomembranes

Geomembranes (GMBs) are flexible, polymeric sheets that have extremely low hydraulic conductivity and are typically used as barriers for water or vapour, (ASTM D4439, 2017). They come in a variety of thicknesses, interface characteristics and polymer types, each having significantly different shear strengths. Raw materials, which include polymer resin and various additives, are used to manufacture geomembranes. These raw materials are processed into various sheets of geomembranes through three methods, *(1) Extrusion, (2) Calendaring,* and *(3) Spread Coating,* (Oriokot, 2014). The method of extrusion is used to manufacture geomembranes such as High-Density Polyethylene (HDPE), Linear Low-Density Polyethylene (LDPE) and Flexible Polyethylene. Polyvinyl Chloride (PVC), chlorinated polyethylene (CPE) and polypropylene (PP) are the commonly extruded geomembranes, (Koerner, 2005).

In landfill applications, the predominantly used geomembrane is HDPE, (Ng & Ramsey, 2012). This is due to its superior hydraulic and mechanical properties in combination with its high chemical resistance, thermal stability, durability and ultraviolet (UV) light degradation resistance, (McCartney et al., 2002). Manufactured as a blown film or flat sheet products, HDPEs are the cheapest (per mm thickness) industrial geomembrane available commercially. The modern HDPE geomembrane includes the mono and double smooth geomembranes and mono and double textured membranes, (Koerner, 2005). The textured features of geomembranes are formed by either spraying of particles onto the geomembrane during formation, by a physical structuring process or by-passing nitrogen gas through the polymer during formation. Once this roughened surface is created through the "texturing" process, it results in a higher friction surface that enhances the frictional resistance of the geomembrane, which improves interfacial stability of the landfill liner system, (Ng & Ramsey, 2012). There is greater interface friction obtained between adjacent geosynthetics with textured geomembranes as compared to smooth geomembranes. Hence, smooth HDPE geomembranes are mainly applied in projects requiring low permeability, excellent chemical and ultraviolet resistance properties. The textured HDPE, however, is generally applied in high shear strength projects due to its highest multi-axial performance, (Buthelezi, 2017; Sikwanda, 2018).

2.3.3.3 Geosynthetic Clay-Liners

Geosynthetic Clay Liners (GCLs) are prefabricated geocomposite materials used as an alternative to Compacted Clay Liners (CCL) in various geotechnical structures such as landfills. GCLs offer ease of construction, lower space requirements, and lower costs due to good hydraulic performance. Typically, GCLs that consist of a thin layer of sodium bentonite sandwiched between two sheets of geotextiles (woven or nonwoven) or mixed with an adhesive and attached to a geomembrane, are referred to as "unreinforced" GCLs. Alternatively, GCLs that made up of a layer of un-hydrated, loose granular sodium bentonite, which is held together by needling, stitching and/or chemical adhesive to give the structure its internal shear resistance, are referred to as "reinforced" GCLs, (Bouazza & Bowders, 2009; Shukla, 2016). Typical cross-sections of unreinforced and reinforced GCLs are shown in **Figure 2-6** and **Figure 2-7** respectively.

When unreinforced GCLs are used in landfills, one concern in terms of slope stability is mid-plane shear through the bentonite layer, (Zhao & Karim, 2018). Although the use of sodium bentonite provides an effective hydraulic seal to the adjacent materials, due to its high swelling capacity and low permeability, they have very low peak shear strength values making them prone to sliding. As a result, their use in engineering applications, i.e. landfill cover or liner system, requires careful assessment of the shear strength prior to installation, (McCartney et al., 2002).To increase the internal strength of GCLs, manufacturers created "reinforced" GCLs in which the two outer layers of geotextile are either needle-punched or stitch-bonded together through the bentonite layer. This gives the GCLs greater internal peak strength due to the presence of fibre reinforcements, (Zhao & Karim, 2018).

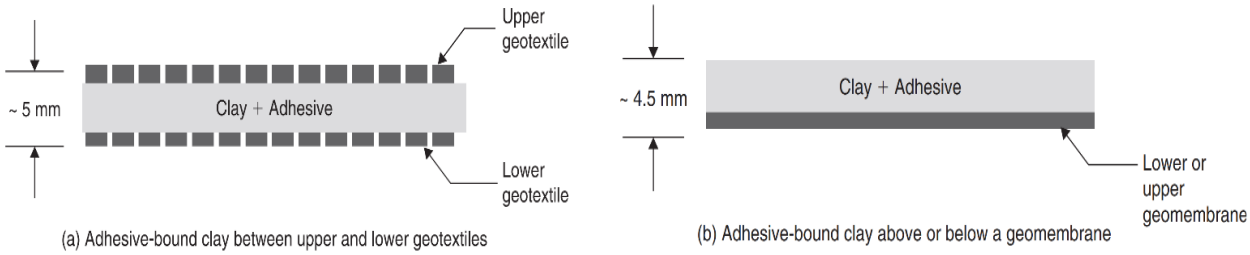

Figure 2-6 Cross sections of typical unreinforced GCLs. (after Bouazza & Bowders, 2009)

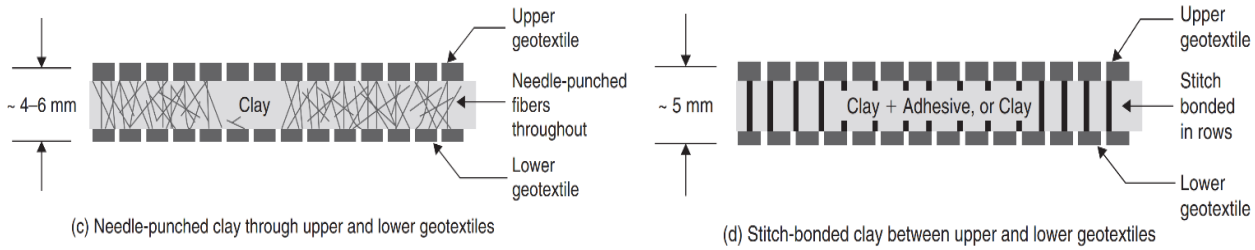

Figure 2-7 Cross sections of typical reinforced GCLs. (after Bouazza & Bowders, 2009)

2.4 Geosynthetic Interfaces in landfills

In a landfill liner, the placement of geosynthetics with similar or dissimilar properties adjacent to each other results in a zone of interaction that is referred to as an "interface", (Karademir, 2011). Relative displacement is most likely to occur at this interface due to the discontinuities, which could make that interface the weakest point in the overall system relative to the adjacent materials in terms of shear strength, (Karademir, 2011). The overall design and stability of more than one material system are often controlled by the interface shear strength. The integration of one geosynthetic material into another geosynthetic material or soil creates an interface, and this generates a potential weakness within the system or soil mass that could lead to failure, (Koerner, 2005; McCartney et al., 2002). The shear behaviour and the state of the interface, as well as the interaction and contact behaviour between the two materials, are defined by their physical and mechanical properties. It is therefore essential to thoroughly evaluate and understand the factors controlling the shear strength-displacement response of that interface to prevent a failure from developing at the interface, (McCartney et al., 2002).

Amongst all the components in composite liner systems, there are three critical geosynthetics and clayey soil interfaces, i.e. GMB/clayey soil; GMB/GTX, and GCL/clayey soil, (Chai & Saito, 2016). The interface shear behaviour between geosynthetics and clayey soils is influenced by both the geosynthetic and the soil properties involved. There are preferential slip planes on the interfaces between the components of the liner system, especially where geosynthetic materials exist. This results in great variability in shear strength due to laboratory testing and material variations, (Chai & Saito, 2016). Hence, caution should be taken when using literature data, since it may not be representative of the conditions on-site. Consequently, site-specific testing should be performed using representative material below and above the interface to reduce the uncertainty associated with interface shear strength variability, (Fowmes et al., 2007).

2.4.1 Interface shear testing Apparatus

To study and thoroughly understand the soil-geosynthetic and geosynthetic-geosynthetic interaction and successfully replicate the representative field conditions in the laboratory, various aspects of shear testing and theoretical analysis can be performed under different conditions, (Moraci et al., 2014). This can be done by carrying out interface shear testing using different devices such as large-scale direct shear apparatus (LDSA), pull-out apparatus (POA), inclined plane device (IPA), and ring (or rotational) shear device (RSA). These apparatus have been developed to quantitatively study the interface shear strength behaviour of soil and geosynthetic interfaces, (Bouazza et al., 2002). In cases where soil mass sliding on reinforcement surfaces occurs, LDSA is mostly used to quantify soil-reinforcement interactions. Alternatively, POA can be used in cases where reinforcement is pulled out. Lastly, in the case of investigating the interface properties under low vertical stresses of inclined barrier and landfill cover systems, the IPA is suitable, (Moraci et al., 2014). Each of these devices is discussed below, briefly stating their use and advantages.

2.4.1.1 Pull-out testing device

Generally, pull-out testing involves the measurement or assessment of the anchorage or pull-out capacity of a geosynthetic specimen out of a soil mass, (Moraci et al., 2014). A pullout test is performed in an apparatus defined by ASTM D6706, and its average normal size is 30 to 50 cm in width, 30 cm in height, and 60 to 100 cm in length. This apparatus consists of four components namely; a large pullout soil box, a vertical load application system, a horizontal force application device, and a geosynthetic clamping system, as can be seen in **Figure 2-8**(a), (ASTM D6706, 2013; Park et al., 2017).

In terms of the pullout coefficient, the soil–geosynthetic interaction along both surfaces of the geosynthetic material in contact with the soil is considered. The interface shear resistance and stiffness properties for applications where the soil is moving relative to the geosynthetic is evaluated, (Moraci et al., 2014). Eventually, this determines the cohesion and pullout friction properties between the soil and reinforcements. The coefficients can then be defined as $\tan\delta/\tan\phi$, where ϕ is the friction angle of the soil and δ is the friction angle of the soil-geosynthetic interface, (Perkins, 2007; Prashanth et al., 2016). Many researchers have previously reported the evaluation of soil–geosynthetic interfacial frictional behaviour through direct shear tests and pull-out tests, (Kalumba, 1998; Moraci et al., 2014; Park et al., 2017; Prashanth et al., 2016). It has been found that shear resistance parameters (cohesion & friction angle) obtained from the pullout test are slightly smaller than those from the direct shear apparatus, (Hegde & Roy, 2018; Kalumba & Scheele, 1999).

2.4.1.2 An Inclined plane testing device

An inclined plane (also known as tilt table) is an apparatus that measures the soil-geosynthetic or geosynthetic-geosynthetic interface shear strength, (see **Figure 2-8**(b)). Shear and normal stresses are induced into the geosynthetic placed on a board by gravity and the angle of the board is increased at a specific rate until failure occurs. This test is commonly used as an alternative to the direct shear test, due to the LDSA not being applicable in cases where normal stress levels are low (less than approximately 50 kPa), i.e. side slopes in landfill covers, (Gourc et al., 2008; Pitanga et al., 2009).

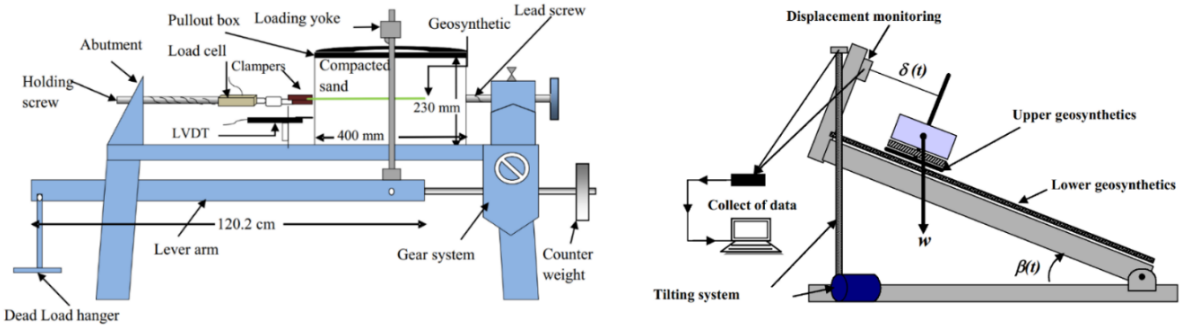

(a) Pull-out test apparatus (b) Inclined plane test apparatus

Figure 2-8 Schematic diagram of interface shear test devices. (Gourc et al., 2004; Prashanth et al., 2016)

Additionally, this apparatus allows testing of much larger geosynthetics than those used in a LDSA, but normal stress is limited (typically below 50 kPa) due to a deadweight loading system on the sloping board and is well suited to creep investigations, (Rouncivell, 2007). Further comparisons between the two apparatus indicate that the shear strength determined using the LDSA is much higher than in inclined plane tests. Moreover, inclined plane tests are regulated by force/gravity, whereas LDSA tests are controlled by displacement, (Lopes et al., 2014; Wu et al., 2008).

2.4.1.3 Ring Shear testing device

The Ring Shear Apparatus (RSA) is a rotational shear test that allows constant shearing of samples, (Li et al., 2017). This device is primarily used for the determination of residual soil strength of soils. It has been successfully used in the study of large strain shear response of cohesive/non-cohesive soils as well as to determine interface shear strengths between soils and other engineering materials such as geosynthetics, (Othman, 2016). One major advantage of this apparatus is that it can place infinite uni-directional shear strains on the sample while maintaining a relatively uniform state of stress on the shear plane, (Orebowale, 2006). It can be used to achieve true residual soil strengths via continuous rotation, thus achieving large displacements. However, due to the presence of non-uniform strains across the shear surface, this apparatus cannot be used to measure peak interface shear strengths, (Othman, 2016).

Due to its finite shear displacement, the RSA is more suitable in investigating the effects of shear displacement at failure and shear displacement rate on the internal shear strength of GCL than using an LDSA, (McCartney et al., 2002). A comparison in the method of obtaining residual interface strengths using LDSA and RSA found that the measured values differ significantly. Such disparities in the values were correlated with the test setup, geosynthetic fixing, the shape of the particles, grading of the cover soils and shearing direction as the main reasons for the differences, (Othman, 2016). **Figure 2-9** shows a schematic diagram of a ring shear device.

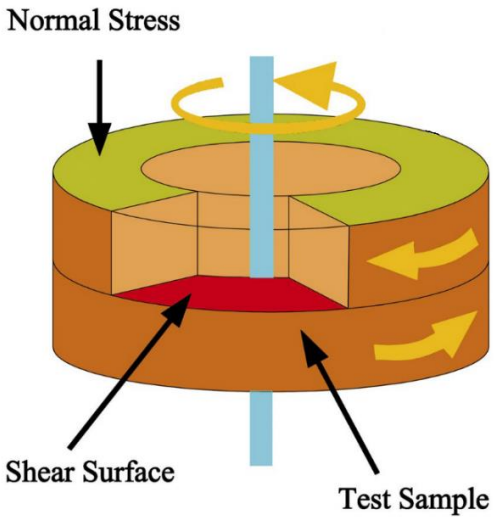

Figure 2-9 Schematic diagram of ring shear apparatus. (adpated from Li et al., 2017)

2.4.1.4 Large direct shear device

LDSA is the most widely utilized testing apparatus in laboratories to measure the shear strength of geosynthetic-geosynthetic or soil-geosynthetic interfaces, (Othman, 2016). It is widely used due to its relatively simple procedures, which are well established and recommended in ASTM D5321/D6243. This device is a modification of the conventional standard direct shear apparatus used to determine the angle of internal friction of soils. Unlike the conventional standard direct shear device, the modified LDSA is best suited to shear soil, different types of geosynthetic products or both. This direct shear device has an advantage over the first in that it can shear relatively large specimens with limited boundary effects during testing. This allows the determination of the residual shear strength of the interface and no generation of regular eccentric loads during shear, (ASTM D5321, 2017; ASTM D6243, 2018).

The LDSA consists of two rectangular or square shearing boxes, the lower/bottom moving part, and the upper/top static part, placed one above the other, as shown in **Figure 2-10**. A constant normal load (N) is applied to the top box to produce a vertical normal stress $\sigma_n = N/A$, where A is the cross-sectional area of the direct shear box. The shearing process is then initiated by applying a steadily increasing tangential (shear) force (F), which causes an increase in horizontal displacement, to the bottom part of the shear box at a user-defined rate. The bottom shear box then slowly starts moving laterally relative to the upper static box. Once the shearing process is initiated, the test machine monitors the relative horizontal displacement of the bottom shear block to the top shear box and the normal force applied, through a connected desktop computer. As a result, respective shear stress versus horizontal displacement relationship graph is plotted, as shown in **Figure 2-11**. The same steps would be taken to determine the frictional characteristics of a soil-geosynthetic or geosynthetic-geosynthetic interface, (Jogi, 2005).

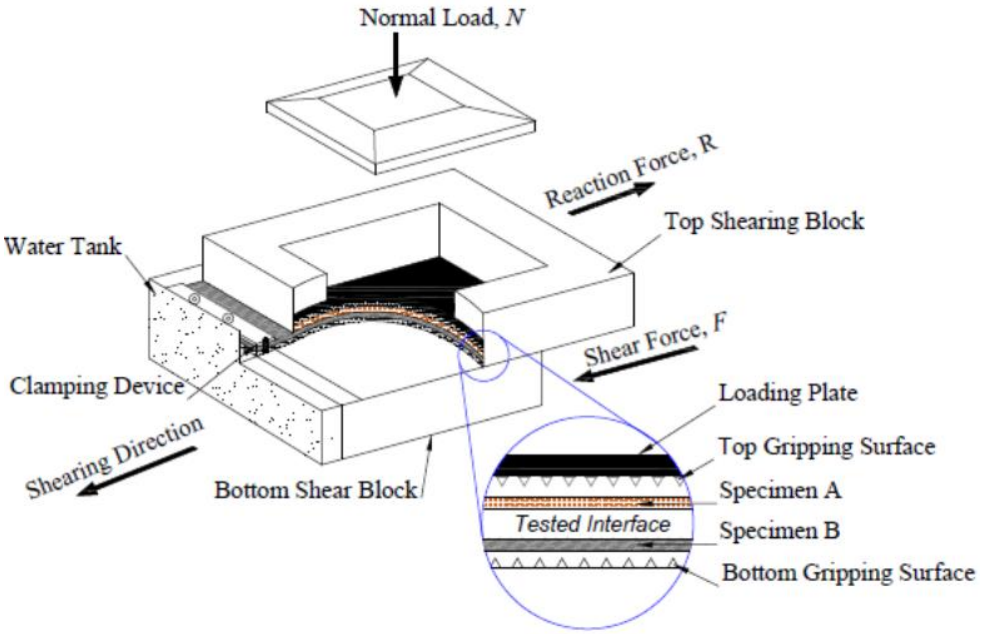

Figure 2-10 Schematic diagram of large-scale direct shear apparatus. (after Sikwanda, 2018)

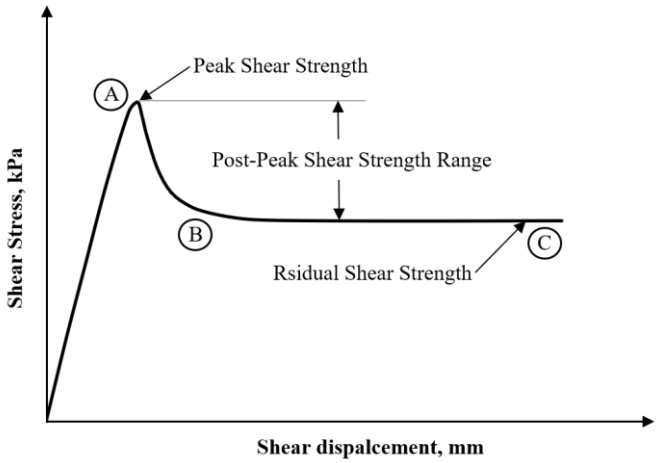

Figure 2-11 Shear stress-displacement curve for a geosynthetic interface, (adapted from Thiel (2001)).

Eventually, maximum shear stress (point A in **Figure 2-11**) is achieved after a certain amount of displacement, which is referred to as the peak shear stress. After the peak, the shear resistance falls off, as shown by region AB, to eventually reach the residual shear stress, shown by point C, in **Figure 2-11**. At this stage, the tested material is going through a plastic deformation state, a process termed strain softening. Once the residual strength is reached, it is considered that the failure of the interface has occurred, (Jogi, 2005; McCartney et al., 2002).

The test is then repeated for at least two additional, yet different, normal stresses to obtain a set of three points in the shear stress versus normal stress graph. By plotting the peak and residual or Large Displacement (LD) shear stress against the corresponding normal pressure, a failure envelope for the interface test series is produced, where interface friction angles and adhesion values can be obtained, (Kalumba, 1998). A typical plot of shear stress vs normal stress obtained from testing of a soil-geosynthetic or geosynthetic-geosynthetic interface is shown in **Figure 2-12**.

2.4.1.5 Mohr-Coulomb Failure Envelope

The relationship between the shear stress at failure and the normal stress applied to the interface is known as the failure envelope. The Mohr-Coulomb failure criterion is used to describe the shear strength envelope for a given interface. This failure criterion assumes that the peak and residual or LD shear strengths vary linearly with normal stress. According to McCartney et al. (2002) and Othman (2016), a generic interface shear strength envelope is described by the general expression:

$$\tau = c_\alpha + \sigma_n \cdot tan\delta$$

Equation 2-1

where τ is the peak or residual shear stress at failure, c_α is the adhesion of the interface (or shear strength at zero normal stress), σ_n is the applied normal stress and δ is the interface friction angle. The above-mentioned relationship is quite useful for most practical purposes for interface shear testing, and is the most widely accepted interface failure criterion, (Jogi, 2005).

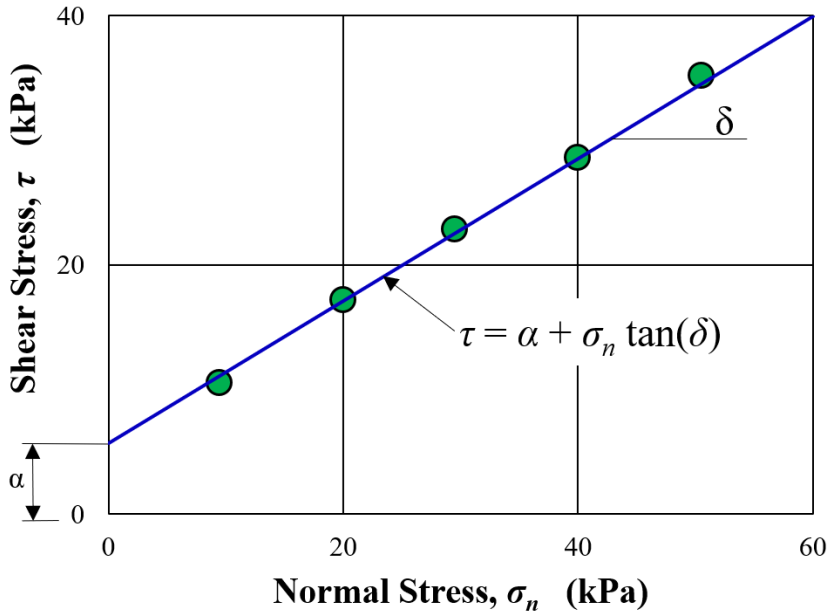

Figure 2-12 Shear stress versus normal stress, (adapted from Jogi, 2005).

Many common models can be used to characterize interface failure envelopes. Fox & Stark (2004) found that the peak and residual interfaces can be linear, multi-linear (e.g. bilinear, trilinear) or non-linear. Linear envelopes were found to be the simplest, with a zero or non-zero intercept. On the other hand, multi-linear envelopes, consisting of two or more- line segments, gave an abrupt change in the friction angle at the point(s) of the intersection, which may in some cases reflect the true nature of shear strength behaviour. Nonlinear envelopes showed a gradual change in tangent friction angle as normal stress increased, (Fox & Stark, 2004). **Figure 2-13** shows the typical examples of failure envelopes for soil and geosynthetic interfaces.

Several researchers using DSA, (i.e. Bacas et al., 2015; Fowmes et al., 2008; Fox & Stark, 2004; McCartney et al., 2002; Triplett & Fox, 2001), have reported non-linear shear vs normal stress relationships. The results obtained by Bacas et al. (2015), for instance, using a DSA (300 x 300 mm), yielded non-linear relations. Although the straight envelopes showed a good fit, it was observed that the non-linear trend curves clearly illustrated a more accurate fit. The friction angle of the non-linear envelope was not constant over the range of the confining pressures tested, (Bacas et al., 2015). Fox & Stark (2004) also acknowledged that selecting and using the proper normal stress range for shear testing was important because a non-linear model seemed more appropriate over large stress ranges.

Jogi (2005) also observed that for many soils and geosynthetics the strength envelope is curved (i.e. non-linear) over a wide range of normal stresses. Consequently, the normal stress range over which tests are carried out often dictates the degree of curvature in the resulting data and the appropriate model to use, (Fox & Stark, 2004).

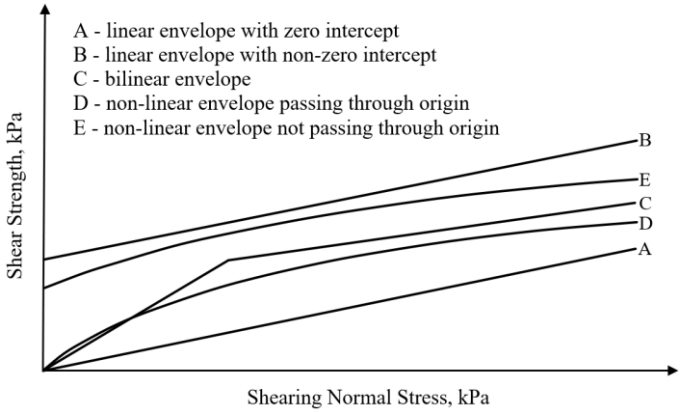

Figure 2-13 Typical examples of linear, bilinear and non-linear failure envelopes. (adapted from Fox & Stark, 2004)

2.4.1.6 Peak, post-peak and residual Interface Shear Strength

The peak strength is defined as the highest level of shear strength measured in a direct shear test under a given normal load. The peak interface shear strengths are generally mobilized at displacements of 1 to 15 mm, (Jogi, 2005). The angle of interface shearing resistance obtained by considering peak shear stresses on the interface is referred to as the peak friction angle of the interface. However, with continued shear displacement there is typically a loss of strength and past the point of peak strength, the shear strength at any given displacement is referred to as "post-peak strength". Eventually, there will no longer be any further loss in shear strength with continuous shear displacement, and this point is referred to as the "residual strength" (see **Figure 2-11**). The angle of interface shearing resistance obtained by considering residual shear stresses on the interface is referred to as the residual friction angle of the interface.

According to Thiel (2001), many of the most common direct shear devices do not allow sufficient displacement to occur which would allow the measurement of true residual strength. Rouncivell (2007) noted that when a 300 mm x 300 mm LDSA device is used, the residual shear strength condition may, in some cases, not be defined due to its limited shear stress displacement. It is therefore not technically correct to refer to end-of-test conditions as representing the "residual" strength, but rather, to refer to "post-peak" strength, while also specifying the amount of displacement. Alternatively, a reduced shear strength condition reached after the strain-softening can as well be referred to as the "large displacement" (LD) strength, (Adeleke et al., 2021; Sikwanda, 2018).

Various researchers have given different suggestions for use of peak or residual strength in design, (Thiel, 2001). Stark & Poeppel (1994) suggested that the most conservative approach to be used in the design is the use of residual strengths for all conditions. Furthermore, Koerner (2003) suggested the usage of residual strength of the interface having the lowest peak strength, which is a concept that applies to multiple geosynthetic interfaces. It is suggested that there is no likelihood of failure when using residual strength in design and so while such an approach is unquestionably extremely conservative, it is unnecessary so, (Jogi, 2005; Koerner, 2003).

2.4.2 Interface shear stress-displacement relationship

The determination of the interface shear stress-shear displacement behaviour and shear force parameters is essential for accurate assessment of the stability of the composite liner interface, (Seo et al., 2003). However, establishing the available shear resistance along an interface that exhibits strain-softening behaviour is difficult. This makes modelling the relationship between shear stress and displacement complex, (Seo et al., 2003). As such, a new constitutive interface model combining a nonlinear hyperbolic model with a displacement-softening model was proposed to describe the nonlinear strain-softening behaviour of the geosynthetic interfaces, (Esterhuizen et al., 2001; Gomez et al., 2000; Wu et al., 2011). This was proposed based on the results of interface shear tests performed by Jones & Dixon (1998).

In nonlinear models, the interface shear stress-displacement relationship is represented by a higher degree of mathematical functions. During shear, the shear stiffness of the interface changes depending on the magnitude of the displacement and any other factor included in the model, (Gomez et al., 2000). The nonlinear strain-softening property of geosynthetic interfaces reduces the shear stress at displacements beyond the corresponding displacement of peak strength, (Wu et al., 2011). Thus, the relationship between shear stress and displacement can be described by three stages: the pre-peak stage, the softening stage, and the residual stage, as shown in **Figure 2-14**. The behaviour of each of these three stages is discussed in brief below.

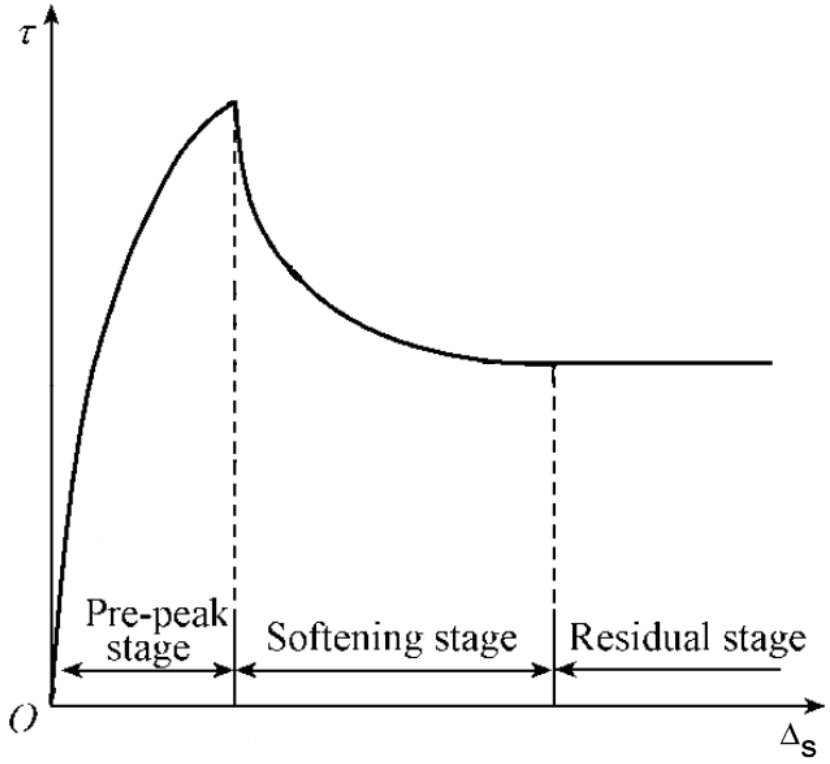

Figure 2-14 Relationship between shear stress and shear displacement of geosynthetic interface divided into three stages: pre-peak, strain softening and residual stages (adapted from Wu et al. (2011)).

2.4.2.1 Pre-peak behaviour

At the pre-peak stage, the shear stress increases with increasing displacement from the origin and typically follows a nonlinear hyperbolic stress-displacement behaviour until reaching a peak value (Wu et al., 2011). This hyperbolic model has been extensively used in the design of geotechnical structures and often provides an accurate approximation of the interface response under constant normal stress, (Gomez et al., 2000). The procedures for identifying the stress-displacement relationship at geosynthetic interfaces are as follows:

(1) Approximation of nonlinear stress-displacement relationship using the hyperbolic equation:

In **Figure 2-15**(a), a hyperbola was used to fit a set of test data from a direct shear test interface, and the hyperbola equation can be written as:

$$\tau = \frac{\Delta_s}{a + b \cdot \Delta_s}$$

Equation 2-2

Where a and b are the parameters evaluated to fit the hyperbola to the experimental data. Equation 2-2 can be rewritten as:

$$\frac{\Delta_s}{\tau} = a + b \cdot \Delta_s$$

Equation 2-3

The same test data used in **Figure 2-15**(a) is plotted in **Figure 2-15**(b), in terms of Δ_s/τ and Δ_s. This is called the transformed plot, and it is plotted using Equation 2-3. If the interface shear stress-displacement behaviour follows a hyperbolic shape, the plot in **Figure 2-15**(b) will be a straight line, and hyperbolic parameters 'a' and 'b' will be the vertical axis intercept and slope of this straight line, respectively. The value of 'a' is the reciprocal of the initial shear modulus K_{si} of the interface, and the value of 'b' is the reciprocal of the asymptotic shear stress value τ_{ult} of the hyperbola, (Gomez et al., 2000; Seo et al., 2003). If the actual interface test data does not exactly follow a hyperbolic relationship, then the plot in **Figure 2-15**(b) must then be fitted to a straight line to determine the hyperbolic parameters 'a' and 'b'.

Duncan & Chang (1970) observed that the transformed plot (**Figure 2-15**(b)) for strength test data in soils diverged from a straight line, both at low and high values of strain. They recommended that the best fit to the data can be obtained when the hyperbola intersected the test data at 70 and 95 percent of the strength. This is shown as points P_1 and P_2, as well as points P_{1t} and P_{2t} in **Figure 2-15**(a) and **Figure 2-15**(b) respectively. Consequently, a straight line can be drawn between P_{1t} and P_{2t}, allowing the hyperbolic parameters (a & b) to be found as illustrated in the figure, (Gomez et al., 2000). The failure ratio (R_f) is calculated from the value of b, which is defined as the ratio of τ_f/τ_{ult}.

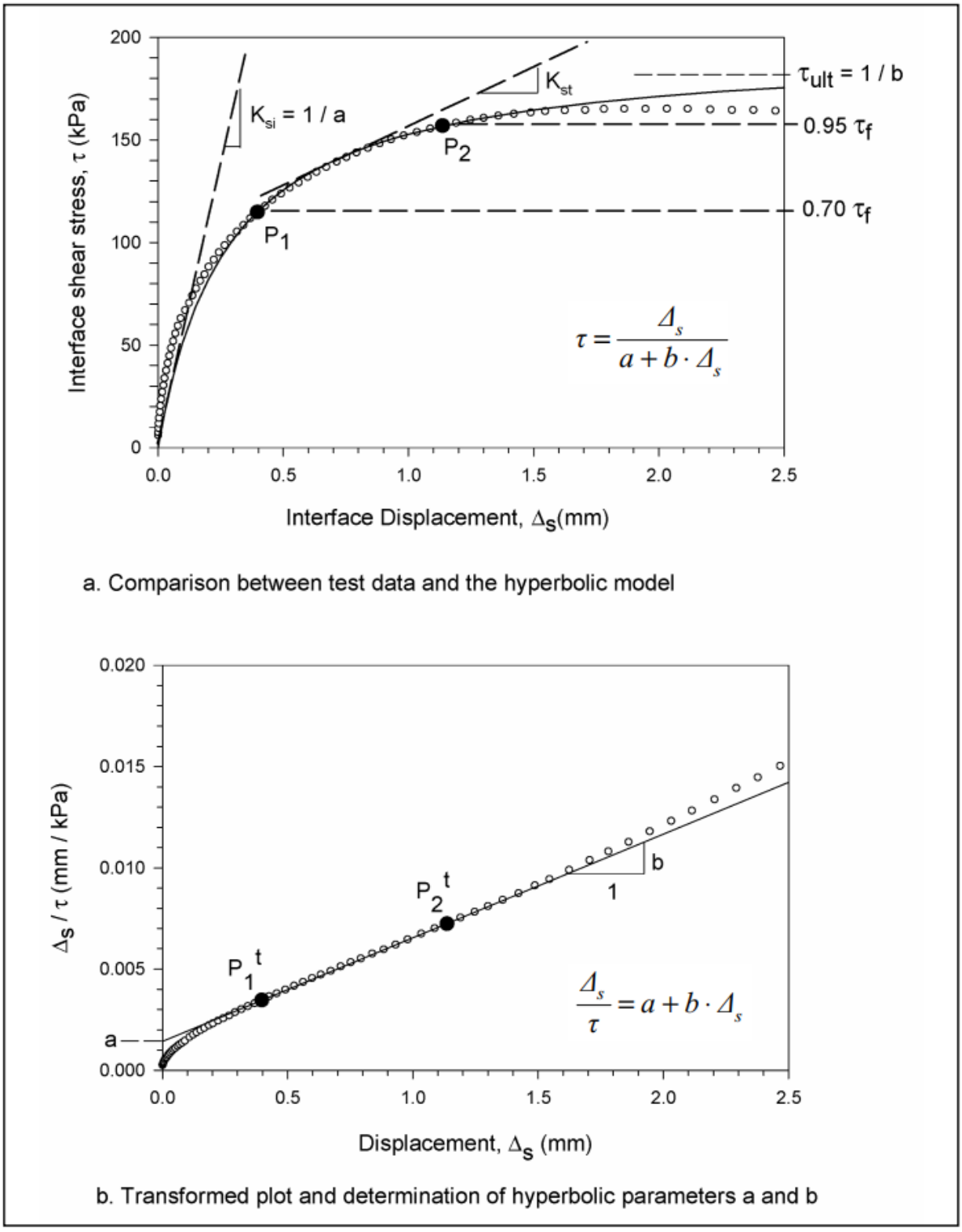

Figure 2-15 Plot showing: (a) comparison between direct shear test data and hyperbolic model and (b) determination of hyperbolic parameters a and b (adapted from Gomez et al. (2000)).

(2) Consideration of stress dependency:

Experimental studies show that the relationship between initial interface shear modulus and normal stress may be calculated using the following expression (Esterhuizen et al., 2001; Gomez et al., 2000; Seo et al., 2003):

$$K_{si} = K \cdot \gamma_w \cdot \left(\frac{\sigma_n}{P_a}\right)^n$$

Equation 2-4

Where K_{si} is the initial shear modulus (kN/m^3), σ_n is the normal stress (kPa), γ_w is the unit weight of water (kN/m^3), K is the dimensionless shear coefficient, P_a is the atmospheric press (kPa) and n is the modulus exponent.

The hyperbolic parameter a, and consequently K_{si}, can be evaluated for every normal stress from a series of interface tests under various normal stresses, (Seo et al., 2003). Values of the dimensionless shear coefficient (K) and modulus exponent (n) can then be determined readily from test results by fitting K_{si}/γ_w and σ_n/P_a values using logarithmic (log-log) axes. The slope of the best-fit line gives the value of n, and the vertical intercept of the line gives the value of K.

(3) Determination of tangent modulus value

Duncan and Chang (1970) proposed that tangent modulus (K_{st}) value for any stress condition can be expressed as (Anubhav & Wu, 2015; Gomez et al., 2000; Seo et al., 2003; Wu et al., 2011):

$$K_{st} = \frac{\Delta\tau}{\Delta s} = K \cdot \gamma_w \cdot \left(\frac{\sigma_n}{P_a}\right)^n \left(1 - R_f \cdot \frac{\tau}{\tau_f}\right)^2$$

Equation 2-5

Where, K_{st} is the tangent shear modulus (kN/m^3), R_f is the failure ratio (τ_f/τ_{ult}), τ_f is the interface shear at peak or failure (kPa) and τ_{ult} is the ultimate interface shear stress (kPa).

Seo et al. (2003) and Gomez et al. (2000) maintained that this expression for tangent modulus can be employed very conveniently in incremental analyses. Seo et al. (2003) also noted that the growing value of n implies that K_{st}'s dependence on normal stress in the pre-peak region increased. Hence, the initial shear modulus depends on the magnitude of normal stress, while the value of the tangent shear modulus varies with the horizontal displacement in the tests.

This proposed hyperbolic interface model has some significant limitations to its use. The hyperbolic formulation does not model displacement softening of the interface. Therefore, another model must be implemented for the remainder of the shear stress versus the displacement graph, (Buthelezi, 2017; Gomez et al., 2000)

2.4.2.2 Softening behaviour

In the softening stage, with the increase of shear displacement, there appears a sharp reduction in shear stress until a constant or residual value is reached. The shear stress-displacement relationship can be represented by a nonlinear displacement-softening model proposed by Esterhuizen et al. (2001). The procedures for displacement softening modelling used by Esterhuizen et al. (2001) are as follows, (Seo et al., 2003; Wu et al., 2011):

(1) Calculation of the strain-softening factor (R):

Transformation of the initial stress vs. displacement curves into new curves that relate the strength degradation to the strain-softening shear displacement, can be achieved using the shear strength strain-softening factor (R). The strain-softening factor can be calculated by normalizing the post-peak strength degradation by the shear strength degradation from the peak to the large displacement value, and it can be defined as follows, (Anubhav & Wu, 2015; Aza-Gnandji et al., 2019; Seo et al., 2003):

$$R = \frac{\tau_p - \tau_{pr}}{\tau_p - \tau_r}$$

Equation 2-6

Where, τ_{pr} is the post-peak shear strength, τ_p is the peak shear strength, and τ_r is the residual shear strength. The parameters, τ_p and τ_r , can be calculated by the Mohr-Coulomb criterion using Equation 2-7 and Equation 2-8:

$$\tau_p = \sigma_n \cdot tan\emptyset_p + c_p$$

Equation 2-7

$$\tau_r = \sigma_n \cdot tan\emptyset_r + c_r$$

Equation 2-8

Where, $\emptyset_p$ & $\emptyset_r$ is the peak & residual friction angle of the interface, and c_p & c_r is the peak & residual cohesion of the interface, respectively.

(2) Calculation of the displacement ratio (D):

The displacement ratio (*D*) can also be calculated by normalizing the strain-softening shear displacement by the maximum strain-softening shear displacement that takes place at large displacement. It can be expressed as follows, (Wu et al., 2011):

$$D = \frac{u^p}{u_r^p}$$

Equation 2-9

Where, u^p is the plastic shear displacement, and u_r^p is the plastic shear displacement where the shear stress just reaches the residual strength, as illustrated in **Figure 2-16**.

(3) Plotting the relationship between R and D.

The normalized nonlinear curves can be approximated by a single hyperbolic relationship between the strength residual factor (*R)* and the shear displacement ratio (*D)*. The typical R-D curve is shown in **Figure 2-17**. The relationship can be described by Equation 2-10 as, (Esterhuizen et al., 2001):

$$R = \frac{K_0 \cdot D}{1 + (K_0 - 1) \cdot D}$$

Equation 2-10

Where, K_0 is the initial slope of the *R-D* curve. From Equation 2-10, K_0 values can be determined, and large values of K_0 would mean that interface shear strength decreased significantly at the early stage after peak strength was mobilized, (Seo et al., 2003).

2.4.2.3 Post-peak/residual behaviour

The shear stress reaches a stable state after reaching the residual stage, with the continuous increase of shear displacement as shown in **Figure 2-16**. The shear stress remains at a constant value equal to the residual shear strength, τ_r (Wu et al., 2011).

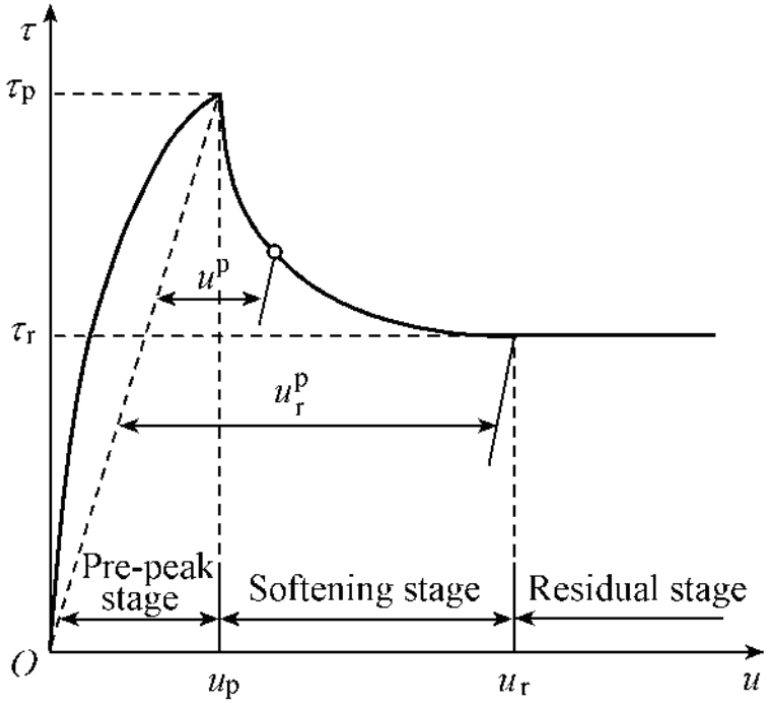

Figure 2-16 Shear stress and displacement relationship of geosynthetic interface. (Wu et al., 2011)

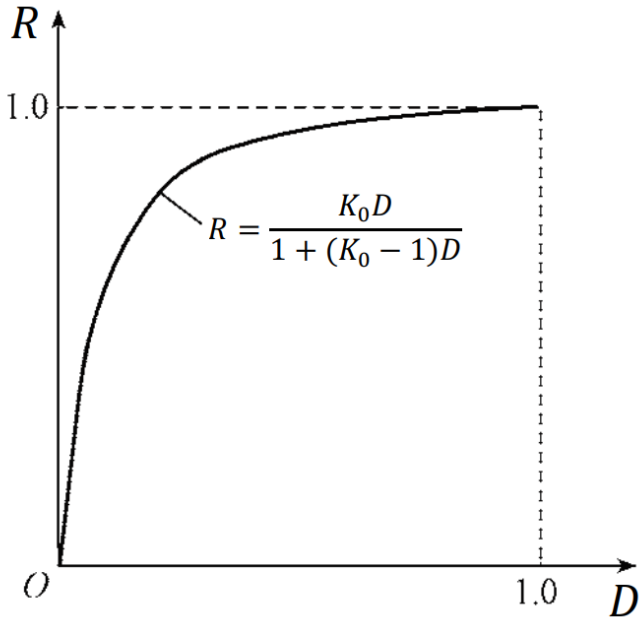

Figure 2-17 Typical strain-softening vs displacement ratio curve (*R-D*) curve.(Wu et al., 2011) .

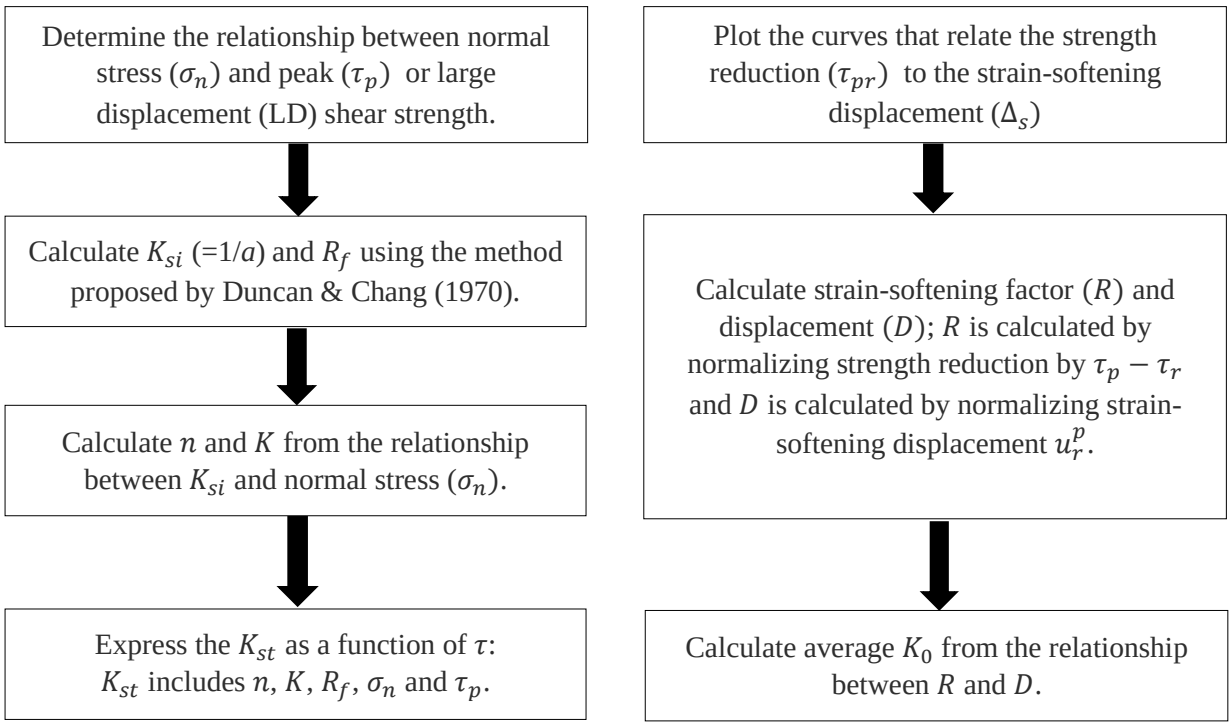

(a) Flow chart for pre-peak region

(b) Flow chart for post-peak region

Figure 2-18 Summary of procedures for interface modelling (adapted from Seo et al. (2003)).

2.4.3 Factors affecting Interface Shear Strength

The main objective of interface shear strength testing is to determine the peak and LD shear strength values at the boundary between one geosynthetic and another geosynthetic or soil. The interface shear strength of geosynthetics can be influenced by several factors and the most important of these are discussed below.

- ***Applied Normal Stress***

ASTM D5321 requires that at least three direct shear tests be performed under three different normal stresses to obtain the interface friction angle for the soil-geosynthetic or geosynthetic/geosynthetic interface. Using this data, both linear and non-linear relationships between the normal stress and the shear stress can be plotted, and the resulting slope will give the interface friction angle (see **Figure 2-12**). However, designers should be conservative when selecting the proper normal stress, based on the function of the application. For example, the normal stress applied to the landfill cap differs from the normal stress at the baseliner. Geosynthetics in bottom liner landfill systems are subjected to normal stress that is initially low and increases to a high value (as large as 1000 kPa or more) with time. Therefore, shear strength tests should be conducted for low, intermediate and high normal stress conditions in this case. On the other hand, geosynthetics placed in cover systems could be tested to low confining pressures due to these liners being subjected to low normal stress (approximately 10-25 kPa) that remains nearly constant after construction (Buthelezi, 2017; Fox & Stark, 2004)

- ***Shear displacement rate***

There are different views regarding the selection of the appropriate rate of shear displacement and its effect on the interface shear strength. Several studies, (i.e. Eid et al., 1999; Fox & Stark, 2004, 2015; McCartney et al., 2002), have demonstrated that the choice of the shear displacement rate affects the measured interface shear strength of geosynthetics. According to Eid et al. (1999), the peak and the residual shear strength of the soil-geomembrane interface do not change significantly due to the use of different shear displacement rates. Nevertheless, the rate of shear displacement affects peak strength more than residual strength, (Alzahrani, 2018; Jogi, 2005). Thus, depending on the interface being tested, the strain rate of the test should be slow enough to give results representative of long-term (slow) shear conditions. Different shearing rates have been used and recommended by previous researchers, (i.e. McCartney et al., 2002; Stark et al., 2015). However, shear rates of between 0.1 mm/min and 1.0 mm/min are usually utilized in geosynthetics interface testing, (Buthelezi et al., 2016; Sikwanda et al., 2018). With lower rates being applied for saturated conditions to permit dissipation of pore water pressures to prevent the existence of excess pore pressure at failure

- ***Hydration***

Consideration of hydration when performing interface shear strength testing of geosynthetics, particularly GCLs, is of utmost importance. GCL contains a material known as bentonite with swelling characteristics, as such stability consideration should be checked before its application in a landfill. This is because the shear strength of the GCL decreases when the bentonite is

hydrated (by rain or moisture from waste) and can affect the stability of the slope. Consequently, if hydration is anticipated in the field, as is usually the case, laboratory tests should be carried out under hydrated conditions to represent the least favorable environments, (Fox & Stark, 2004; Sikwanda, 2018). At the time of hydration, ASTM D6243 standards recommend that the hydration of the GCL test specimens should be carried out under the normal stress anticipated in the field. The standard does not provide the specific time for hydration, most production testing laboratories hydrate GCLs for 24 to 48 hours because if shearing occurs at the same normal stress a slight decrease in shear strength is expected. On the other hand, the geotextile/geomembrane interface test can be hydrated for an hour. The one hour is to allow sufficient time to engage the geotextile and geomembrane before shearing, (ASTM D6243, 2016; Fox & Stark, 2015; Sikwanda, 2018; Stark et al., 2015).

- ***Consolidation Time***

According to Jogi (2005), consolidation of the clay layer in the composite liner may take place under the imposed loads, and a substantial increase in the shear strength of the interface may occur during this consolidation. Consequently, when conducting interface shear testing, the immediate application of the normal stress (unconsolidated loading) would potentially simulate the relatively rapid placement of waste during landfilling operations. Hence, to model the long-term response of the liner, the clay must be allowed to consolidate under the imposed normal loads before the interface shear test is conducted. However, it should be noted that there is no guarantee and control over whether the clay will be fully consolidated or not during interface shear testing and various researchers have used varying consolidation time frames including 24 hours, 1 hour or less, (Fox & Stark, 2004; Jogi, 2005; Sikwanda, 2018).

- ***Specimen gripping systems***

When performing geosynthetic interface shear tests, a combination of the gripping surface and clamping devices to form a gripping system may be used to secure the test specimens to the lower and upper shear blocks of the DSA, (Sikwanda, Buthelezi, et al., 2018; Sikwanda, Kalumba, et al., 2018). Gripping surfaces are used during shearing to provide adequate resistance between the test samples and the shearing blocks, to prevent slipping of the specimens. This simulates the anticipated resistance of the field interface between two geosynthetics or geosynthetics and the adjacent material, (Kalumba, 1998; Sikwanda et al., 2020; Sikwanda, Kalumba, et al., 2018). The effect of insufficient gripping can result in inaccurate measurements of shear stress–displacement behaviour and strength mainly by reducing peak (but not residual) shear strength and increasing the displacement at peak strength achieved, (Buthelezi, 2017; Fox & Stark, 2004).

Several authors have demonstrated success using a variety of different gripping surfaces, i.e. (Bacas et al., 2015; Fox & Stark, 2004; Sikwanda, Kalumba, et al., 2018; Triplett & Fox, 2001). Examples of gripping surfaces used include textured steel plates, nail plates, adhesive glue bonding, and sandpapers (see **Figure 2-19**). The ASTM standards currently state that the textured surface and flat jaw-like clamping device are normally sufficient, but work is still ongoing to define the best type and textured surfaces that can be used to minimize or eliminate the errors associated with the gripping of the specimen, (ASTM D5321, 2017; ASTM D6243, 2018).

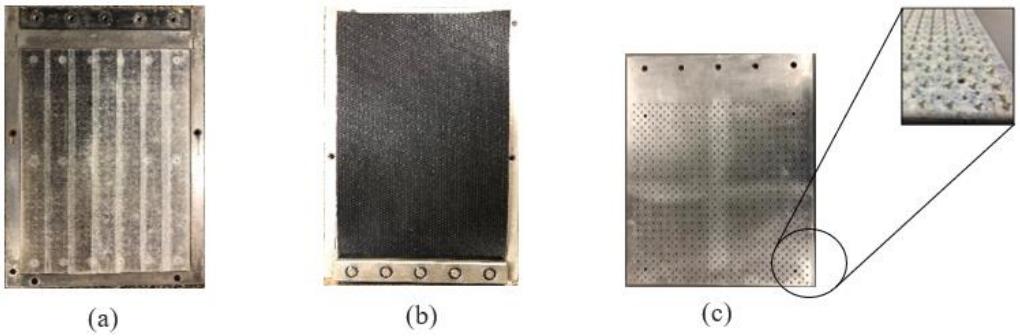

Figure 2-19 Gripping mechanisms used: (a) sandpaper, (b) clamping device and (c) nail plate.

However, a combination of clamping devices and sandpaper was used for the gripping surface in this study during direct shear testing. The clamping devices used are manufactured together with the *ShearTrac-III* large direct shear apparatus, and the sandpaper can be installed to provide slip resistance in dry, wet, or oily conditions, making it suitable for use even in saturated conditions.

2.4.4 Multi-layer Interface Tests

Composite landfill liner systems consist of multiple geosynthetic interfaces. An important feature of these composite liner systems, in terms of slope stability, is the shear resistance available along with the different component interfaces and the internal shear strength of each component. According to Stark et al. (2011), to date, substantial investigations on the shear behaviour of geosynthetic interfaces have been carried out using single interface tests (**Figure 2-20**) but there have been limited studies published on comparisons between single interface and multi-layer interface shear tests (**Figure 2-21**).

Stark et al. (2015) stated that comparing results from multi-layer interface tests with results from at least one single interface test, such as the critical interface for a given normal stress, is beneficial since there are fewer variables involved in single-interface testing compared to multi-interface testing. Multi-layer interface tests are becoming more prevalent in laboratory testing and the design of composite liner systems. The advantages and disadvantages of multi-layer interface tests over single interface tests are briefly discussed below.

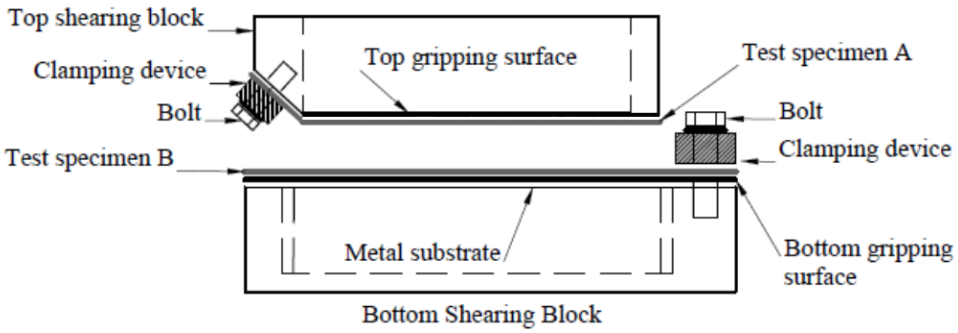

Figure 2-20 Schematic diagram of single interface shear test configuration.(after Sikwanda, 2018)

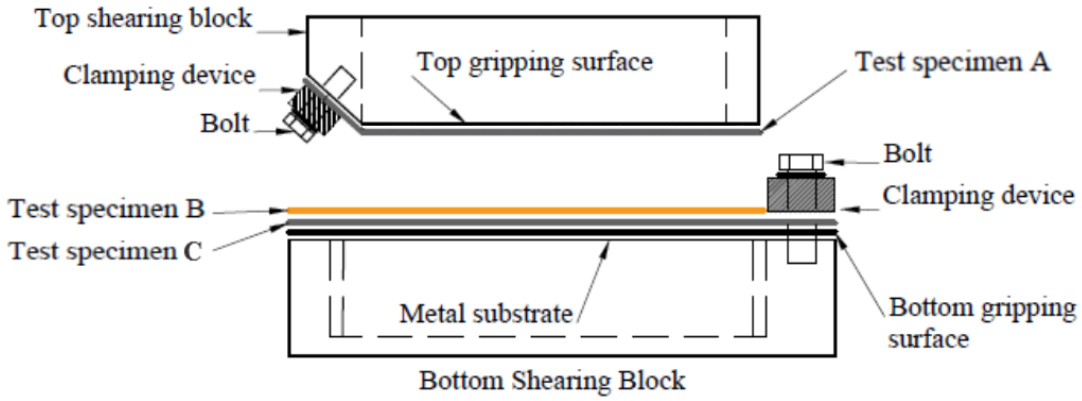

Figure 2-21 Schematic diagram of multi-layer interface shear test configuration. (after Sikwanda, 2018)

2.4.4.1 Advantages of Multi-layer Interface Tests

In single interface tests, the failure surface is forced to occur along with a specific geosynthetic interface that is not a true representation of the field condition, (Stark et al., 2015). This is because in a composite liner system, shear movement in the field can occur on more than one interface plane. These limitations, however, can be captured in multi-layer interface tests, where interfaces are tested simultaneously and allow failure to occur along with the weakest interface as anticipated in the field, (Stark & Choi, 2004).

Multi-layer interface shear testing can reduce the amount of testing, and the time needed to test and design by simultaneously testing multiple interfaces and materials which are part of the liner system. Also, Stark & Choi (2004) described the possibility of using multi-layer interface tests to determine peak and large displacement (LD) design strengths envelopes, rather than developing combination peak and LD failure envelopes from the results of several single interface tests (Stark et al., 2011).

2.4.4.2 Disadvantages of Multi-layer Interface Tests

Multi-layer interface tests have a limitation in that the strength parameters obtained are only for the critical failure surface of the system being tested, and no other interface. The combination failure envelope obtained in multi-layer interface tests does not show how close other materials are to failure (Rouncivell, 2007; Stark et al., 2015). The results of single interface testing can be used to develop envelopes of peak and LD strength for the appropriate range of normal stresses for each test interface. Multi-layer interface tests, however, only provide envelopes of peak and LD strength for the critical fault surface of the system identified at each normal stress (Fox & Stark, 2004). Besides, multi-layer interface tests are difficult to set up, execute, and interpret. As a result, to avoid errors and erroneous assumptions, it is necessary for design engineers and testing laboratories to be experienced in specifying and performing these tests, respectively, (Stark & Choi, 2004).

2.4.5 Review of previous research

To understand the shear response of an entire landfill geosynthetic liner system, Sikwanda et al. (2019), developed an approach to compare the shear strength between single and multi-interface test configurations, as can be seen in **Figure 2-22**, using a 305 mm x 305 mm large direct shear test. The multi-layer interface test allowed multiple interfaces and materials to be tested. To replicate the landfill interface conditions, Sikwanda et al. (2019) utilized three geosynthetics that are commonly used in landfill liners, namely GTX, GMB and GCLs. The interface testing was carried out at five normal stresses, i.e. 50, 100, 200, 295 and 400 kPa. **Figure 2-23** shows the curves obtained after testing. From the plots, it was evident that the rate of the shear stress development increased with increasing shear displacement until reaching the maximum/peak interface shear strength, regardless of the test configuration utilised. Previous studies, (Adeleke et al., 2019; Bacas et al., 2015, 2011; Buthelezi, 2017), observed similar patterns in the shear stress curves as those obtained by Sikwanda et al. (2019).

Moreover, a relation between the clamping device and the higher peak and LD strength values was observed. According to ASTM D5243/6243, clamping devices provide enough shear resistance to prevent non-uniform displacement of the tested geosynthetics. The two specimens in single-interface tests were each confined to one end of the shear block during shearing (see **Figure 2-22** (a)), while only the top and bottom specimens were clamped in multi-layer interface tests, leaving the two middle test specimens unconfined (see **Figure 2-22** (b)). Also, in both single and multi-layer interface tests, a nail plate and sandpaper were used as the top and lower gripping surfaces respectively, as can be seen in **Figure 2-22**. As a result, failure of the specimen tested, using a single interface, occurred at a pre-determined interface as the test samples were fixed to the shear blocks, (Fox & Stark, 2004). In multi-layer interface tests, the test samples were able to slip between each interface, and failure could have occurred at any of the interfaces available depending on which plane was the weakest. This represented a better field configuration simulation for a composite liner system, where multiple layers of geosynthetics are installed as stated by Stark et al. (2015).

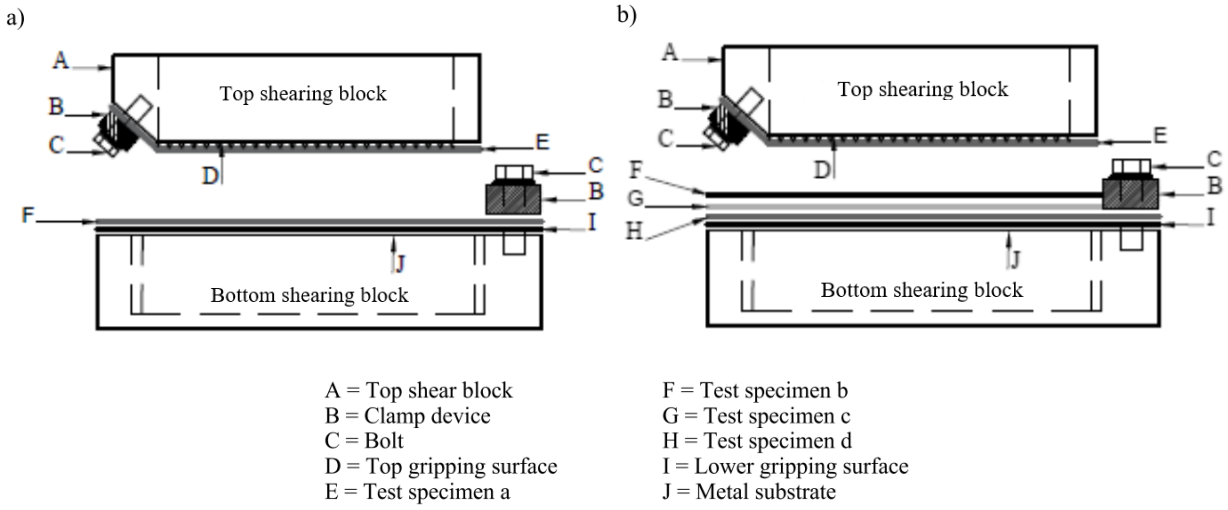

Figure 2-22 Test specimen configuration: a) single interface and b) multi-layer interface test, (adapted from Sikwanda et al., 2019)

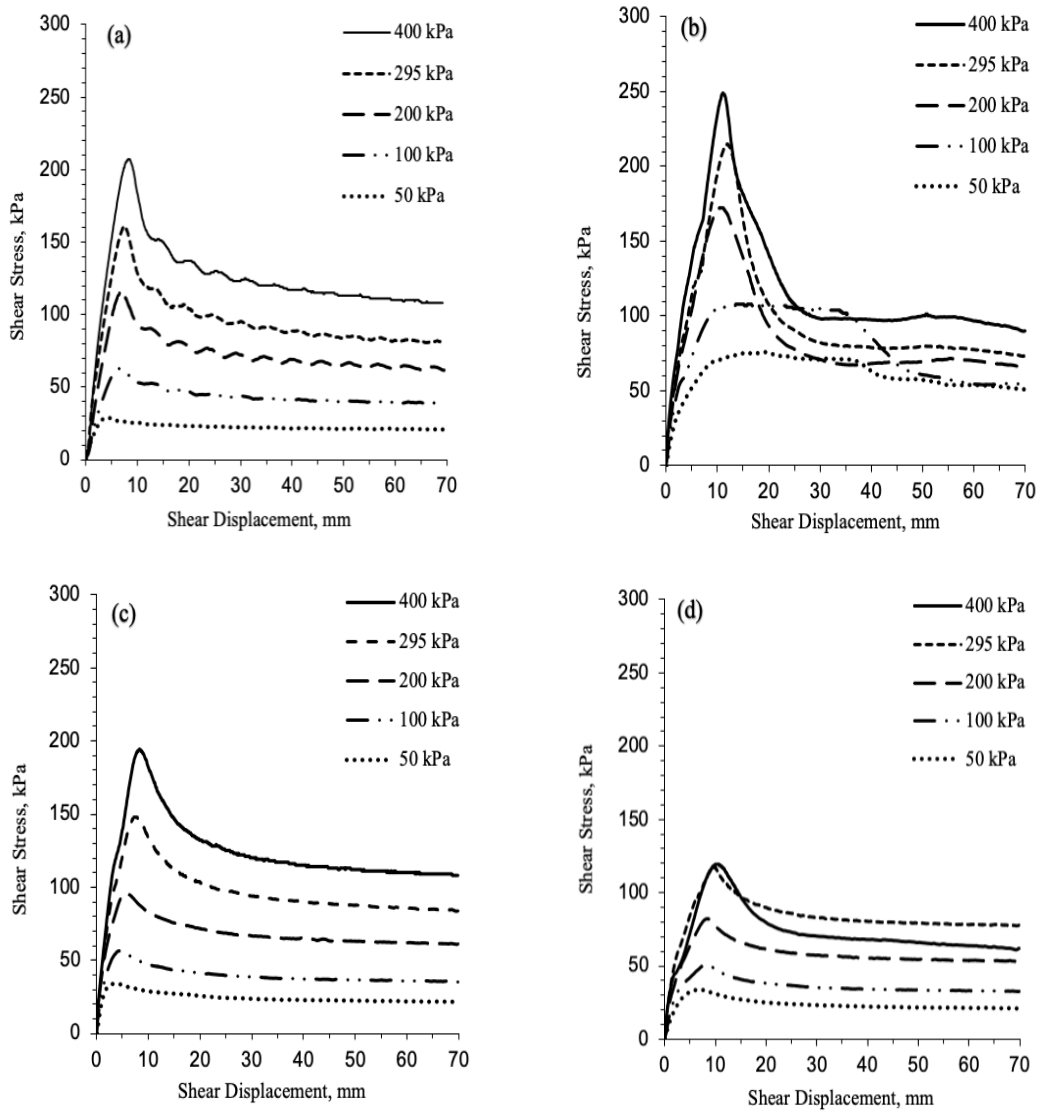

Figure 2-23 Showing shear stress-displacement results: (a) to (c) single interface tests and (d) multi-layer interface test. (after Sikwanda et al., 2019)

Also, as can be seen in **Table 2-4**, Sikwanda et al. (2019) compiled a summary of the peak and LD strength values obtained from both single and multi-layer interface tests. At all normal stress, except 50 kPa, higher peak and LD strength values were observed from single-interface tests than multi-layer interface tests. With an increase in normal stress applied, this dissimilarity in shear stresses increased, thus indicating that the shear strength is also dependent on stress. Therefore, the results obtained by Sikwanda et al. (2019) concluded that, the use of multi-layer interface shear tests can lead to an underestimate of the peak and LD strength. This observation was found to be consistent with the findings of previous researchers, (i.e. Eid & Stark, (1997)), who reported that single interface testing has a disadvantage of overestimating the interface shear resistance of some geosynthetics, (Stark et al., 2011). This was, however, in contrast with the findings of Stark et al. (2015).

Table 2-4 Summary of the peak and LD strength values. (adapted from Sikwanda et al., 2019)

Normal Stress σ_n	Single-interface						Multi-interface	
	GTX-A/GMB		GMB/GCL		GCL/GTX-B		GTX-A/GMB/GCL/GTX-B	
	Peak (kPa)	LD (kPa)	Peak (kPa)	LD (kPa)	Peak (kPa)	LD (kPa)	Peak (kPa)	LD (kPa)
50 kPa	29	20.6	75.8	51	33.9	21.5	33.4	20.9
100 kPa	63	39.2	108	54.8	56.3	35.3	50.7	32.9
200 kPa	116	61.6	172	66	95.8	61.2	82.6	53.5
295 kPa	161	81.4	215	73	148	83.9	118	72.5
400 kPa	207	108	249	89.8	194	108	119	61

In a similar study, Stark et al. (2015) presented a comparison of strength envelopes from single- and multi-interface strength tests for a proposed landfill liner system configuration (see **Figure 2-24**). Peak and LD combination strength envelopes from single and multi-interface direct shear tests for the same geosynthetic/geosynthetic and soil/geosynthetic interfaces were compared. Likewise, the interface shear test was performed at five normal stresses, i.e. 70, 170, 690, 1380, and 2070 kPa, using a 300 mm × 300 mm LDSA. To better define the stress-dependent nature of the strength envelopes at low effective normal stresses, the test program included low normal stress of 70 and 170 kPa. All interface shear tests were limited to shear displacements of about 75 mm. If the constant minimum strength was reached before 75 mm, the resulting strengths were referred to as LD strengths and not residual strengths, (Stark & Choi, 2004).

Four test series were carried out for single-interface testing, while two test series were conducted for multi-layer interface testing. **Figure 2-25** shows the schematic diagrams of the setup of both single and multi-layer interface test configurations as conducted by Stark et al. (2015). It can be observed that in single interface testing, a clamping device was also used as a gripping system to confine the geosynthetic specimen to one end of the shear block (see **Figure 2-25**). This approach is similar to that of Sikwanda et al. (2019). In addition, due to the GCL being encapsulated by two geomembranes, GCL hydration in the multi-layer interface test was a challenge. Therefore, four small holes of 6.35 mm in diameter were drilled through the primary and secondary geomembranes to facilitate hydration of the GCL to simulate the worst-case scenario for defects in the geomembranes during installation (see **Figure 2-25**(b)). This allowed the inner portion of the GCL as well as the edges to be hydrated without removing, from both geomembranes, a significant amount of the textured surface.

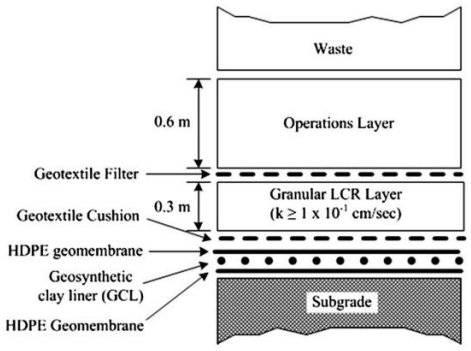

Figure 2-24 Proposed landfill liner system configuration. (after Stark et al., 2015)

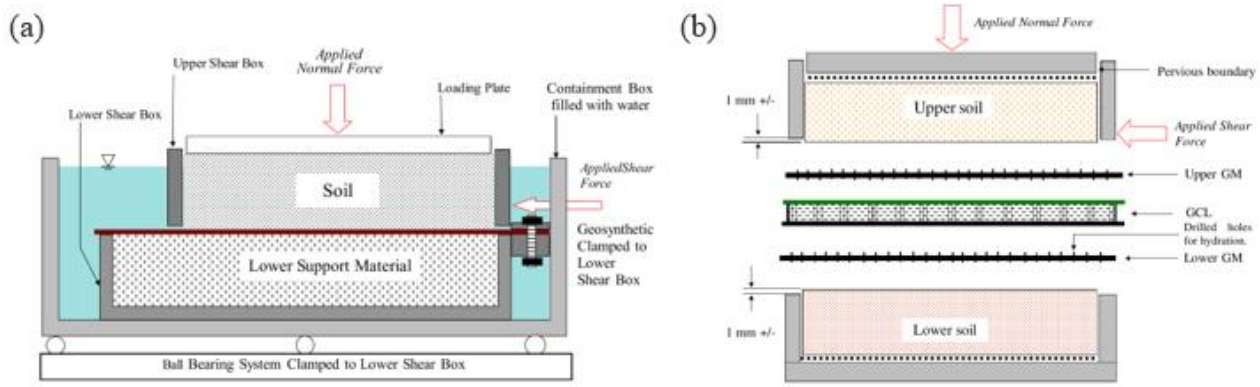

Figure 2-25 Schematic diagram of laboratory direct shear test configuration: (a) single interface and (b) multi-layer interface with five layers, (after Stark et al., 2015).

From the plots in **Figure 2-26**, it is evident that the rate of development of shear stress increased with increasing shear displacement up to the maximum/peak shear strength of the interface, regardless of the test configuration used. This is similar to observations made by Sikwanda et al. (2019). The shear strengths (peak and LD) of both single and multi-layer interface tests were comparable for lower normal stresses (170 and 690 kPa). However, multi-layer interface testing resulted in higher peak and LD strengths for higher normal stresses (1380 and 2070 kPa) than the single interface tests. These curves are similar to those from a study by Sikwanda et al. (2019), as previously shown in **Figure 2-23**.

Peak and LD combination strength envelopes were obtained from GMX/GCL/HDPE (hydrated), GMX/GCL (pre-wetted), GTX/GMX (pre-wetted), and GMX/subgrade (pre-wetted), for single interface tests. These peaks and LD combination strength envelopes were compared to those obtained from GMX/GCL/GMX/Subgrade (un-hydrated & hydrated) for multi-layer interface tests, as can be seen in **Figure 2-27**. This comparison was appropriate because the above combinations involve all the interfaces/materials that were tested for the respective liner system in the two multi-layer interface tests.

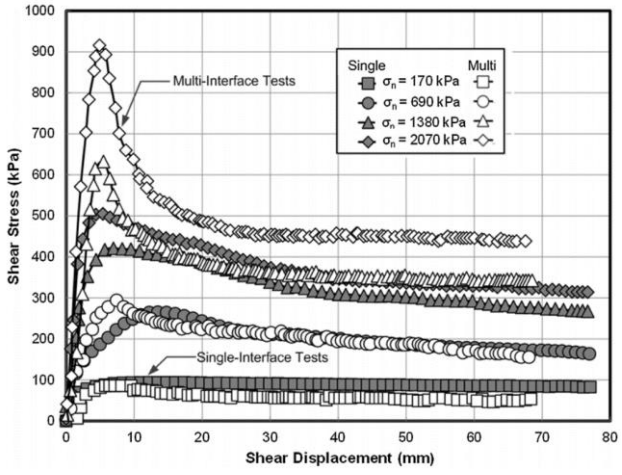

Figure 2-26 Shear stress vs shear displacement relationship for single and multi-layer interface tests involving GM-X textured HDPE geomembrane. (after Stark et al., 2015)

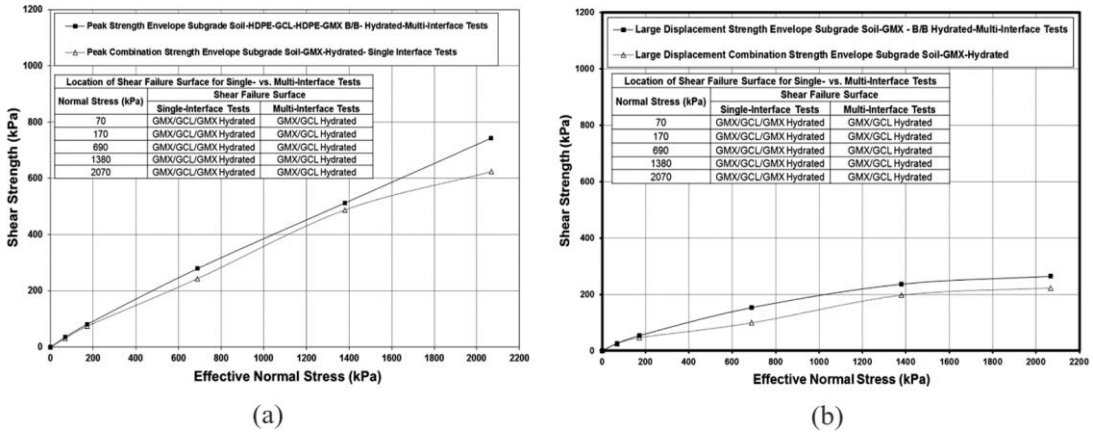

Figure 2-27 Peak and LD combination strength envelopes from: (a) single interface and (b) multi-layer interface, respectively. (after Stark et al., 2015)

It can be observed from **Figure 2-27**(a) that the critical interface is the same for both test methods, i.e., GMX/GCL (Hydrated), for the range of normal stresses considered. However, at high normal stresses the peak strength is slightly lower for single interface tests. These differences might have resulted from these tests being conducted in isolation and not influenced by surrounding geosynthetics, such as geonets embedded in multiple geosynthetics. Moreover, as can be seen in **Figure 2-27**(b), higher LD strengths were obtained from multi-layer interface tests than for single interface tests. This is consistent with higher peak strengths in the multi-layer interface tests shown in **Figure 2-27**(a). The consistency may be due to differences in shear displacement between single and multi-layer interface tests on the critical interface.

Single interface testing appears to have generally provided somewhat underestimated peak and LD strength values than multi-layer interface testing, which is consistent with previously published data in Triplett & Fox (2001). This observation, however, was found to be inconsistent with findings in Sikwanda et al. (2019). The reason for this inconsistency could be the difference in the test procedures that were followed in each study, i.e. clamping of the geosynthetics. In the study by Sikwanda et al. (2019), the two specimens in single interface testing were each clamped and confined to one end of the shear block during shearing. However, in this study the two specimens were not clamped during single interface testing, but rather adhered to a rigid substrate. This is a mini-spiked steel plate placed either in the lower half of the shear box, or both, depending on the type of test performed, i.e. geosynthetic/geosynthetic or soil/geosynthetic interface. Thus, the lower LD strengths observed in single interfaces were probably caused by the rigid clamping of the geosynthetics, which resulted in some tensile strains in the geosynthetics.

Furthermore, in another study, Khilnani et al. (2017) compared single and multiple geosynthetic interface shear strength tests conducted on soil/geosynthetic and geosynthetic/geosynthetic interfaces, for both side-slope and baseliner systems of a landfill expansion project as shown in. Three single series of interface strength tests (i.e. GCL/ Foundation Layer soil (FLS), GM/GCL & GM/GC) was performed before acceptance of geosynthetic materials to verify compliance with design strengths.

Additionally, two multi-layer interface test series (i.e. Gravel/GM/GCL/FLS & Operations Soil/GC/GM/GCL/FLS) were conducted to confirm the single interface test results. These tests were performed following test procedures specified in ASTM D5321 and D6243. **Table 2-5** shows a summary of the peak and post-peak strength test results for the three single and two multi-layer interface test series. These results were then plotted to evaluate the minimum interface strength envelope for side and baseliner systems.

The side-slope liner interface test results are shown in **Figure 2-28**. From **Figure 2-28**(a), the GM/GC interface (series 3) was found to be the weakest or critical interface from single interface testing. The multi-layer interface test (series 5) confirmed this, showing that shear displacement occurred along the GM/GC interface for all the normal stresses tested. Moreover, the multi-layer interface test (series 5) essentially yielded the same peak strength envelope as the single interface tests (series 5), which is consistent with similar findings in Stark et al. (2015). This consistency between single and multi-layer interface testing confirmed that the GM/GC interface was the critical interface for the tested side-slope liner system materials and was used to create the post-peak strength envelope, as shown in **Figure 2-28**(b).

From **Figure 2-28**(b), it was observed that for normal stress greater than 239.4 kPa, the post-peak strength envelope for GM/GC was higher than the GCL/FLS interface. However, it was suggested that the GCL/FLS post-peak strength envelope should not be used for side-slope design. This is because the GM/GC interface would fail before the GCL/FLS interface fails, leading to post-peak condition development along the GCL/FLS interface before the GM/GC fails, as Stark & Choi (2004) described it. The GCL/FLS post-peak strength envelope decreased in strength with increasing normal stress (383.2 kPa). Likewise, the GM/GCL post-peak strength envelope also decreased in strength at the highest normal stress (574.8 kPa). This was due to the GCL failing internally and the measured strengths corresponding to the shear resistance provided by the bentonite in the GCL (see **Figure 2-28**(b)). As a result, it was suggested that the GCL/FLS interface strength envelope should not be used for side-slope liner design because it would be overly conservative, as described by Stark & Choi (2004).

Table 2-5 Summary of single and multi-layer interface test results (adapted from (Khilnani et al., 2017).

Normal Stress σ_n	Single-interface						Multi-interface			
	Series 1 GCL/FLS		**Series 2** GM/GCL		**Series 3** GM/GC		**Series 4** Gravel/GM/GCL/FLS		**Series 5** Operations Soil/GC/GM/GCL/FLS	
	Peak (kPa)	Post-Peak (kPa)	Peak (kPa)	Post-Peak (kPa)	Peak (kPa)	Post-Peak (kPa)	Peak (kPa)	Post-Peak (kPa)	Peak (kPa)	Post-Peak (kPa)
0	0	0	0	0	0	0	0	0	0	0
47.9	36.3	31.1	34.5	21.4	28.7	17.9	32.2	25.7	30	17.5
191.6	132.4	112.8	114.7	77.9	107.1	55.3	114.3	73.2	101.9	54.4
287.4	171.6	29.5	167.1	94.7	144.3	70.8	165.1	86.8	142.2	70.2
383.2	220.1	37.9	215.8	112.8	181.7	83.1	205.6	105.1	179.2	81.3
574.8	274.2	46.4	271.5	77.1	251.1	109.2	285.9	114.5	252.4	111.2
574.8	340.2	57.3	N/A	N/A	N/A	N/A	262.3	75.5	N/A	N/A

Table 2-6 Summary of single and multi-layer interface tests by several authors.

Author	Shear device size (mm)	Shear rate (mm/min)	Normal Stress (kPa)	Horizontal Displacement (mm)	Characteristics of Geosynthetics		Interface tested	Peak		LD	
								δ_p (°)	$c_{a\text{-}p}$ (kPa)	δ_{LD} (°)	$c_{a\text{-}LD}$ (kPa)
Sikwanda et al. (2019)	305 x 305	0.1 & 1.0	50 - 400	70	GTX-A	Bidim A10	GTX-A/GMB	26.7	9.9	13.5	11.9
					GMB	DST GMB	GMB/GCL	26.6	59.2	6.2	44.4
					GCL	Envirofix X800	GCL/GTX-B	24.6	9.3	13.9	10.4
					GTX-B	F-25 SA	GTX-A/GMB/GCL/GTX-B	14.7	25.9	7.4	21.1
Shenthan et al. (2019)	300 x 300	0.1 & 1.0	100 - 1500	75	GMB	Double-side textured (DST)	GMB/GCL/GMB	-	-	-	-
					GCL	Encapsulated between Two NW GTX & needle-punched	GMB/GCL/Subgrade	-	-	-	-
					GTX	Non-woven	GMB/CSL	-	-	-	-
					GC	Drainage Geocomposite	GMB/GCL/GTX or GC	-	-	-	-
Khilnani et al. (2017)	Not reported	Not reported	47.9 - 574.8	Not reported	GCL	Needle-punched & reinforced	GCL/FLS	24.1	34.3	1.7	26.5
							GMB/GCL	24.4	25.7	6.0	45.4
					GC	Drainage Geocomposite	GMB/GC	22.6	19.1	9.5	17.3
					GMB	Double-side textured (DST)	Gravel/GMB/GCL/FLS	25.6	18.6	9.3	32.3
							Operations Soil/GC/GMB/GCL/FLS	22.7	17.0	9.8	15.9
Stark et al. (2015)	300 × 300	1.0	170 - 2070	75	GTX	410 g/m^2 cushion	GTX/GMB	-	-	-	-
							GMB/GCL/GMB (Unhydrated)	-	-	-	-
					GMB	1.5 mm Double-side textured (DST)	GMB/GCL/GMB (Hydrated)	-	-	-	-
							GMB/Subgrade soil	-	-	-	-
					GCL	Needle-punched & reinforced	GTX/GMB/GCL/GMB/Subgrade soil (Unhydrated)	-	-	-	-
							GTX/GMB/GCL/GMB/Subgrade soil (Hydrated)	-	-	-	-

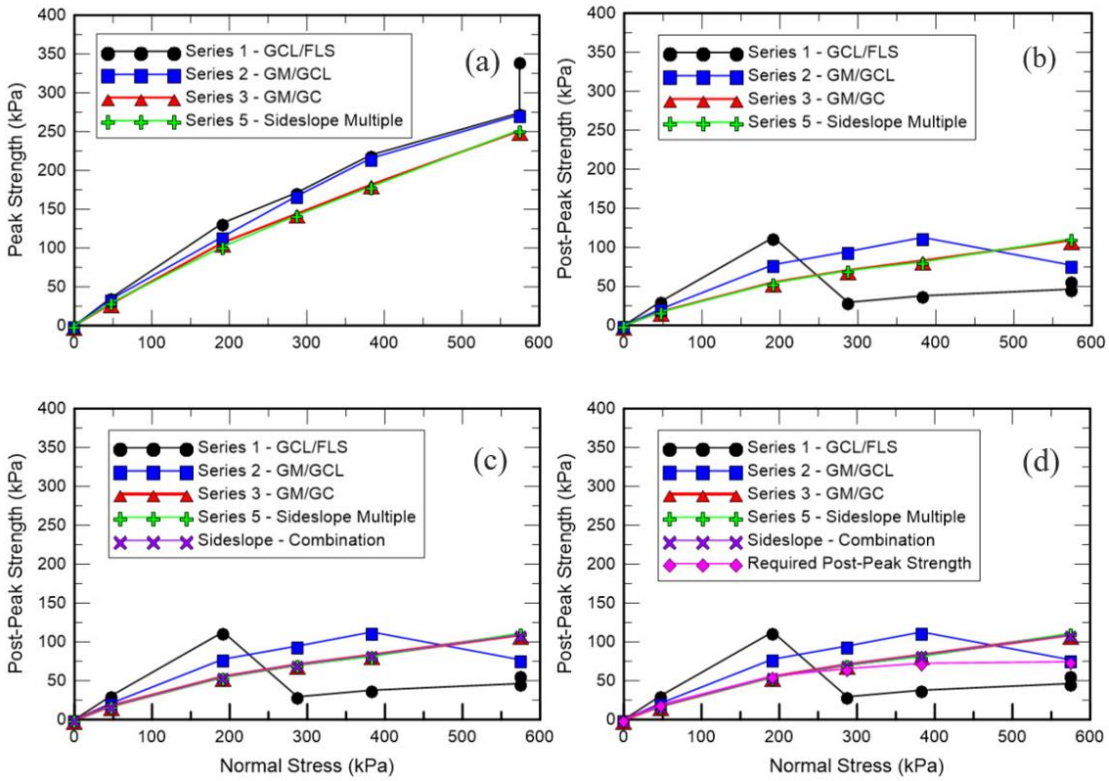

Figure 2-28 Side-slope liner system: (a) peak strengths, (b) post-peak strengths, (c) combination post-peak strength envelope, and (d) comparison of combination post-peak strength envelope and design required post-peak strengths. (after Khilnani et al. (2017).

The combination post-peak strength envelope for the side-slope liner system was shown in **Figure 2-28**(c). This curve coincided with the post-peak strength envelope for the GM/GC interface because sliding occurred along with this interface for all the normal stresses tested in the single and multi-layer interface tests. Stark & Choi (2004) described that the combined strength envelope would also change interfaces if the critical interface changes with increasing normal stress, but this was not the case for this testing. The GM/GC post-peak strengths for the side-slope liner system met or exceeded the project specified post-peak strength envelope, as can be seen in **Figure 2-28**(d). Therefore, Khilnani et al. (2017) concluded that the critical interface for the side-slope liner system materials tested was the GM/GC interface.

The peak interface strengths results are shown in **Figure 2-29**(a) for single interface tests (series 1 & 2), for the baseliner system. In this case, test series 3 was not relevant, since there was no GC layer in the baseliner system. Additionally, the multi-layer interface test results (series 4) base liner system were included for comparison purposes. From **Figure 2-29**(a), it can be observed that the interface strengths for test Series 1 and 2 are not significantly different. It was therefore beneficial that a multi-layer interface test was carried out using materials from the baseliner system to further investigate the shear behaviour of the baseliner system. Single and multi-layer interface tests yielded similar peak strengths in line with Stark et al. (2015). It was therefore confirmed that the critical interface for the baseliner system is the materials tested in the GM/GCL interface.

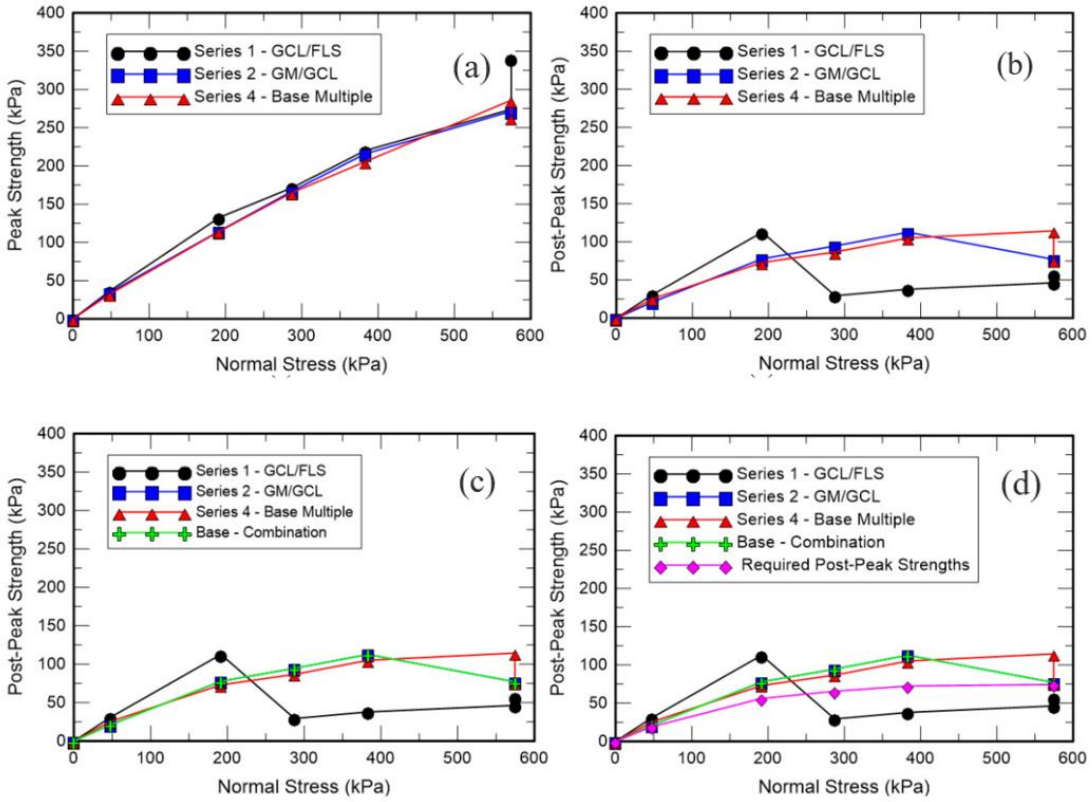

Figure 2-29 Base liner system: (a) peak strengths, (b) post-peak strengths, (c) combination post-peak strength envelope, and (d) comparison of combination post-peak strength envelope and design required post-peak strengths. (after Khilnani et al. (2017).

2.5 Summary of the Literature Review

2.5.1 Key Points

The literature review presented above focused on the topics that were relevant to this research. The key points from the reviewed studies are summarized below:

1. Many devices had been adopted for interface shear testing. A review of past literature, however, demonstrated that the LDSA was the most popularly used testing apparatus in laboratories to measure the shear strength of geosynthetic-geosynthetic or soil-geosynthetic interfaces. This was because of its relatively simple procedures and its ability to test large specimens at the largest possible range of normal stresses.

2. Modelling the interface shear stress-shear displacement behaviour along with an interface that exhibits strain-softening behaviour was complex. From past literature, however, a new constitutive interface model combining a nonlinear hyperbolic model with a displacement-softening model was proposed. This model described the nonlinear strain-softening behaviour of the geosynthetic interfaces. This modelling was performed by

dividing the entire shear stress versus displacement graph into three regions, pre-peak region, strain-softening region and residual region.

3. The review of past studies demonstrated that when a 300 mm x 300 mm LDSA device is used for interface testing, the residual shear strength condition may, in some cases, not be defined due to its limited shear stress displacement. Therefore, a residual shear strength condition reached after the strain-softening was referred to as the to "post-peak" or "large displacement" (LD) shear strength,

4. The interface shear strength of geosynthetics can be influenced by several factors, namely; applied normal stress, shear displacement rate, hydration, consolidation time, and gripping systems. In terms of shearing rate, it was recommended that interface tests containing GCL be sheared at a maximum displacement rate of 1 mm/min or 0.1 mm/min if the failure occurs within a hydrated GCL. Also, hydration of GCLs for 24 to 48 hours was recommended before testing.

5. The determination of interface shear strength using a LDSA can be achieved by using two approaches, namely; single and multi-layer interface shear testing. Comparative studies were needed to assess the viability of a multi-layer interface test in understanding the shear interface in composite liner systems. Hence, multi-layer interface test results should be compared to at least one single interface test, such as the critical interface for a given normal stress.

6. While some studies had stated that single interface testing underestimates peak and LD strength values compared to multi-layer interface testing, the opposite had been found by other studies. One reason for this incoherence was the difference in the test procedures that each study followed.

7. Further research was therefore required to better understand the shear behaviour of both single and multi-layer interface tests using experimental data from LDSA.

2.5.2 Gaps in Knowledge

From the literature reviewed, it was found that many experimental studies have used single interface experiments to examine the shear behaviour of soil and geosynthetic materials and interfaces. Just a few experimental studies have used a multi-layer interface testing configuration to investigate shear tests of soil/geosynthetics and geosynthetics/geosynthetics interfaces. Also, in a multi-linear failure envelope, little research has been done to determine the critical confining stress under which the linear failure envelope becomes non-linear. This encouraged further research to better understand the mechanical behaviour of both soil and geosynthetic interfaces when tested using multi-layer interface configurations. The purpose of this research project is to fill in these knowledge gaps and possibly provide new insights.

3 RESEARCH MATERIALS AND METHODOLOGY

3.1 Introduction

This chapter provides an overview of the experimental procedures, research materials, testing equipment and methodological approach followed to achieve the objectives of this research. In this study, three different types of geosynthetics, i.e. geotextiles (GTX), geomembranes (GMB), and geosynthetic clay liner (GCL), constitute the critical interface components of a lining system in a modern landfill liner and two soils were used.

The physical properties of the three geosynthetics were obtained from their respective manufacturer's handbooks (Kaytech Engineered Fabrics & AKS Lining Systems). A summary of those properties was presented in section 3.2. To fully understand the nature of both soil materials, mechanical tests were carried out and results were briefly discussed in section 3.2. A 305 mm x 305 mm large direct shear device was used to measure the interface shear parameters at these critical interfaces, as recommended by internationally recognized standards, (ASTM D5321, 2017; ASTM D6243, 2018). The procedures followed were briefly described in section 3.4. Finally, the chapter was concluded with a summary of the test program and the measures adopted to ensure consistency of the results.

3.2 Research Materials

3.2.1 Mechanical properties of selected soil materials

Two types of soils were selected for this study: *river sand* and *clay*. The river sand was brownish, whereas the silty sand was reddish-brown (see **Figure 3-1**) and both these soils were sourced from Durban, South Africa. The soils were selected due to their availability and significant presence in Durban. The river sand was clean and easy to work with, thus making it possible for the results to be repeatable. On the other hand, the clay was consistent and easily controllable, which enabled repeatability of results. The mechanical properties of both soils were determined by performing standard tests in the Geotechnical Laboratory of the Department of Civil Engineering, University of Cape Town. **Table 3-1** presents the various tests which were conducted along with the standards utilized.

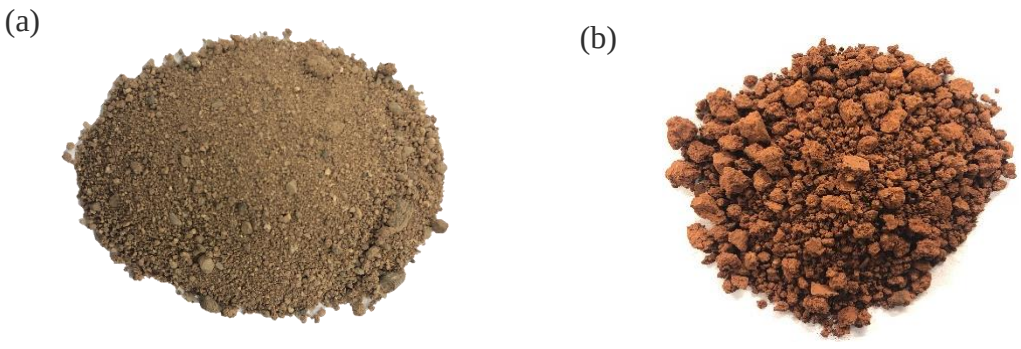

Figure 3-1 Selected soil materials: (a) river sand and (b) clay

Table 3-1 Test methods for soil classification.

Test Performed	Test Methods	Standards
Grain size distribution Test	Dry sieving	BS 1377: Part 2: 1990
	Wet sieving	BS 1377: Part 2: 1990
	Hydrometer	BS 1377: Part 2: 1990
Atterberg Limits Test	Casagrande	BS 1377: Part 2: 1990
	Plastic Limit	BS 1377: Part 2: 1990
	Linear shrinkage	BS 1377: Part 2: 1990
Specific Gravity Test	Small pyknometer	BS 1377: Part 2: 1990
Compaction Test	Standard Proctor	BS 1377: Part 4: 1990
Direct Shear Test	Small Direct Shear box	BS 1377: Part 7: 1990

The tests conducted on the two soils were in accordance with the British Standard (BS). To assess their mechanical and physical properties, the characterisation of the soil materials was carried out and the Unified Soil Classification System (USCS) was used to classify the soils. Some of the properties were considered significant in the preparation of soil samples while others were useful in the interpretation of the results.

Sieve analysis results for both soils are presented in **Figure 3-2**. From the curve, the river sand comprised of 99.2 % sand and 0.8 % fines (passing the 0.075 mm sieve). It had a coefficient of uniformity of 2.4 and a coefficient of curvature of 1.2. According to the Unified Soil Classification Systems (USCS), the soil was classified as a poorly graded sand (SP) with soil particles ranging from 3.350 mm to 0.075 mm. The clay had a liquid limit of 47.7 %, a plastic limit of 17.5 % and a plasticity index of 30.2 %. According to the Unified Soil Classification Systems (USCS), the soil was classified as lean clay with sand (CL).

Additionally, the dry density/optimum moisture content relationships of the two research soils were obtained in accordance with the standard proctor test procedure. The two curves obtained were then fitted (dashed lines) on a characteristic-compaction-curves for typical soils (solid lines) published by Head (2006), as shown in **Figure 3-3**. The river sand results showed it had two distinct peaks of density at two optimum moisture content. This was found to be similar to the double peak obtained by Head (2006) for the fine uniform sand compaction curve and by a study done by Kalumba (1998) for the cape flats sand. To select an appropriate density for the river sand to be used in the direct shear tests to be performed, it was decided to compact the sand to the higher of the two optimum moisture content obtained. On the other hand, as can be seen in **Figure 3-3**, the clay showed a density peak similar to that of heavy clay.

A summary of the results obtained from the characterisation tests is presented in **Table 3-2**. The detailed data are presented in **Appendix A** for both river sand and clay.

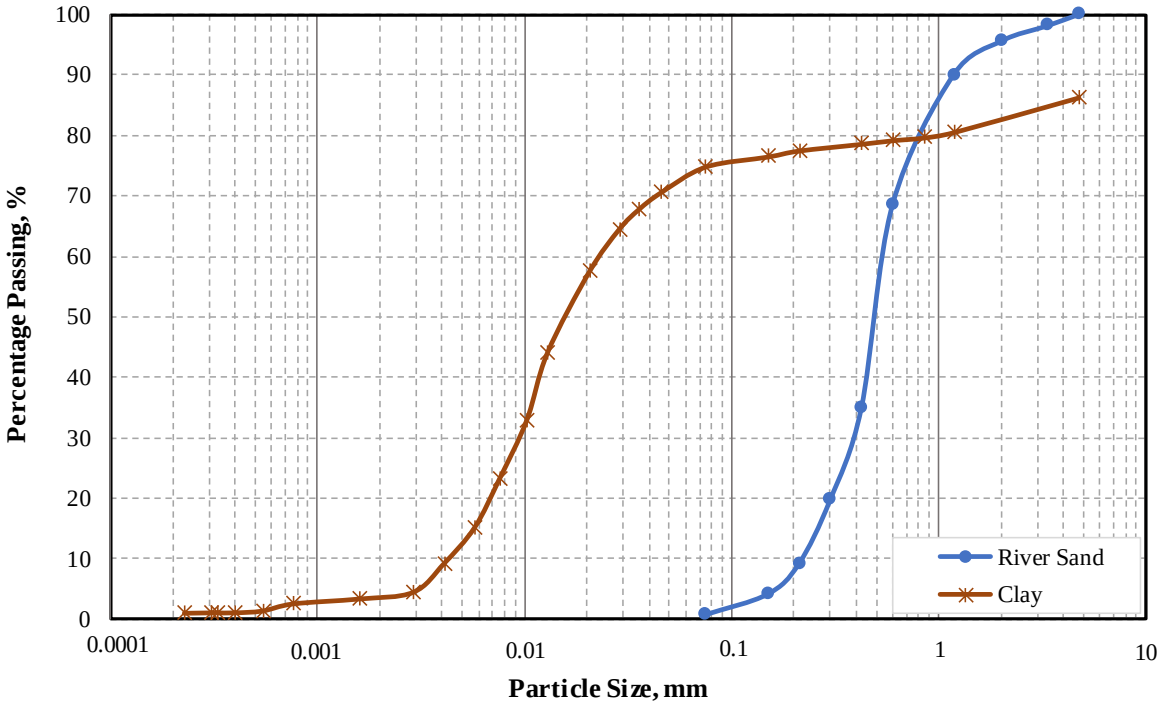

Figure 3-2 Grain size distribution of river sand and clay.

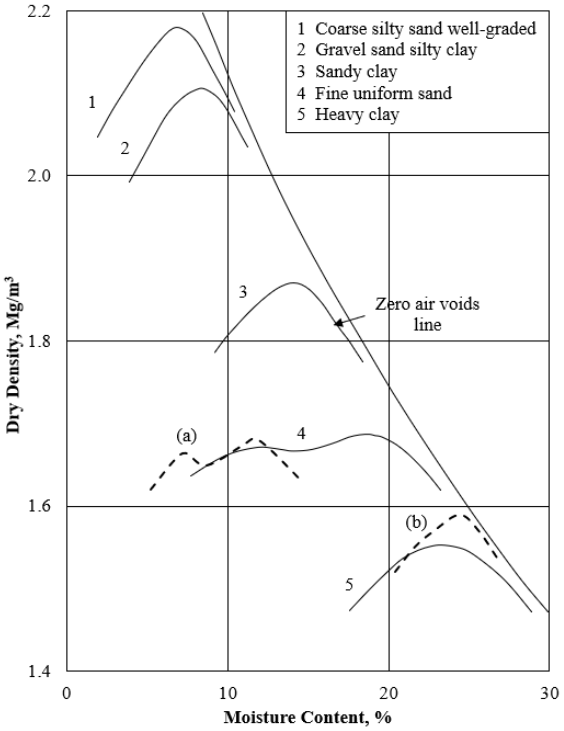

Figure 3-3 Compaction curves (after Head, 2006) and results for: (a) river sand and (b) clay.

Table 3-2 Soil mechanical properties of red clay and river sand.

Properties	Units	River sand	Clay
Specific Gravity, G_s	-	2.6	2.8
Cohesion, c'	kPa	0	20.9
Angle of Internal Friction, ϕ'	Degrees	43	38.7
Optimum Moisture Content, *OMC*	%	11.5	24.3
Maximum Dry Density, *MDD*	Mg/m^3	1.7	1.6
Particle size range	mm	0.063 - 3.35	-
Coefficient of uniformity, C_u	-	2.4	-
Coefficient of curvature, C_c	-	1.2	-
Liquid Limit, *LL*	%	-	47.7
Plastic Limit, *PL*	%	-	17.5
Plasticity Index, *PI*	%	-	30.2

3.2.2 Geotextile

The bidim® A10 geotextile was used in this study. The bidim® type of geotextile was one of the most extensively used in landfill liners in South Africa, which made it suitable for simulating the anticipated field conditions, (Sikwanda, 2018). One of the reasons this product was selected for use in this study was because Kaytech Engineered Fabrics manufactured it in Cape Town, South Africa, making it readily available. It also met the minimum requirements, as specified by the Geosynthetic Institute (GSI) to be used as a cushion in a landfill. **Table 3-3** shows the physical, mechanical, hydraulic, and durability properties of the bidim® A10 provided by the manufacturers Kaytech Engineered Fabrics Ltd.

Table 3-3 Properties of bidim® A10 Geotextile, (after Kaytech Engineered Fabrics Ltd, 2019)

Properties*	Test Method	Units	M A R V
Mass per unit area	ASTM D5261	g/m^2	1080
Thickness**	SANS 9863	mm	6.4
Tensile Strength	SANS 1525	kN	50
		%	50 - 70
Grab Strength	ASTM D4632	kN	3700
		%	50 - 80
Trapezoidal Tear Strength	ASTM D4533	kN	1950
Static Punctured (CBR) Strength	SANS 12236	kN	11
UV Resistance	ASTM D4355	%	70
Permeability	SANS 11058	m/s	0.0026
Pore Size, $O_{95\,W}$	SANS 12956	µm	< 75

* All values are Minimum Average Roll Values (M A R V) except UV resistance; it is a minimum value.
** under 2 kPa load

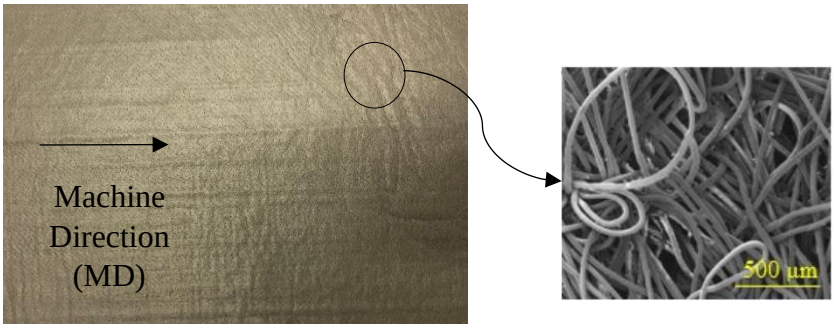

Figure 3-4 Surface and microscopic view of selected Bidim® A10 geotextile.

Bidim® was a continuous filament, nonwoven, needle-punched geotextile (**Figure 3-4**) manufactured from 100 % recycled polyester from discarded bottles of cool-drinks. This geotextile was used in various applications of engineering, i.e. liner protection, erosion control etc, due to its versatility, (Kaytech Engineered Fabrics Ltd, 2017). Bidim® A10 was normally selected as the appropriate geotextile protection for the HDPE liner in a landfill due to its thickness, long-term creep, and abrasion and piercing resistance, while retaining high tensile strength. Additionally, its ease and speed of installation was a great advantage compared to sand protection layers, especially on slopes, (Kaytech Engineered Fabrics Ltd, 2019). The dark green bidim® A10 utilized had a design life of over 120 years. The bidim® A10 had a thickness of 6.4 mm and a mass per unit area of 1080 g/m^2.

3.2.3 Geomembrane

The geomembrane (GMB) used in the study was a 2 mm thick black double textured HDPE manufactured in Cape Town, South Africa by AKS Liner Systems (Pty) Ltd. This product was factory-made from HDPE resin under controlled conditions and international specification of GRI–GM13, (AKS Lining Systems (Pty) Ltd, 2019). The GMB was specifically selected because it was the most popular GMB used in landfill applications in South Africa, (Sikwanda, 2018). GMBs are mainly installed in landfills between the GTX-cushion and the GCL, and act as an impermeable layer creating a liquid barrier between contaminated fluids and surrounding soil and groundwater, (Buthelezi, 2017).

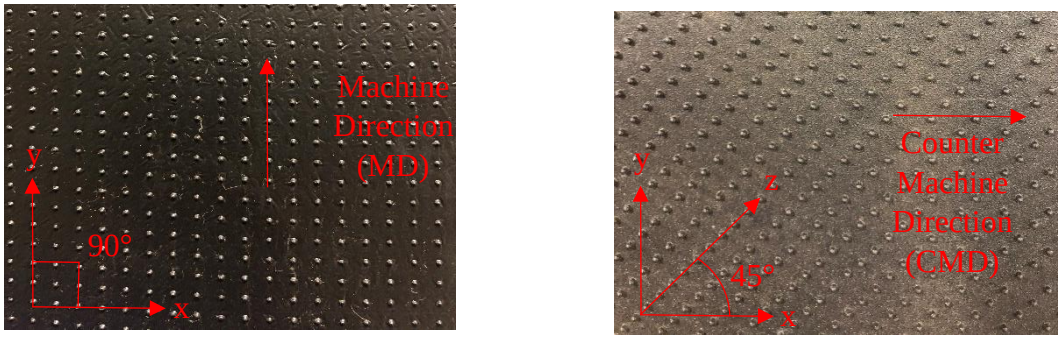

(a) (b)

Figure 3-5 Asperity height difference of the HDPE used: (a) 0.80 mm and (b) 1.80 mm

The physical properties were measured using a digital dial gauge (asperity height), 100 mm x 100 mm sheet metal (asperity density) and a measuring ruler (asperity spacing). The GMB had an average surface asperity height of 0.80 mm on one side (side A – minor spikes) and 1.80 mm on the other side (side B – major spikes), as can be seen in **Figure 3-5**. The difference in height asperities was mainly influenced by field placement, so that, due to higher asperities, side A mobilized more interface shear resistance, (Sikwanda, 2018). The average asperity density was found to be 338 per 10000 mm^2 (side A) and 225 per 10000 mm^2 (Side B). **Table 3-4** below, shows the relevant material specifications such as thickness, formulated density, carbon black percentage, and tear and puncture resistance, as obtained from AKS Liner Systems.

Table 3-4 Properties of the GMB and the standards used for determining the specifications.

Properties	Specification	Units	M A R V	Test Method
Asperity height	Side A - Minor spikes	mm	0.8	
	Side B - Major spikes		1.8	
Asperity density	Side A - Minor spikes	per 10000 mm^2	338	
	Side B - Major spikes		225	
Thickness*		mm	2.0	ASTM D5994
Formulated Density*		g/cc	≥ 0.94	ASTM D1505
Carbon black content*		%	2.5	ASTM D4218
Tear resistance*		N	249	ASTM D1004
Puncture resistance*		N	534	ASTM D4833
UV Resistance*		%	50	ASTM D5885

*(AKS Lining Systems (Pty) Ltd, 2019) M A R V = Minimum average roll value

3.2.4 Geosynthetic Clay Liner

The geosynthetic clay liner (GCL) used in this study was selected from GCLs known as EnviroFix®. This needle-punched GCL was chosen because it was the most common type of reinforced GCL used in Landfills in South Africa, (Buthelezi, 2017; Kaytech Engineered Fabrics Ltd, 2015a). EnviroFix® X 2000 was produced by distributing a uniform layer of sodium bentonite between two geotextiles. The fibres of the upper non-woven geotextile were then needle-punched through the bentonite layer and incorporated into the lower geotextile (**Figure 3-6**). This process resulted in a strong mechanical bond between the fabrics making it a versatile hydraulic barrier, (Kaytech Engineered Fabrics Ltd, 2015b). The needle-punched fibres were modified and more permanently locked in place using a proprietary heat treatment process known as the Thermal Lock^{TM}. This resulted in combined properties such as low permeability and high internal shear resistance, (Kaytech Engineered Fabrics Ltd, 2015a).

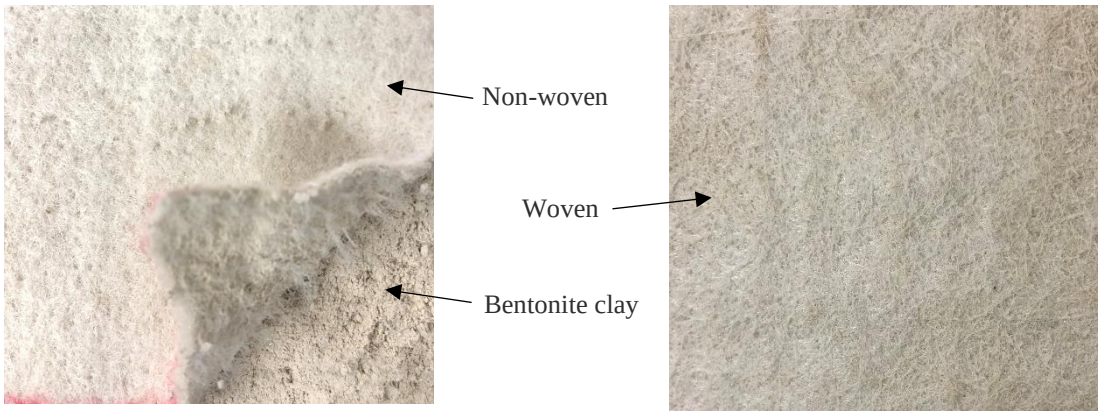

Figure 3-6 Envirofix X2000 GCL: (a) Smooth non-woven side and (b) Rough woven side.

The sodium bentonite clay used in EnviroFix® Thermal Lock^{TM} was a naturally occurring clay mineral that swells between its clay platelets as water enters. The bentonite swells when hydrated under confinement to form a low permeability clay liner with the equivalent hydraulic protection of about one meter of compacted clay. Consequently, the application of GCL's as a replacement for the traditional compacted clay in landfill liners had become common practice, (Sikwanda, 2018). **Table 3-5** illustrates the properties of EnviroFix® X 2000 as specified in the manufacturer's handbook.

Table 3-5 Properties of the EnviroFix® X 2000 GCL, (Kaytech Engineered Fabrics Ltd, 2015b).

Properties	Specification	Units	M A R V	Standards
Geotextile Cover Layer	PP non-woven, white	g/m^2	200	ASTM D5261
Geotextile Carrier Layer	PP slit film, woven	g/m^2	110	
	PP non-woven, white		200	
	Composite		310	
Bentonite Layer (bentonite mass at 0% moisture content	Quality	Montmorillonite content > 75% Sodium Cation Na^+ > 60 %		
	Sodium Bentonite Powder	g/m^2	3 700	ASTM D5993
	Swell Index (minimum)	mℓ/2 g	≥ 24	ASTM D5890
GCL Mass per Unit Area		g/m^2	4 210	ASTM D5993
Bonding Process		Needle punched and Thermal Lock^{TM}		
Grab Strength	Machine Direction (MD)	N	1 500	ASTM D4632
	Cross Direction (XD)	N	1 500	
CBR Burst	Strength	N	2 500	ISO 12236
	Elongation	%	≥ 50	
Hydraulic Conductivity (maximum)		m/s	≤ 1.92×10^{-11}	ASTM D5887
Peel Strength (excluding Edge treatment)		N/m	> 600	ASTM D6496

PP = Polypropylene M A R V = Minimum average roll value

3.3 Testing Apparatus

3.3.1 Large direct shear

The free-standing large direct shear apparatus, *ShearTrac-III*, was used to perform the interface shear tests in the Geotechnical Engineering Laboratory at the University of Cape Town, South Africa. Designed and manufactured by Geocomp Corporation, USA, the device was capable of running fully automated consolidated and shear phases of direct shear tests. The equipment consisted of a top (static) shear box with plane dimensions of 305 mm x 305 mm and 100 mm in depth, and a lower (moving) shear box with plane dimensions of 460 mm x 355 mm and a depth of 100 mm. Also, the shear device was equipped with a water tank (for hydration), two load cells (horizontal and vertical), two displacement transducers (horizontal and vertical), and a computer-controlled unit. The transducers ensured quality test control and prevented the *Shear Trac-III* from running beyond its physical limitations. The device had a maximum load capacity of 44.5 kN and was able to apply a constant shear rate of up to 15 mm/min and maximum normal stress of 450 kPa, according to the manufacturer, Geocomp. The tests were monitored through the computer-unit which graphically displays data during the tests in real-time.

Figure 3-7 Automated large direct *ShearTrac-III* apparatus (Front & back).

Figure 3-7 shows a general configuration of the apparatus. This *ShearTrac-III* system generated a fairly homogeneous state of shear stress throughout the specimen, providing initial stress condition, stress path, and deformation configuration that more closely models numerous field loading conditions than any other test, (Sikwanda, 2018). The interface friction properties between geosynthetic/geosynthetic and soil/geosynthetic were determined using this device. The device was suitable for this investigation as it met the minimum requirements stipulated by the standards of ASTM D5321 (2017). Besides, previous studies by various researchers, i.e. (Alzahrani, 2018; Aza-Gnandji et al., 2019; Buthelezi et al., 2016; Buthelezi, 2017; Sikwanda, 2018), relating to geosynthetics had used the same apparatus to determine interface shear parameters.

3.4 Test Preparation

The interface shear tests were divided into two test configurations: single and multi-interface tests. Five different samples were used in this study. For this study, the simulated composite liner consisted of three geosynthetics, namely GMB, GTX and GCL, sandwiched between two soils, namely sand and clay (see **Figure 3-8**). All tests were conducted in accordance with ASTM D5321 (2017), which examines soil/geosynthetic and geosynthetic/geosynthetic interfaces, and ASTM D6243 (2018), which examined geosynthetic clay liner (GCL) interfaces. The following steps were performed on the test samples in each test to be carefully prepared to obtain similar test conditions throughout all of the experiments.

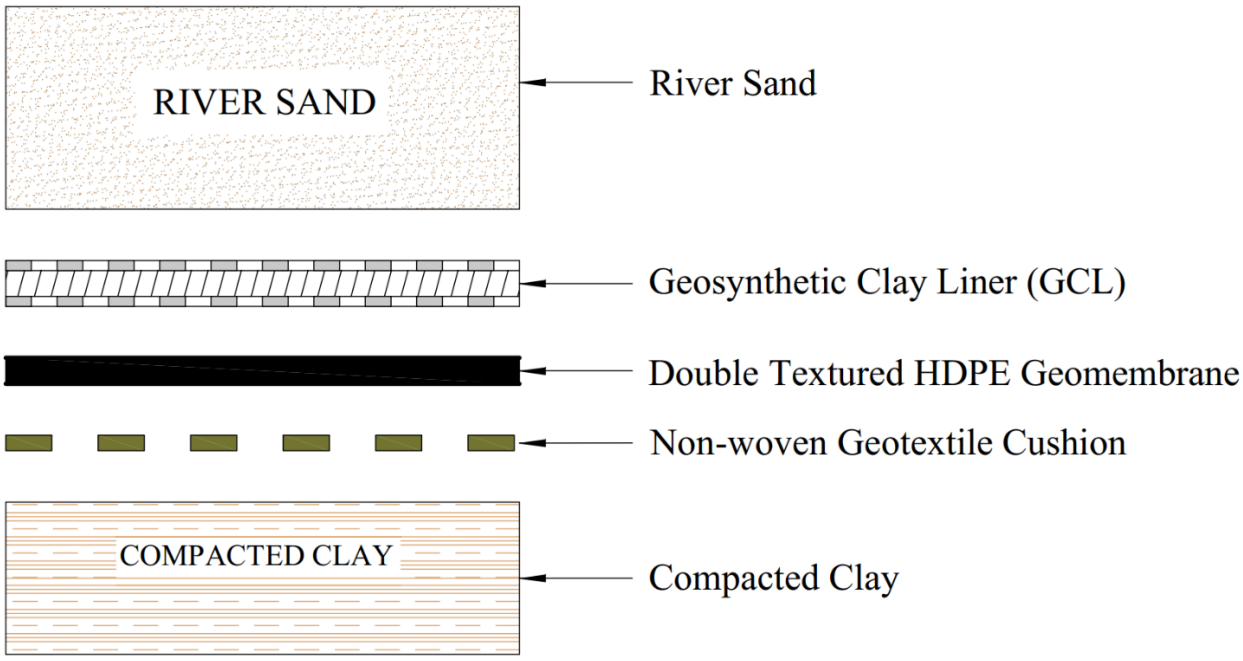

Figure 3-8 Schematic of simulated composite liner.

3.4.1 Shear box set up

As described in ASTM D5321, a metal substrate that served as a replacement for soil material was gently placed inside the bottom shearing box when a geosynthetic/geosynthetic interface was being carried out. The substrate was specifically designed for the direct shear box and supplied with the direct shear device. According to Buthelezi (2017), it was reported that the metal substrate, which had plane dimensions of 400 mm x 300 mm and a height of 100 mm, increased the accuracy and reproducibility of test results. Alternatively, for the top shearing block, an aluminium dead weight of 3.3 kg with dimensions of 300 mm x 300 mm x 12 mm was used as a substrate. This aluminium plate was selected based on its ability to withstand corrosion, making it suitable for use in wet conditions during testing. When a soil/geosynthetic interface test was performed the metal substrate for the bottom shearing box remained in place, while the aluminium plate for the top shearing box was removed and placed above the soil sample after the test was set up. This will be further discussed in detail later in this section.

3.4.1.1 Gripping surface

Sikwanda, et al. (2018) recommended that sandpaper be used as a gripping surface, as it made it possible to simulate the friction characteristics between geosynthetics with the direct shear device, as applicable in field conditions, (Kalumba, 1998). The sandpaper, which was 50 mm wide, was cut according to the length of each substrate through a pair of scissors and was carefully placed to act as a gripping surface on each of the two respective substrates. The cut pieces were then carefully glued to each respective substrate and left for about 15 minutes (without placing anything atop) to cure and form a gripping surface.

It was imperative to replace the sandpaper before carrying out new tests. Firstly, to replace the sandpaper, a sharp blade was used to remove the worn-out sandpaper and then all the impurities on the substrate surface were eradicated using paraffin oil. The substrate was then further cleaned with a brush by washing it with soap and water. A suitable solvent for plastic and synthetic fibres known as acetone, was then used to dissolve glue particles stuck on the substrate. Lastly, the surface was left for at least 1 hour to dry, and the new sandpaper was installed.

3.4.2 Test Sample preparation

3.4.2.1 Geosynthetic/geosynthetic Interface

Preparation of the GTX and GMB samples was done following the guidelines set out in ASTM D5321 (2017), whereas the preparation of samples for GCLs was done following ASTM D6243 (2018). Before the shear box set up, geosynthetics samples were carefully cut into required sizes at random sections from the respective supplied geosynthetic rolls. This cut was done based on standard geosynthetic-templates and parallel to the factory roll direction (machine direction) from their respective geosynthetic rolls supplied by different manufacturers. The cut was carried out to a precision of approximately ± 0.5 mm. Since two of the geosynthetics, i.e. GTX and GCL, were made from fabrics that were not too rigid, they were cut using a pair of scissors.

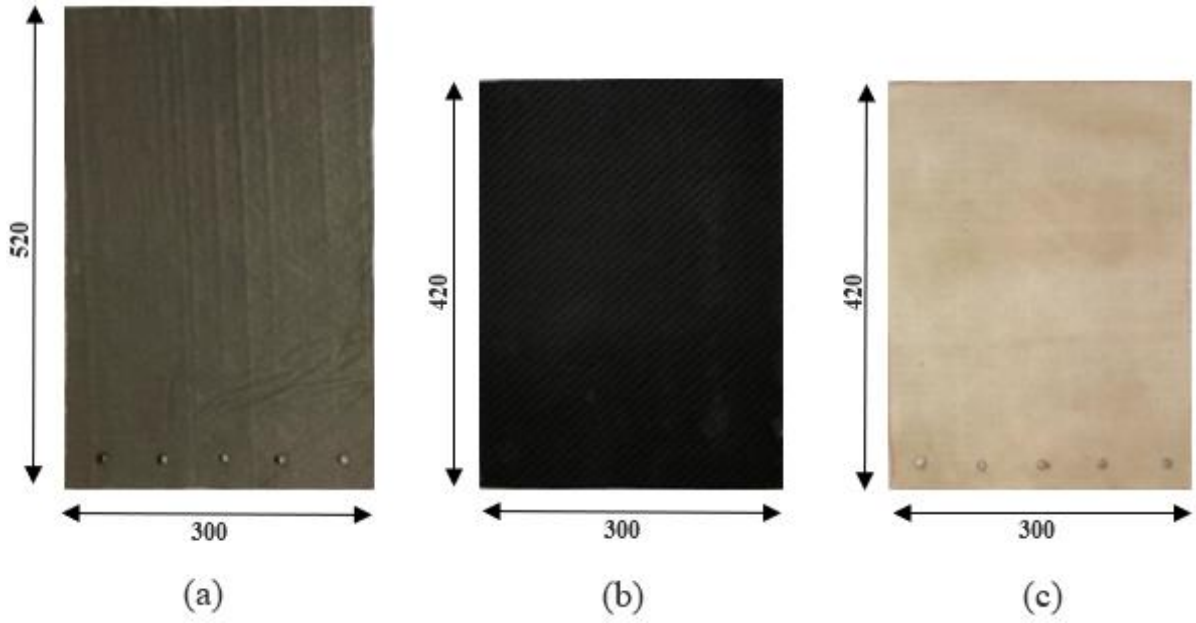

Figure 3-9 Plan view of geosynthetic specimen: (a) GTX, (b) GMB and (c) GCL, (all dimension in mm).

However, due to their high tear-resistance, the GMBs were cut to the required dimensions using a mechanical saw machine at the Civil Engineering workshop, University of Cape Town. The geosynthetics were cut into sample sizes that were dependent on the size of the box upon which each sample was to be fixed. Samples to be fixed on the upper box were cut to 300 x 420 mm, while those to be fastened on the lower box was cut to 300 x 520 mm, as can be seen in **Figure 3-9**. These sample sizes were sufficient to cover the entire top and/or bottom surface of the shear box, so that no area correction was necessary.

Figure 3-10 Tools and equipment used in sample preparation: (a) pair of scissors, (b) mechanical hole puncher, (c) rubber hammer, (d) ratchet bolt driver and (e) mechanical saw machine.

Once all the geosynthetic samples were cut to their respective sizes, a mechanical-hole puncher with a diameter of 10 mm and a rubber hammer were used to make five gripping holes, with a precision of ± 0.5 mm, at one edge of each trimmed test specimen. To ensure accurate marking and punching of the holes, a geosynthetic-template similar to that used for cutting the geosynthetics was used. These holes were necessary to secure the test specimen with the clamping system (washers and nuts) to the shear box and to provide sufficient resistance to keep the test samples in position and enforce failure of the specimen to occur at the desired interface. The trimmed geosynthetic specimens were then fastened to either top or bottom box depending on the interface being tested by clamping, using metal strips and bolts (see **Figure 3-11**). The bolts were fastened to the metal strip using the bolt-driver ratchet.

3.4.2.2 Soil/geosynthetic Interface

In this case, once the geosynthetic was secured on the bottom shear box, the top shear box was carefully fixed atop the bottom shear box through alignment screws. Preparation of soil samples was done following the guidelines set out in ASTM D5321 (2017). A weighing scale was used to determine an approximate mass (around 3.0 - 4.0 kg) of three soil samples required for testing. The soil samples were carefully mixed to the OMC of the soil using a mechanical mixer. Then, the soil samples were poured in three equal layers into the top shear box in direct contact with the geosynthetic. A 20 mm thick solid plate covering the entire soil area was placed gently on top of each layer before being subjected to tamping with a hand tamper, as schematically shown in **Figure 3-12**. The hand tamper consisted of a steel shaft rod attached to a solid rectangular plate measuring 300 mm x 300 mm with a drop weight of 4 kg. For sand and clay, each layer received 20 and 40 drop weights, respectively, from a height of 300 mm.

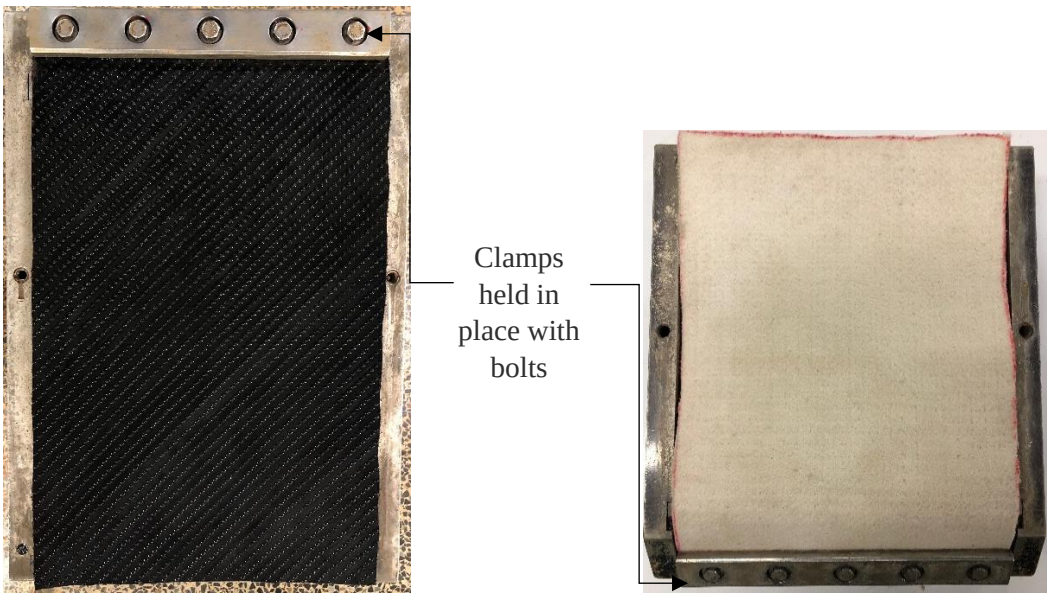

(a) Bottom shear box (305 mm x 450 mm) (b) Top shear box (305 mm x 325 mm)

Figure 3-11 Fastening of geosynthetics to bottom and top shear box.

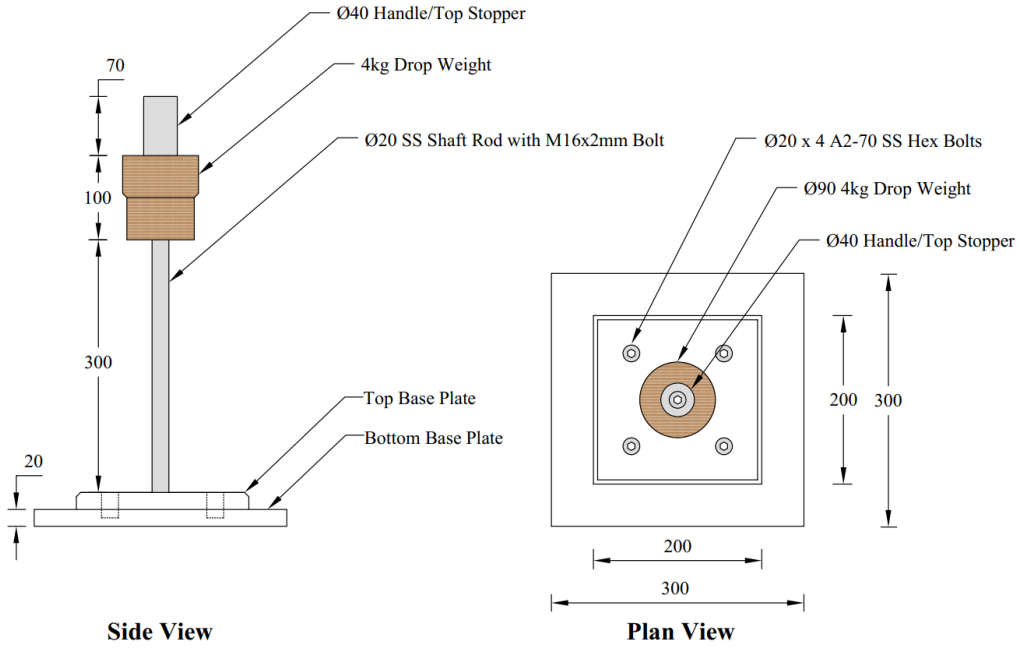

Figure 3-12 Schematic view of hand tamper (or drop weight) compactor (all dimensions in mm).

3.5 Test configuration

3.5.1 Single Interface Test

In the case of singe interface testing, both soil/geosynthetic and geosynthetic/geosynthetic interface tests were carried out. For geosynthetic/geosynthetic interface testing, i.e. GTX/GMB, the two trimmed geosynthetic samples to be tested were carefully fixed, through a clamping device and bolts, at one end of the respective shear boxes. As illustrated in **Figure 3-13**(a), the top shear box with the clamped test specimen, i.e. GTX, was then carefully placed on top of the bottom shearing box with the clamped test specimen, i.e. GMB. The top shearing box was then gently aligned using two alignment screws and held in place with the bottom shearing box to prevent any movement during handling. The top gripping surface was placed inside the shear box with care, such that the topside of the gripping surface was in contact with the upper test specimen.

On the other hand, for soil/geosynthetic interface testing, i.e. sand/GCL, only one trimmed geosynthetic sample, i.e. GCL, was fixed to the bottom shear box using a clamping device and bolts. Similarly, the top shearing box was gently placed on top of the bottom shearing box and aligned using two alignment screws to keep it in place and prevent any movement during handling. Then, as highlighted in Section 3.4.2.2, the soil sample, i.e. sand, was poured in three equal layers into the top shear box in direct contact with the geosynthetic. To achieve the specified moisture and density, each layer of soil was compacted, uniformly and carefully, 20 times using the steel tamper, as shown in **Figure 3-12**, (Alzahrani, 2018). **Figure 3-13**(a) & **Figure 3-13**(b) show the setup of both geosynthetic/geosynthetic and soil/geosynthetic interface tests respectively.

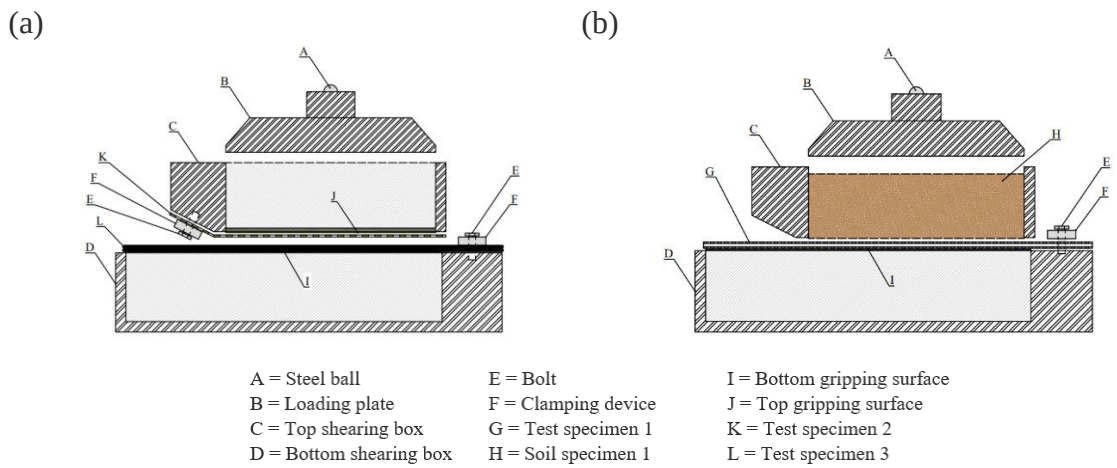

Figure 3-13 Test sample configuration for single interface testing: (a) geosynthetic/geosynthetic and (b) soil/geosynthetic.

3.5.2 Multi-layer interface tests

The procedures adopted in multi-layer interface test configurations were identical to those followed in the preparation of the single interface tests. Similar to single interface tests, both soil/geosynthetic and geosynthetic/geosynthetic interface tests were carried out. However, to simulate the anticipated field condition, one or more additional test specimens were added. For geosynthetic/geosynthetic/geosynthetic interface testing, i.e. GTX/GMB/GCL, two of the three trimmed geosynthetic samples to be tested, referred to as test specimen 1 & 2 (i.e. GTX & GCL) in **Figure 3-14**(a), were carefully fixed to one end of the respective shear boxes through a clamping device and bolts. In a smoothly but carefully stretched mode, test specimen 3 (i.e. GMB) was placed on top of test specimen 1 (i.e. GTX) without being clamped, so that it was between the test specimen 1 and 2, as shown in **Figure 3-14**(a). This was to allow failure to occur at the weakest interface during interface shearing. As was done in single-interface testing, the top shear box with the clamped test specimen 2 (i.e. GCL) was then carefully placed on top of the bottom shearing box.

Alternatively, testing procedures for soil/geosynthetic interfaces were similar to those discussed above, except for adding or removing one test specimen, depending on the simulated field conditions. For soil/geosynthetic/geosynthetic/geosynthetic interface testing, one soil sample was tested together with three geosynthetic specimens, (i.e. sand/GCL/GMB/GTX). Similarly, one trimmed geosynthetic specimen, i.e. GTX, which is referred to as test specimen 1 in **Figure 3-14**(b), was fastened to the bottom shear box through a clamping device and bolts. Then test specimens 3 & 4, i.e. GCL & GMB, were carefully placed on top of test specimen 1, i.e. GTX, without being clamped, such that they were in contact with test specimen 1. This was to allow failure to occur at the weakest interface during interface shearing, (Sikwanda, 2018). The top shear box was then placed gently on top of the bottom shear box and aligned with two alignment screws. Then, the soil sample, i.e. sand, was poured in three equal layers into the top shear box in direct contact with the geosynthetic. To achieve the specified moisture and density, each layer of soil was compacted uniformly and carefully 20 times using the steel tamper (see **Figure 3-12**).

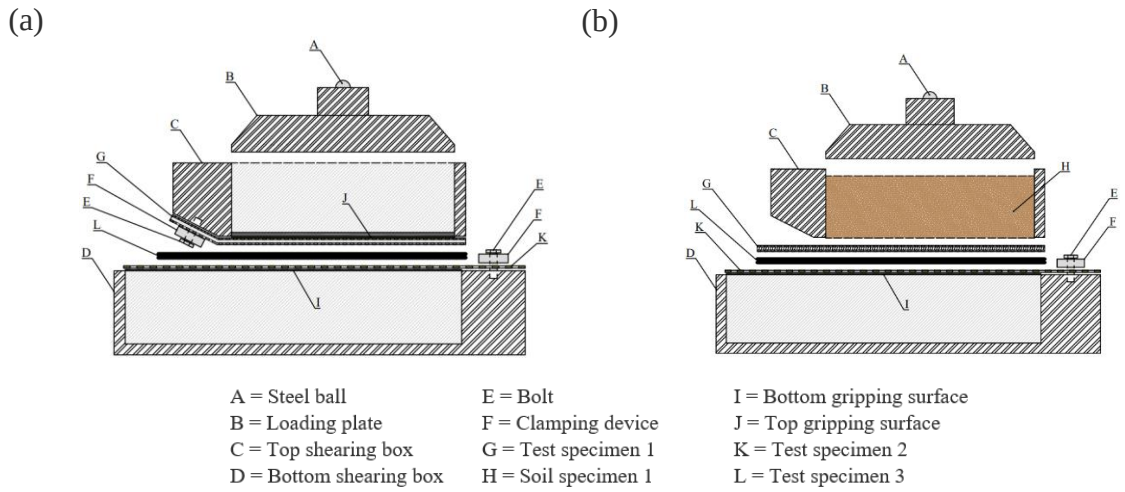

Figure 3-14 Test sample configuration for multi-layer interface testing: (a) geosynthetic/geosynthetic/geosynthetic and (b) soil/geosynthetic/geosynthetic/geosynthetic

For soil/geosynthetic/geosynthetic/geosynthetic/soil interface testing, both soil samples were tested together with the three geosynthetic specimens as one system, (i.e. sand/GCL/GMB/GTX/clay). Firstly, the less compressible soil (i.e. sand) was poured in three equal layers into the bottom shear box and each layer was compacted 20 times to achieve the specified moisture and density. The soil was compacted such that it was protruding above the shear box by a height of approximately 1 - 5 mm. Then the trimmed three geosynthetic specimens, i.e. GCL, GMB & GTX, were carefully placed on top of compacted soil, without being clamped, such that they were in contact with soil specimen, as can be seen in **Figure 3-15**. This was to allow failure to occur at the weakest interface during interface shearing, (Sikwanda, 2018). The top shear box was then placed gently on top of the bottom shear box and aligned with two alignment screws. Then, the second soil sample, i.e. clay, was poured in three equal layers into the top shear box in direct contact with the geosynthetic. To achieve the specified moisture and density, each layer of soil was compacted uniformly and carefully 40 times using the steel tamper (see **Figure 3-12**).

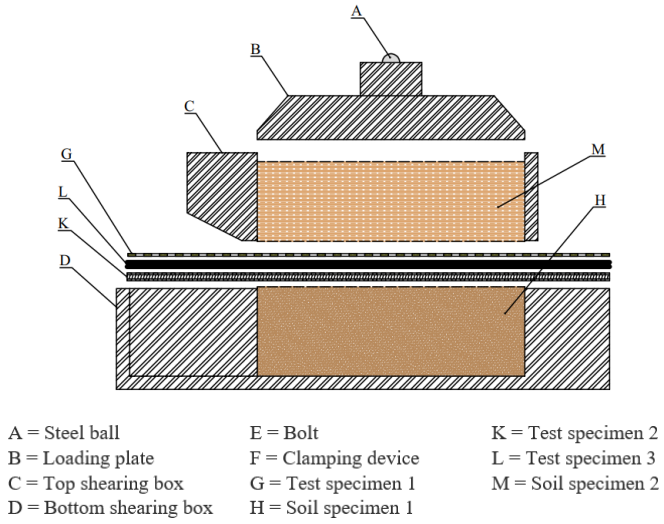

Figure 3-15 Test sample configuration for multi-layer interface testing

3.5.3 Final Assembling of Apparatus

Once all the test preparation was completed in either single or multi-interface setup, a loading plate weighing 10 kg and measuring 300 mm x 300 mm x 22 mm was carefully placed inside the upper shear box and over the top gripping surface or the soil specimen, as described by the direct shear manufacturer. Also, a ball-bearing made of steel and weighing 79.1 g with a diameter of 26.6 mm was then gently placed on the loading plate in the spherical seat, as specified by Geocomp (2020). The loading plate was designed and supplied by Geocomp together with the *ShearTrac-III* large direct shear apparatus, and its primary purpose was to distribute the normal force applied to the test samples in a shear box.

After this was complete, the entire assembly was moved to the starting position and carefully pushed into the low-friction machine testbed by sliding it into the base container of the *ShearTrac-III*. The entire assembly within the base container was then adjusted by lowering the vertical loading cell and moving the combined shear boxes horizontally using the connected desktop computer until the vertical loading device coincided with the steel ball placed on the loading cover. Two steel reaction beams spanning on top of the test chamber were screwed to the machine frame to hold the entire assembly in position. The beams provided the top shearing box with the reaction force to ensure that only the bottom shearing block moved during shearing. Once all was in order, the two aligning screws holding the top shearing block to the bottom shearing block were carefully removed with the consciousness that no displacement between the two shearing blocks was caused. Finally, normal stress was applied, and nuts and bolts were used to secure the upper and lower shear boxes in the *ShearTrac-III* base container.

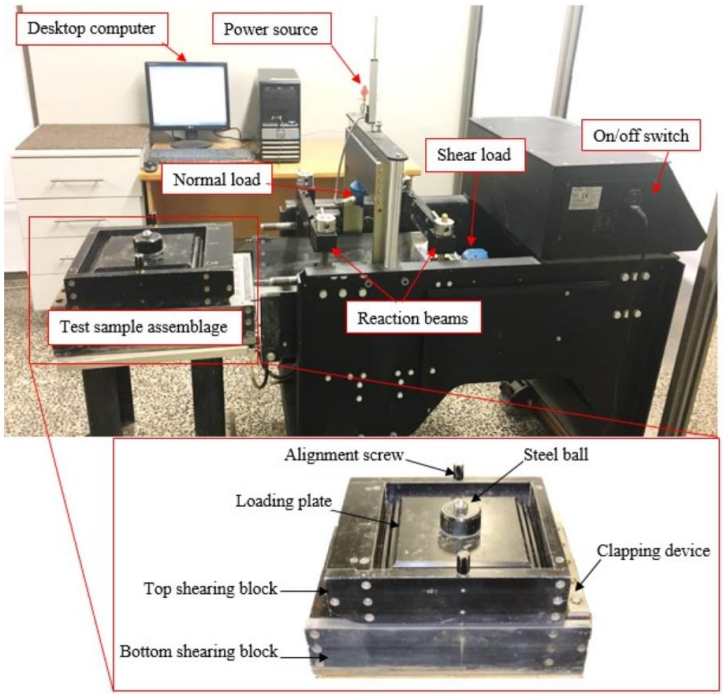

Figure 3-16 Final Assemblage of *ShearTrac-III* large direct shear apparatus. (after Sikwanda, 2018)

3.6 Testing Procedures

After setting up the direct shear device and all test samples in order, the *ShearTrac-III* software was opened and used to manually enter the test parameters required for each test to start testing. These parameters included normal stress, shear rate, calibration values, horizontal displacement, and consolidation time.

Each test was conducted at four normal stresses of 50, 100 , 200, and 400 kPa to represent the varying load conditions experienced by the liner system during the design life of a landfill, (Sikwanda, 2018). ASTM D5321 (2017) & ASTM D6243 (2018) recommend performing at least three normal stresses to develop a shear resistance envelope. For the GTX/GMB single-interface shear test a constant shear rate of 1.0 mm/min was used as it did not involve GCLs or clay specimens and therefore no excess pore pressure was anticipated at the interface. On the other hand, all other interface tests involved either clay or GCLs samples, hence a recommended shear rate of 0.1 mm/min was used, (ASTM D6243 2018). This shearing rate was relatively slow to ensure the insignificant accumulation of excess pore pressure during failure.

Although ASTM D5321/6242 standards recommend a minimum shear displacement of 50 mm in geosynthetic interface shear tests, the direct shear device used for the tests had a maximum displacement of 75 mm. A shearing displacement of 75 mm was used throughout the experiments. The resulting 'residual' strengths were therefore referred to as large displacement (LD) shear strengths, as explained in section 2.4.3. Calibration of the shear device was performed following the manufacturer's manual. The horizontal and vertical transducers used in the system were calibrated for each test before shearing was initiated to ensure uniformity of results, as recommended by the manufacturer.

A consolidation time of 30 minutes was adopted from previous research papers (i.e. Fox & Stark, 2004; Sikwanda, 2018) and used throughout all the experiments. This consolidation time was anticipated to be sufficient for the gripping surfaces to fully engage with the test samples and also to allow the excess pore pressure to decrease substantially to zero before shearing was started. The test was then initiated, and the test samples were allowed to pre-consolidate until the time for 100 per cent primary consolidation (t_{100}) was reached. At this stage approximately 15 litres of tap water were carefully poured into the water tank of the apparatus until all the test specimens were completely submerged for hydration.

For the GTX/GMB interface, a hydration time of one hour was used because no soils had to be consolidated and the interfacial contact time was sufficient before shearing; (Stark et al., 2011; Stark et al., 2015). All the interface tests containing either clay or GCL specimens were hydrated for 24 hours under their respective normal stresses. Previous researchers, i.e. (Eid & Stark, 1997; Fox & Stark, 2004) reported that the selection of the 17 kPa was to simulate the possible initial load that would be imposed on the lining system prior to disposal of waste. Also, it was recommended to hydrate the GCL at low normal stress as it resulted in more water being absorbed into the bentonite particle double layers, thus presenting the worst-case scenario, (Fox & Stark, 2004; Sikwanda, 2018).

Once the hydration was completed, a gap between the upper and lower shear box of approximately 1 mm to 5 mm was created to prevent friction between the two shear boxes during shearing, (ASTM D5321, 2017). Finally, the shearing test was then initiated, whereby a shear force calculated by the direct shear program was applied through a 37.5 mm diameter lead screw to produce shear stress on the bottom shear block from the motor apparatus. As a result, the bottom section of the shear box moved at a user-specified shear rate in relation to the top static shear box. The *ShearTrac-III* software program continuously recorded all the data sensors during the shearing phase, made necessary corrections to maintain the shear rate, graphically displayed the test data on the computer screen and captured the data in an output file. Eventually all of the tests ended automatically when the 75 mm horizontal displacement was reached.

3.7 Testing Program

Using both the single and multi-interface test configurations, a series of 36 direct shear tests were carried out. These tests were tested at varying normal loads namely 50, 100, 200 and 400 kPa. In the single interface test configuration, 16 tests were conducted, while the other 20 remaining tests were carried out using a multi-layer interface test configuration. **Table 3-6** presents the complete test program performed and the key factors considered that have significant effects on the direct shear test results.

Table 3-6 Testing Schedule for the Large Direct Shear box.

Interface Test Configuration		Consolidation Time (hours)	Shearing rate (mm/min)	Normal Stress (kPa)				No. of tests
Single Interface	CLAY/GTX	24	0.1	50	100	200	400	4
	GTX/GMB	1	1.0	50	100	200	400	4
	GMB/GCL	24	0.1	50	100	200	400	4
	GCL/SAND	24	0.1	50	100	200	400	4
Multi -layer Interface	CLAY/GTX/GMB	24	0.1	50	100	200	400	4
	GTX/GMB/GCL	24	0.1	50	100	200	400	4
	GMB/GCL/SAND	24	0.1	50	100	200	400	4
	GTX/GMB/GCL/SAND	24	0.1	50	100	200	400	4
	CLAY/GTX/GMB/GCL	24	0.1	50	100	200	400	4
	CLAY/GTX/GMB/GCL/SAND	24	0.1	50	100	200	400	4
							Total number of tests	**40**

3.8 Data Analysis

3.8.1 Shear Output processing

Once each test was completed, data recorded on the computer-unit connected to the automated *ShearTac-III* was exported to a similar template for data analysis in Microsoft Excel software

(MEs). Shear strength graphs such as shear stress versus horizontal displacement and shear strength versus normal stress were plotted. For any normal stress applied, the shear strength data points were connected by a best-fit line(s) or curve generated within the MEs to establish the Mohr-Coulomb failure plane. This was eventually used to determine the friction angle and adhesion values of the interface.

3.8.2 Failure envelope criterion

Using the peak and large displacement shear strength values and corresponding normal stresses allows for the Mohr-Coulomb failure envelopes to be developed. A properly defined Mohr-Coulomb shear strength envelope, represented by Equation 3-1, describes the linear relationship between the shear and normal stress performed at three or more different normal stresses, according to ASTM D5321 (2017).

$$\tau = c_\alpha + \sigma_n \cdot tan\delta$$

Equation 3-1

where τ is the peak or LD shear stress at failure, c_α is the adhesion of the interface (or shear strength at zero normal stress), σ_n is the applied normal stress and δ is the interface friction angle.

Contrary to the linear failure envelope represented by the Mohr-Coulomb criterion used in the technique above proposed by Anubhav & Basudhar (2010) to estimate peak and residual shear stresses for the geosynthetic interfaces, this research also considered a non-linear failure envelope for their estimation. This approach was consistent with the studies conducted by Aza-Gnandji et al. (2019), Esterhuizen et al. (2001) & Bacas et al. (2015) which observed that the experimental tests on the behaviour of geosynthetic–soil interface usually exhibit non-linear shear stress versus normal stress relationship. For this study, the considered non-linear expression was as follows:

$$\tau = a{\sigma_n}^2 + b\sigma_n + c_\alpha$$

Equation 3-2

where τ is the peak or LD shear stress at failure, c_α is the apparent adhesion which corresponded to the inclination of the vertical axis, σ_n is the applied normal stress and $a\ and\ b$ are hyperbolic functions obtained through a curve fitting technique using the experimental data.

3.9 Quality Assurance

3.9.1 Measures Implemented

The following measures were implemented in each test conducted to ensure that all tests were conducted up to standard:

- In each set-up, to ensure consistency, all of the outlined test preparation and procedure guidelines were followed in great detail.

- In each experiment, new geosynthetic test specimens were trimmed to the same respective dimension in accordance with the machine direction of the industrially supplied geosynthetic rolls without damage.
- A new set of test specimens were used for each interface shear experiment to ensure that no geosynthetic samples were reused.
- After a thorough cleaning of the water tank apparatus, fresh tap water was used in each test for hydration to ensure no contamination of the test samples.
- The equipment used during the entire study was calibrated as recommended by the direct shear manufacturer, Geocomp, and ASTM standards D5321/6243.
- All tests were conducted under similar physical and climatic conditions as recommended by the ASTM D5321/6243 standards (air-conditioned laboratory at 22 C and humidity between 50 - 70 percent).

3.9.2 Repeatability Test results

The testing procedures and results in this study were verified for reproducibility by performing at least two replicate tests of both single interface and multi-layer interface tests. These repeated tests were conducted on the GTX/GMB single interface, and the GTX/GMB/GCL multi-layer interface at the same applied normal stresses considered in this study, namely 50, 100, 200 and 400 kPa. Each set of the two curves, presented in **Figure 3-17**(a) & (b) signifies the behaviours of the first and second interface shear tests for identical specimens.

The behaviour of shear stress for the repeated tests is presented in **Figure 3-17**. It was evident from **Figure 3-17**, that the plots showed a similar shear stress relationship response for each considered interface at any particular normal stress. The shear strength increased to reach the maximum (peak) shear strength at a certain horizontal displacement with increasing normal stress. In each interface tested, the shear stress declined beyond the maximum shear stress to approach a large displacement (LD) strength (see **Figure 3-17**). The close match of measured responses from these tests confirms the repeatability of the test results.

In analysing the results obtained in this study, the percentage difference (% *D*) in mobilized peak and large displacement (LD) strength was calculated using Equation 3-3.

$$Percentage\ Difference\ (\%\ D) = \frac{|E_1 - E_2|}{\left[\frac{E_1 - E_2}{2}\right]}$$

Equation 3-3

Where $E_1$is the first experimental value and E_2 is the second experimental value.

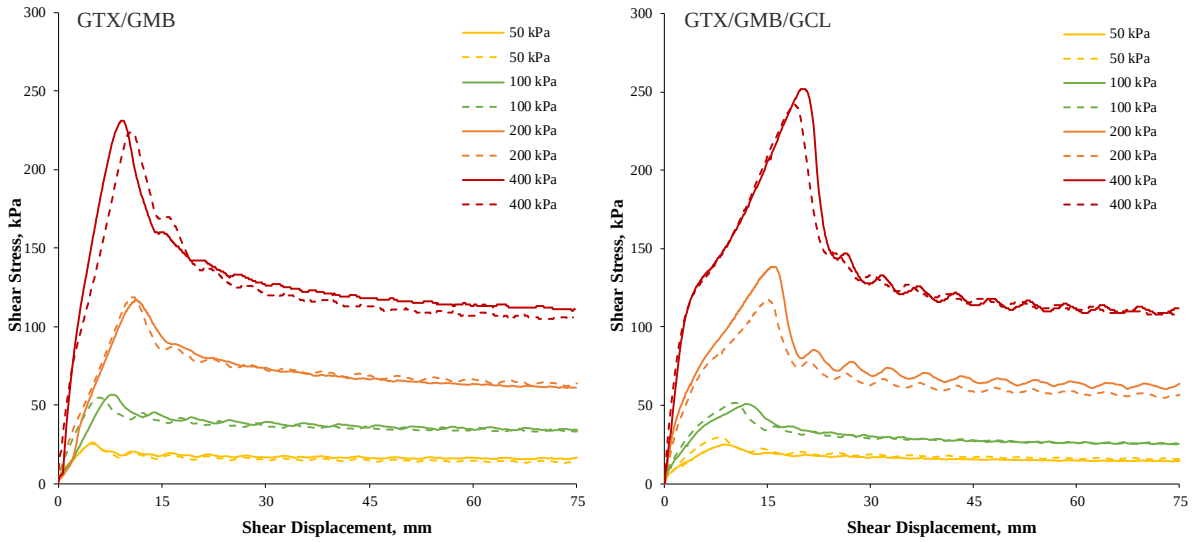

Figure 3-17 Shear Stress versus shear displacement: (a) single interface and (b) multi-layer interface.

If the respective PD was less than 10 %, it was assumed that this would be evidence of repeatability, (Taylor, 2002). It can be observed in **Table 3-7** that the maximum deviation from the mean of peak and LD stress was 2.0 % and 9.1 %, respectively. According to Taylor (2002), the degree of accuracy obtained from the interface shear test was within the maximum allowable deviation from the mean value. Hence, as seen from the consistency of the results, the experimental procedure followed was reproducible and repeatable. Thus, the repeatability tests verified that the testing procedures and sample preparation followed in conducting the tests were consistent, as the PD was all below the 10 percent capping value in peak stress and LD stress.

Table 3-7 Repeatability results analysis for GTX/GMB and GTX/GMB/GCL interfaces

Interface Configuration		Normal Stress (kPa)	Peak Stress (kPa)	Mean Peak Stress (kPa)	Deviation from mean		LD Stress (kPa)	Mean LD Stress (kPa)	Deviation from mean	
					kPa	%			kPa	%
Single Interface	GTX/GMB	50	26.5	26.0	0.5	1.9	16.8	15.5	1.3	7.7
			25.5		-0.5	2.0	14.2		-1.3	9.2
		100	56.5	55.7	0.9	1.5	34.1	33.7	0.4	1.3
			54.8		-0.9	1.6	33.2		-0.5	1.4
		200	117.0	118.0	-1.0	0.9	61.2	62.6	-1.4	2.3
			119.0		1.0	0.8	64.0		1.4	2.2
		400	231.0	227.5	3.5	1.5	111.0	108.5	2.5	2.3
			224.0		-3.5	1.6	106.0		-2.5	2.4
Multi-layer Interface	GTX/GMB/GCL	50	29.2	27.0	2.3	7.7	15.6	15.0	0.7	4.2
			24.7		-2.3	9.1	14.3		-0.6	4.5
		100	51.3	51.0	0.3	0.6	25.6	25.5	0.1	0.6
			50.7		-0.3	0.6	25.3		-0.2	0.6
		200	138	127.5	10.5	7.6	63.7	60.2	3.6	5.6
			117		-10.5	9.0	56.6		-3.6	6.3
		400	252	247.0	5.0	2.0	112	109.5	2.5	2.2
			242		-5.0	2.1	107		-2.5	2.3

4 RESULTS, ANALYSIS, AND DISCUSSION

4.1 Introduction

In this chapter, the results of all direct shear tests conducted at the soil/geosynthetic and geosynthetic/geosynthetic interfaces using both single and multi-layer interface configurations are presented in detail. For both single and multi-layer interface tests, the findings were illustrated in the form of interface shear stress development versus horizontal displacement diagrams. This was followed by an in-depth analysis of the failure envelopes for both test configurations. Finally, from the research findings, a detailed examination of the critical interfaces was provided.

4.2 Shear Stress versus Horizontal Displacement

4.2.1 Introduction

This section presents the development of all the shear stress versus shear displacement relationships for both single and multi-layer interface shear tests performed in this study. A separate graph was produced for every interface test considered. The tests were carried out at four different normal stresses, i.e. 50, 100, 200 and 400 kPa, thus each graph contains four plots of a different type of line, as shown in the legend.

4.2.2 Single Interface Tests

A total of four single interface shear tests were carried out. From these four tests conducted, the GTX/GMB interface test was performed after an hour of the test samples being fully submerged in water. The use of one-hour hydration was to allow the GTX and the GMB enough time to engage before shearing, (Stark et al., 2015). On the other hand, the other three interface tests, (i.e. CLAY/GTX, GMB/GCL & GCL/SAND), were performed after 24 hours of hydration, at their respective shearing loads. This was due to each interface test containing either clay or GCL, and this hydration time was commonly used and found to be sufficient for a sound conclusion to be drawn from previous studies, (Buthelezi, 2017; Fox & Stark, 2004, 2015; McCartney et al., 2002; Sikwanda, 2018).

Furthermore, for the GTX/GMB interface test, a recommended constant shearing rate of 1.0 mm/min was used as no excess pore pressures were expected on the interface, (ASTM D6243, 2018). However, either clay or GCL samples were involved in all the other interface tests, as such a recommended shearing rate of 0.1 mm/min was utilized, (ASTM D6243, 2018). This shearing rate was relatively slow to ensure the minimal accumulation of excess pore pressure during failure. The relationships for shear stress versus shear displacement for each of the four single interface shear tests conducted are shown in **Figure 4-1**. Additionally, a quantitative summary of the peak and LD shear strength values obtained from the single interface tests was presented in **Table 4-1**.

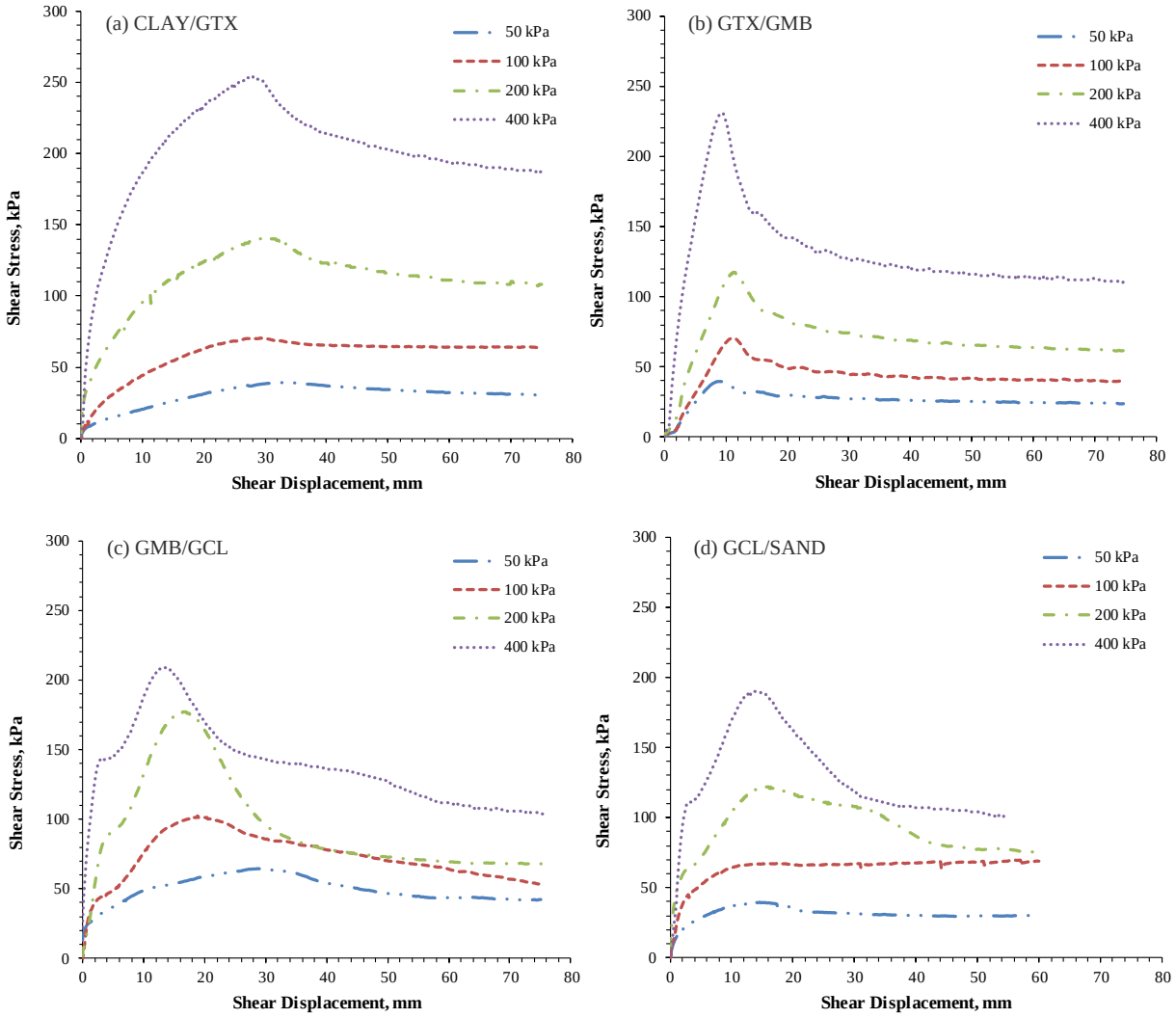

Figure 4-1 Shear stress versus shear displacement results for single interface tests.

4.2.2.1 CLAY/GTX Interface

The clay with a reddish-brown colour was used in this interface test. The geotextile (GTX), on the other hand, was a continuous filament of non-woven needle-punched geotextile with a thickness of 6.4 mm, made of 100 percent recycled polyester from discarded cool-drink bottles. Shearing was performed between these two specimens and **Figure 4-1**(a) shows the resulting shear stress versus shear displacement plots.

In general, it was observed from **Figure 4-1**(a) that as normal pressure increased, the rate of development of shear stress with shear displacement increased. At 50 kPa, the peak shear stress was mobilized at a shear displacement of 32.6 mm, whereas at 400 kPa, it was mobilized at a lower shear displacement of 27.7 mm as compared to 50 kPa, as can be seen in **Figure 4-1**(a) and **Table 4-1**. As such, it can be seen that the maximum (peak) shear resistance was mobilized faster at higher applied normal stresses as compared to lower normal stresses.

Table 4-1 Summary of the peak and LD strength obtained from single interface tests.

Normal stress (kPa)	Single Interface															
	CLAY/GTX				GTX/GMB				GMB/GCL				GCL/SAND			
	τ_p (kPa)	Δ_{s-p} (mm)	τ_{LD} (kPa)	Δ_{s-LD} (mm)	τ_p (kPa)	Δ_{s-p} (mm)	τ_{LD} (kPa)	Δ_{s-LD} (mm)	τ_p (kPa)	Δ_{s-p} (mm)	τ_{LD} (kPa)	Δ_{s-LD} (mm)	τ_p (kPa)	Δ_{s-p} (mm)	τ_{LD} (kPa)	Δ_{s-LD} (mm)
50	39.4	32.6	30.4	75.0	39.3	8.6	23.5	74.7	64.7	28.9	42.5	74.9	39.4	14.4	30.2	60.0
100	70.7	29.2	64.1	75.0	70.9	11.1	39.6	74.8	102.0	18.8	53.3	75.0	66.9	18.7	66.6	60.0
200	141.0	30.0	108.0	75.0	117.0	11.1	61.2	74.9	177.0	16.4	67.6	75.3	122.0	15.3	76.0	60.0
400	254.0	27.7	187.0	75.0	231.0	9.1	111.0	74.8	209.0	13.0	104.0	75.4	190.0	13.5	103.0	55.0

Moreover, before reaching a peak shear strength, the shear stresses increased gradually with cumulative shear displacement. Once the peak strength was reached, a gradual decrease in the shear strength occurred, with the shear displacement increasing further, a phenomenon known as strain-softening. The shear stresses eventually reached a steady-state interface shear stress value referred to as the large displacement (LD) strength, with increasing shear displacement. Under further shear displacement, the LD strengths remained stable until a shear displacement of 75 mm was reached to end the experiment. The results of the shear stress versus shear displacement relationship obtained in this test were very similar to other soil/geosynthetic interface test results published in past literature, (Chai & Saito, 2016; Evangelou & Markou, 2018; Feng & Cheng, 2014; Markou, 2018).

4.2.2.2 GTX/HDPE Interface

The 2 mm thick double textured HDPE produced from the virgin polymeric resin was the geomembrane (GMB) used for this test, (AKS Lining Systems (Pty) Ltd, 2019). The average surface asperity height of this GMB was 0.80 mm on one side (side tested against GTX) and 1.80 mm on the other. **Figure 4-1**(b) shows the investigated shear stress versus horizontal shear displacement relationships for the GTX/GMB interface tests.

It can be observed from **Figure 4-1**(b) that the shear strength curves followed a theoretical pattern of the shear stress versus shear displacement relationship for geosynthetic interfaces. This is contrary to the shear strength curves observed for the clay/GTX interface test in **Figure 4-1**(a), which followed a theoretical pattern of soil/geosynthetic interface tests. The development of interface shear stress increased with corresponding horizontal shear displacement until the maximum (peak) interface shear strength was reached. At all normal stress levels, a well-defined peak shear stress is observed at the failure points. The peak shear resistance at the lowest and highest applied normal stress of 50 and 400 kPa were mobilized at 8.6 and 9.1 mm of shear displacement, respectively. On the other hand, at normal stresses of 100 and 200 kPa, the maximum shear resistance was mobilized slower at 11.1 mm of shear displacement, as can be seen in **Table 4-1**.

The shear strengths of the tested samples decreased rapidly beyond the failure point until it reached a constant LD strength. During this stage, the test samples were considered to be going through a state of plastic deformation, a process referred to as strain-softening, (Buthelezi, 2017; Sikwanda, 2018). The strain-softening, which was associated with the dislocation movements

generated within the crystal structure of the tested specimens, became higher with increasing applied normal stress, as can be seen in **Figure 4-1**(b), (Sikwanda, 2018). These shear responses followed similar trends to the corresponding findings of other researchers,(Adeleke, 2020; Adeleke et al., 2019; Bacas et al., 2015, 2011; Buthelezi, 2017; Sikwanda, 2018).

4.2.2.3 GMB/GCL Interface

The EnviroFix® X2000 needle-punched geosynthetic clay liner (GCL) was used for these tests. The GCL was a composite reinforced product consisting of a soft non-woven geotextile cover layer, a sodium bentonite layer and a non-woven geotextile carrier layer from top to bottom, as explained in section 3.2.4. The soft non-woven GCL surface was the interface tested against the GMB side with an asperity height of 1.80 mm. **Figure 4-1**(c) presents the shear stress versus horizontal displacement relationships for the GMB/GCL interface tests performed.

From **Figure 4-1**(c), it can be observed that all GMB/GCL interface experiments resulted in a complete failure of the tested samples based on shear strength response observation. For any normal stress considered, the general trend of increasing shear stress with further horizontal displacement development to reach peak strengths was identified. However, at low normal stresses of 50 and 100 kPa, a gradual increase in shear stress was observed, whereas a rapid increase in shear stress to peak strength was detected at higher normal stresses of 200 and 400 kPa. Once the peak strengths were achieved, with continuous progress in horizontal displacement to approach the LD strengths, a gradual decrease in shear stresses occurred. All the tests ended automatically at a horizontal displacement of 75 mm, and the measured plots were all non-linear, as shown in **Figure 4-1**(c).

Furthermore, the curves showed distinct pre-peak stresses at all normal stresses, which can be described as a '*skew*' behaviour at various horizontal displacements. This skewed trend has been observed and attributed to the interaction between the test samples and the gripping surface (i.e. sandpaper) used by previous researchers, including Sikwanda (2018) and Soleimanian (2016). This skew behaviour was observed at shear displacements between 2 mm and 6 mm. It was anticipated that the gripping systems were fully involved with the tested specimens as the normal stress increased, thus developing a strong interlocking bond.

4.2.2.4 GCL/SAND Interface

The sand with a brownish colour was tested against the non-woven surface of the EnviroFix® X2000 needle punched GCL. Ultimately, shearing was performed between these two specimens and the resulting shear stress versus shear displacement graphs are shown in **Figure 4-1**(d).

Similar to previous test results, it can be observed that for any normal stress considered, the general trend of increasing shear stress with further horizontal displacement development to reach peak strengths was identified. However, at lower stresses of 50 and 100 kPa, the interface shear behaviour observed can be characterized by little to no post-peak shear strength softening or reduction. This behaviour was again obtained when these tests were repeated at the same applied normal stresses. This little to no post-peak shear strength softening behaviour was similar to what Fox & Stark (2004) and Rouncivell (2007) presented in their study.

Furthermore, these interface tests ended at a horizontal displacement of 60 mm, as opposed to automatic termination at a displacement of 75 mm. This was done to prevent the development of a second peak at lower stresses of 50 and 100 kPa. The peak shear resistance at the lowest and highest applied normal stresses of 50 and 400 kPa were mobilized at 14.4 and 13.5 mm of shear displacement, respectively. On the other hand, at normal stresses of 100 and 200 kPa, the maximum shear resistance was mobilized slower at shear displacements of 18.7 and 15.3 mm, respectively (see **Table 4-1**).

4.2.3 Double Interface Tests

In this section, a total set of three multi-layer shear tests consisting of double interfaces were carried out and the results are shown in the form of graphs. These tests were performed at a constant shear rate of 0.1 mm/min to a horizontal displacement of 75 mm, after 24 hours of hydration, at their respective shearing loads. The resultant shear stress versus horizontal displacement relationships of each of the three interface shear tests conducted are shown in **Figure 4-2**. Also, **Table 4-2** presents a quantitative summary of the peak and LD strength values obtained from the double interface tests.

4.2.3.1 CLAY/GTX/GMB Interface

In this multi-layer interface test, the GMB (clamped to the bottom shear box) was sheared against the GTX (placed unclamped on top of GMB) and clay (placed and compacted into the top shear box). Similar steps to those carried out in the CLAY/GTX interface setup were followed in placing and compacting the clay in the top shear box. Eventually, shearing was performed between the three specimens and **Figure 4-2** shows the resulting shear stress versus shear displacement of the interface test.

It was observed, in **Figure 4-2**(a) that the measured shear stress responses for this interface test were all non-linear for all normal stress applied. It can be seen that the shear stress responses obtained at normal stresses of 50, 100 and 200 kPa were similar to those obtained at the CLAY/GTX single interface test. This could be an indication that shearing took place in particular along the CLAY/GTX interface at those three applied stresses, as opposed to the GTX/GMB interface. The interface shear behaviour detected can be characterized as hyperbolic with little to no strain-softening or reduction of post-peak shear strength. This behaviour was again achieved when these tests were repeated at the same normal applied stresses. This was similar to the results presented by Fox & Stark (2004) and Rouncivell (2007) in their studies.

At the highest normal stress of 400 kPa, the shear stress increased with an increase in shear displacement, exhibiting a ‘smooth’ pre-peak strength behaviour until reaching a peak value. However, once the peak strength was mobilized, the shear stress decreased rapidly with continuous progress in horizontal shear displacement to approach the LD strengths. This “*rapid*” decrease in the shear stress after pre-peak behaviour could have been attributed to the transfer of the shear stress within the system. It was anticipated that, similar to other normal stresses, shearing would take place along the CLAY/GTX interface. However, the shear stress could have

been transferred to the GTX/GMB interface once the pre-peak strength was mobilized, hence the rapid reduction in shear stress at the post-peak stage.

4.2.3.2 GTX/GMB/GCL Interface

This interface test consisted only of three geosynthetics, with the GTX clamped to the bottom shear box, the GMB placed unclamped on top of the GTX and the GCL clamped to the top shear box, as was shown in **Figure 3-14**(a). The GTX was sheared against the GMB side with 1.80 mm asperity height, whereas the GCL was sheared against the GMB side with 0.80 mm asperity height. The experiments were carried out after test samples were hydrated for 24 hours at a constant shear rate of 0.1 mm/min to a horizontal displacement of 75 mm. The shear stress versus horizontal displacement relationships for this GTX/GMB/GCL multi-layer interface test are presented in **Figure 4-2**(b).

In general, it was observed from **Figure 4-2**(b) that as applied normal stress increased, there was a rise in the rate of development of shear stress with horizontal displacement. Moreover, with rising horizontal displacement before reaching a peak shear strength, the shear stresses of all plots grew rapidly. Once the peak strength was reached, with further cumulative horizontal shear displacement, a gradual reduction of the shear strength occurred. It was also observed that there was a drop-off (strain-softening) in shear stresses following the failure points. It was noticed that with cumulative peak strengths of the shear responses, strain-softening became clearer (see **Figure 4-2**). The peak shear resistance at the applied normal stress was mobilized faster at lower normal stresses as compared to higher normal stresses. At 50 and 100 kPa, the maximum shear resistance was mobilized at 8.4 and 12.0 mm of shear displacement, respectively. On the other hand, at normal stresses of 200 and 400 kPa, the maximum shear resistance was mobilized slower at 16.2 and 18.3 mm of shear displacement, as can be seen in **Table 4-2**.

Table 4-2 Summary of the peak and LD strength obtained from double interface tests.

Normal stress (kPa)	**Double Interface**											
	CLAY/GTX/GMB				GTX/GMB/GCL				GMB/GCL/SAND			
	τ_p (kPa)	Δ_{s-p} (mm)	τ_{LD} (kPa)	Δ_{s-LD} (mm)	τ_p (kPa)	Δ_{s-p} (mm)	τ_{LD} (kPa)	Δ_{s-LD} (mm)	τ_p (kPa)	Δ_{s-p} (mm)	τ_{LD} (kPa)	Δ_{s-LD} (mm)
50	47.4	34.6	41.9	75.0	24.7	8.4	14.3	75.0	30.1	8.8	34.4	74.9
100	79.7	31.2	65.9	75.0	50.7	12.0	25.3	74.9	66.0	35.2	41.7	75.1
200	137.0	32.9	121.0	74.9	117.0	16.2	55.7	74.9	139.0	18.2	100.0	75.0
400	211.0	30.6	117.0	75.0	210.0	18.3	95.8	74.7	191.0	14.6	50.6	74.9

4.2.3.3 GMB/GCL/SAND Interface

In this section, the shear stress-horizontal displacement behaviour of the GMB/GCL/SAND interface is presented and discussed. The GMB was clamped to the bottom shear box, with the GCL placed unclamped on top of the GMB. Similar to the GCL/SAND single interface, the sand was placed in the top shear box and compacted using a steel tamper (see **Figure 3-14**(b)).

It was observed in **Figure 4-2**(c) that at the lower normal applied stresses of 50 and 100 kPa, a slight strain-softening response that is hyperbolic was observed. At higher applied normal stresses of 200 to 400 kPa, however, significant strain-softening responses were detected. This response may have been attributed to the transfer of the shear stress within the system. At lower normal stresses, shearing could have occurred between the GCL/SAND interface, whereas at higher normal stresses, shearing could have occurred at the GMB/GCL interface. Additionally, there was a rapid decrease in strength at a normal stress of 400 kPa at the post-peak stage, whereas only a slight decrease in shear stress was observed at 200 kPa.

Moreover, the curves showed distinct pre-peak stresses at higher normal stresses (i.e. 200 and 400 kPa), which can be described as a '*skew*' behaviour at various horizontal displacements. This skewing behaviour was observed at shear displacements between 2 mm and 6 mm. The interaction between the test samples and the gripping surface (i.e. sandpaper) was attributed to this skewing behaviour by previous researchers., (Adeleke, 2020; Sikwanda, 2018; Soleimanian, 2016).

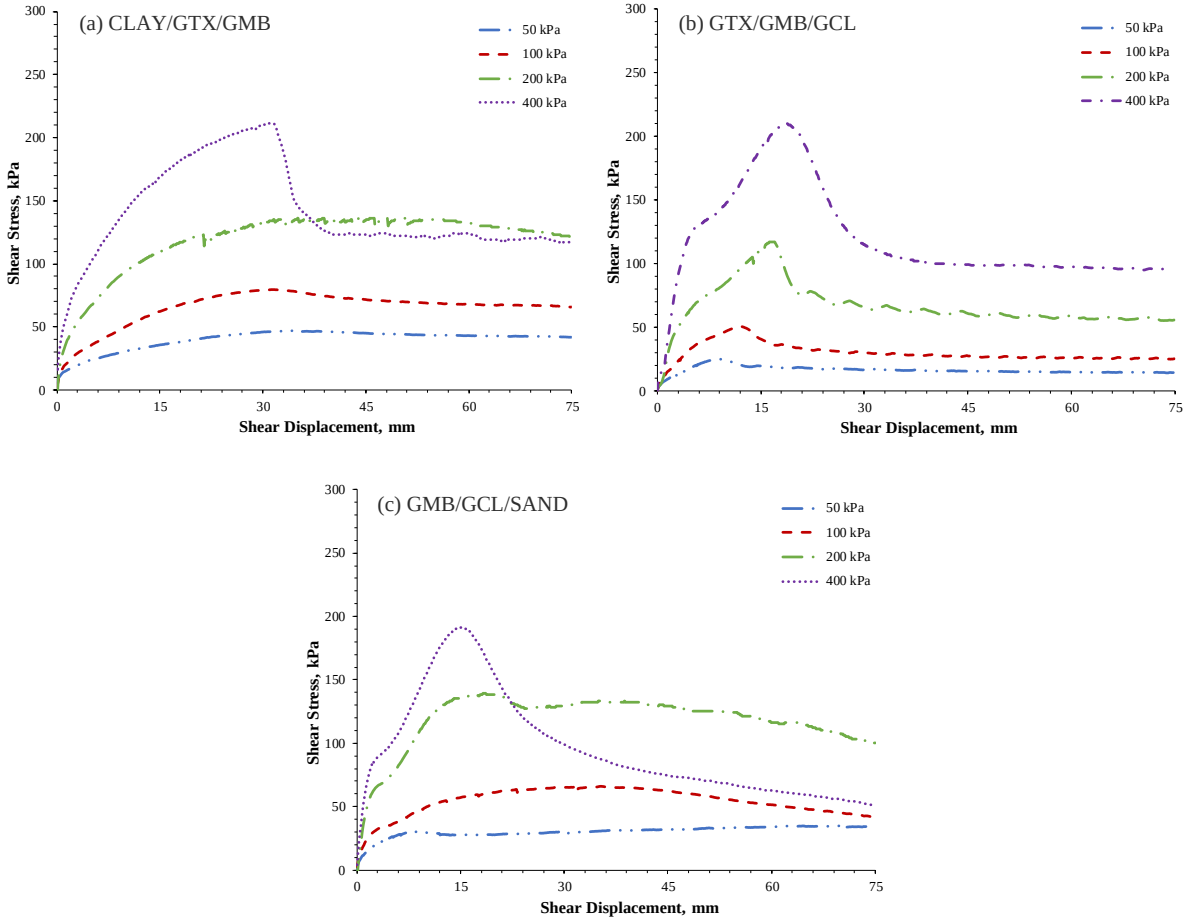

Figure 4-2 Shear stress versus shear displacement results for double-interface tests.

4.2.4 Triple Interface Tests

Two sets of multi-layer interface shear tests consisting of triple interfaces were conducted, and the results are presented in terms of shear displacement graphs. These interface tests involved testing the three interfaces simultaneously as a system. Similarly, these tests, at their respective shear loads, were carried out at a constant shear rate of 0.1 mm/min to a horizontal displacement of 75 mm after 24 hours of hydration. **Figure 4-3** illustrates the resulting shear stress versus horizontal displacement relationships of each of the two interface shear tests performed. Moreover, a quantitative summary of the peak and LD strength values obtained from the triple interface tests is provided in **Table 4-3**.

4.2.4.1 CLAY/GTX/GMB/GCL Interface

This interface test involved soil/geosynthetic interfaces consisting of three geosynthetics, i.e. GTX, GMB and GCL, and one soil, which was classified as clay according to the USCS classification system. In this test, the GCL was clamped to the bottom shear box and both the GTX and GMB were placed unclamped on top of the GCL, to allow failure to occur at the weakest interface during shearing. The clay was placed in the top shear box and compacted 40 times, using a steel hand tamper (see **Figure 3-12**) to achieve the specified moisture content and density. Eventually, shearing was conducted and the resultant shear stress versus horizontal displacement is shown in **Figure 4-3**(a).

It was observed from **Figure 4-3**(a) that the plots showed a smooth hyperbolic gradient in the "pre-peak" stage that was similar to that observed for the CLAY/GTX single interface test and the CLAY/GTX/GMB double interface test. This showed that shearing could have taken place along the interface of the CLAY/GTX, which could have made it the weakest interface in this configuration. In order to reach the failure points, the shear strength plots increased with increasing normal stresses. The peak shear resistance at 50 kPa was mobilized around 20.0 mm of shear displacement, while for 100, 200 and 400 kPa the shear strength was mobilized between 39.1 mm and 46.2 mm, as can be seen in **Table 4-3**. In this interface test, the peak shear strengths were mobilized slower compared to single and double-interface tests. The shear stress in the interface test examined decreased smoothly to a stable LD strength under further development in horizontal displacement once the peak strengths were mobilized.

Table 4-3 Summary of the peak and LD strength obtained from triple and quadruple interface tests.

Normal stress (kPa)	Triple Interface								Quadruple Interface			
	CLAY/GTX/GMB/GCL				GTX/GMB/GCL/SAND				CLAY/GTX/GMB/GCL/SAND			
	τ_p (kPa)	Δ_{s-p} (mm)	τ_{LD} (kPa)	Δ_{s-LD} (mm)	τ_p (kPa)	Δ_{s-p} (mm)	τ_{LD} (kPa)	Δ_{s-LD} (mm)	τ_p (kPa)	Δ_{s-p} (mm)	τ_{LD} (kPa)	Δ_{s-LD} (mm)
50	28.0	19.9	17.5	75.0	68.8	24.6	64.6	74.8	48.8	44.5	45.3	75.5
100	74.5	41.8	61.2	75.0	89.7	22.8	85.5	75.0	76	22.9	41.5	75
200	133.0	39.1	72.5	74.9	149.0	22.3	98.7	75.0	129	27.7	43	74.9
400	224.0	46.2	134.0	74.9	213.0	19.7	77.2	74.6	154.0	20.9	52.7	75

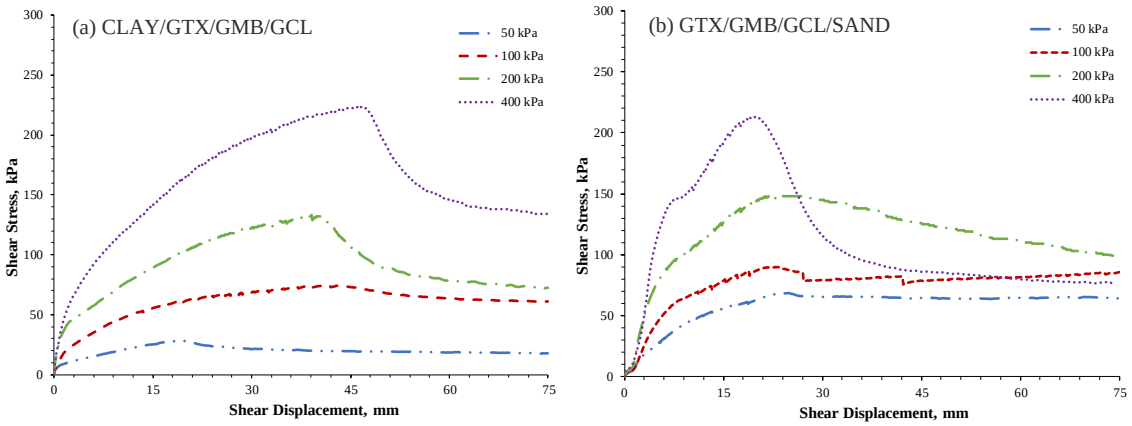

Figure 4-3 Shear stress versus shear displacement results for triple-interface tests.

At lower normal stresses of 50 and 100 kPa, only a slight decrease in post-peak shear stress was observed. On the other hand, a gradual decrease in shear stresses was observed at applied stresses of 200 and 400 kPa, with continuous progress in horizontal displacement to approach the LD strengths. The observed difference in the decrease in strain-softening can be attributed to the normal stress applied. The higher the applied normal stress, the higher the strain-softening became. This strain-softening behaviour was associated with the dislocation movements generated within the crystal structure of the tested soil and geosynthetic specimens, (Sikwanda, 2018). These outcomes of the relationship between shear stress and shear displacement were found to be very similar to the results of other soil/geosynthetic interface tests published in previous literature, (Chai & Saito, 2016; Evangelou & Markou, 2018; Feng & Cheng, 2014; Markou, 2018).

4.2.4.2 GTX/GMB/GCL/SAND Interface

This interface test involved the shearing of all three geosynthetics in a sandwich along with sand. The GTX was clamped to the bottom shear box and the GMB and GCL were both placed unclamped on top of the GTX to allow failure to occur during shearing at the weakest interface. The sand was then placed in the top shear box and compacted by a steel hand tamper 20 times (see **Figure 3-12**) to achieve the specified moisture content and density. Shearing was eventually performed, and **Figure 4-3**(b) shows the resulting shear stress versus horizontal displacement graph.

It was found, from **Figure 4-3**(b), that general soil/geosynthetic and geosynthetic/geosynthetic interface patterns were exhibited in the plots. As a result, little to no tension will develop within the layers. Observations during and after testing showed that shearing within the system could have occurred along with the GCL/SAND interface at the lowest stress of 50 kPa. At a normal stress of 100 kPa, it could be said that shearing originally occurred along with the GCL/SAND interface, but, as can be seen in **Figure 4-3**(b), at a shear displacement of 27 mm, a transfer of the shearing interface within the system could have occurred from the GCL/SAND interface to the GMB/GCL interface. It was again observed at a shear displacement of 65 mm that a similar transfer in the interface being sheared from the GMB/GCL interface to the GTX/GMB interface

could have occurred. According to Swan & Stark (2019), when conducting a multi-layer interface shear test, once the system begins to shear (fail), the shear stress gets transferred within the system from one interface to another. However, it was noted that shearing could have taken place along the GCL/SAND and GTX/GMB interfaces at the applied normal stresses of 200 kPa and 400 kPa respectively. The resulting stress-displacement plot at 400 kPa exhibited a similar trend to that of the GTX/GMB/GCL double interface (see **Figure 4-2**(b)).

Furthermore, the shear stress responses exhibited a skewing behaviour at the "pre-peak" phase. At the highest stress of 400 kPa, this skewing trend was most visible, whereas only slight skewing was observed at all the other normal stresses. It was examined that after the peak strengths were mobilized, only a slight decrease in the shear stresses (strain-softening) was experienced before reaching LD strength at normal stresses of 50, 100, and 200 kPa. Conversely, a rapid decrease in shear stress was detected at the highest normal stress of 400 kPa.

4.2.5 Quadruple Interface Test

Interfaces are simultaneously tested in a multi-interface test and this allows failure to occur on the weakest interfaces as anticipated in the field. Hence, instead of developing combined peak and LD failure envelopes from the results of several single interface tests, the peak and LD design strengths are determined directly from a one multi-layer interface failure envelope. In this section, all the single interfaces considered in the entire simulated composite liner were tested at the same time to form a multi-layer interface consisting of quadruple interfaces (see **Figure 3-15**). Similarly, this test was carried out at a constant shear rate of 0.1 mm/min to a horizontal displacement of 75 mm after 24 hours of hydration. **Figure 4-4** illustrates the resulting shear stress versus horizontal displacement relationships of the interface shear test performed.

4.2.5.1 CLAY/GTX/GMB/GCL/SAND Interface

In this section, the shear stress versus horizontal shear displacement behaviour of the CLAY/GTXGMB/GCL/SAND interface was presented and discussed. As was shown in **Figure 3-15**, this interface involved a system consisting of three geosynthetics, i.e. GTX, GMB and GCL, and two soils, namely clay and sand. In this test, the sand was placed in the bottom shear box since it was less compressible, and the clay was placed in the upper shear box due to being more compressible. Eventually, shearing was carried out and in **Figure 4-4** the resulting shear stress versus horizontal displacement is shown.

All the interfaces considered in the single interface test configuration (see **Figure 4-1**) were included in the shear stress responses for the multi-layer quadruple interface test presented in **Figure 4-4**. The shear strength graphs showed that before reaching the peak strength, all experiments conducted showed a pre-peak strength with increasing horizontal displacement, regardless of the test configuration, for all the single (see **Figure 4-1**) and multi-layer quadruple interface test (see **Figure 4-4**) considered. In both the single and multi-layer interface test, the strain softening behaviour was observed at higher stresses of 200 and 400 kPa to achieve a steady-state strength beyond the peak strength. However, the interface shear behaviour observed can be characterised by little to no post-peak shear strength softening or reduction at lower

stresses of 50 and 100 kPa. The disparity in strain-softening observed can be due to the normal stress applied, as a result the strain-softening increased as the applied normal stress increased. The disparity in strain-softening observed can be due to the normal stress applied. The strain-softening increased as the applied normal stress increased. Therefore, the dislocation movements created within the crystal structure of the tested soil and geosynthetic specimens were linked to the strain-softening behaviour, (Sikwanda, 2018). As observed in **Figure 4-1** and **Figure 4-4**, this was evident in all experiments conducted. A quantitative summary of the peak and LD strength values obtained from the quadruple interface tests are presented in **Table 4-3**.

From the 'pre-peak' stage of **Figure 4-4**, it was observed that the plots displayed 'smooth' shear stress development curves of a hyperbolic nature as a result of shearing occurring along the CLAY/GTX interface at lower normal stresses of 50 and 100 kPa. On the other hand, as a result of shearing occurring along the SAND/GCL, the "pre-peak" stage at higher normal stresses of 200 and 400 kPa showed "skewing" behaviour at shear displacements between 3 mm and 7 mm, respectively. At 100 kPa, a phenomenon known as “stick-slip” behaviour was observed and it can be attributed to the inadequacy of the gripping system, i.e., slippage between the test specimen and gripping surfaces, this is according to Soleimanian (2016). No strain-softening behaviour was observed at 50 kPa, whereas slight strain-softening was exhibited at 100 kPa. Before reaching LD strength at normal stresses of 200 and 400 kPa, a rapid decrease in the shear stresses (strain-softening) was experienced.

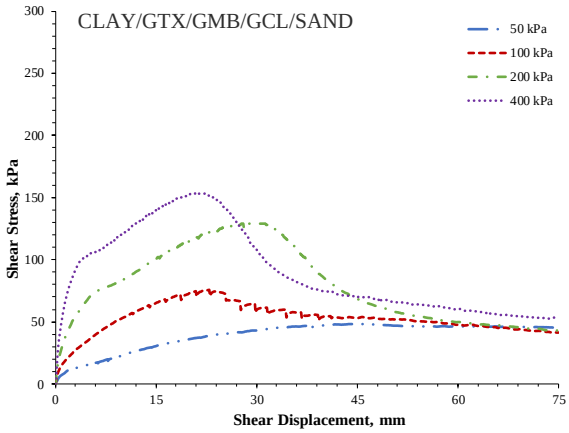

Figure 4-4 Shear stress versus shear displacement results for quadruple-interface tests.

4.3 Shear Stress versus Normal Stress

4.3.1 Introduction

According to ASTM D5321, a minimum of three test points is required for the development of a Mohr-Coulomb shear strength envelope of soil/geosynthetics or geosynthetic/geosynthetic interfaces at three distinct normal loads. In this study, single and multi-layer interface tests were carried out at four applied normal stresses, and the respective peak and large displacement (LD) interface shear stresses were obtained and presented in **Table 4-1** to **Table 4-3**. In this section, failure envelopes using a best-fit line were produced for each respective single and multi-layer

interface from the peak and LD shear stress values obtained. Additionally, multi-layer interface failure envelopes were compared to the combination peak and LD strength failure envelopes, which were constructed using segments of single interface strength envelopes representing the lowest peak or LD strength for a range of normal stresses applied.

4.3.2 Single interfaces

The peak and LD shear strength values of single interfaces, read-off from **Table 4-1**, are connected through best-fit straight lines with the corresponding applied normal stress in **Figure 4-5**. Each linear envelope was characterized using Equation 3-1 to determine the interface friction angle (δ) and apparent adhesion (c_α) parameters. The inclination of those lines to the horizontal axis corresponded to the friction angle of the shear resistance of the tested interfaces, whereas the vertical intercept represented the adhesion. In **Table 4-4**, the respective interface friction angles and adhesions obtained from **Figure 4-5** are presented. This is followed by a comparative analysis, as well as a discussion summary. Figure **4-5**(a) showed that the weakest interface was transferred between the various interfaces tested as the normal stresses applied increased. The CLAY/GTX interface exhibited the lowest peak shear stress at applied normal stresses below 50 kPa, as such it was regarded as the weakest interface. However, as the applied stress increased beyond 50 kPa, the peak shear stress of the CLAY/GTX interface increased and as a result, at higher applied stresses, it becomes the strongest interface. It can be noted that the GCL/SAND interface is the weakest interface at pressures beyond 100 kPa. The LD shear stresses of the four single interfaces tested were also demonstrated in **Figure 4-5**(b). It was found that at lower applied stresses, the GTX/GMB exhibited the lowest LD shear stress, thus making it the weakest interface. In addition, the weakest interface was transferred from the GTX/GMB to the GCL/SAND interface as the applied stresses increased beyond 300 kPa. The strongest interface at stresses above 100 kPa was observed to be the CLAY/GTX.

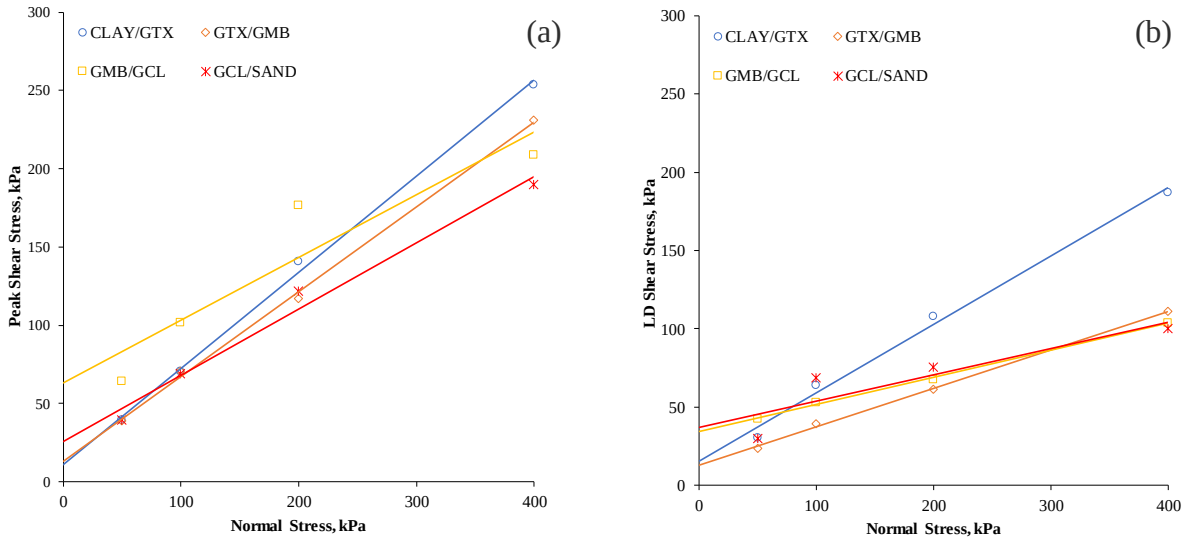

Figure 4-5 Shear stress versus normal stress for single interfaces: (a) peak and (b) LD shear stress.

From Figure **4-5**, the peak and LD failure envelopes were determined for the four single interfaces in terms of strength parameters and summarized in **Table 4-4**. The respective results were calculated by analysing the best-fit straight line governed by the Mohr-Coulomb failure envelope equation.

It was clear from **Table 4-4** that there is a difference between the four single interfaces in friction angle and apparent adhesion. The CLAY/GTX interface exhibited the highest peak and LD friction angles as compared to the other three single interfaces. As was observed in **Figure 4-5**, this interface was considered to be the strongest interface. The peak and LD interface friction angles obtained for this interface were 31.5° and 23.5° respectively. On the other hand, the GMB/GCL and GCL/SAND interfaces exhibited the lowest peak and LD interface friction angles, respectively. The GMB/GCL interface exhibited the lowest friction angle in terms of peak shear strength, thus making it the weakest interface. The GCL/SAND interface, however, showed the lowest interface friction angle in terms of LD shear strength, which makes it the weakest interface.

Based on these results, it is therefore safe to conclude that the GCL/SAND interface is in terms of peak shear strength, the weakest interface among all the single interfaces tested. On the other hand, at normal stresses below 300 kPa, the GTX/GMB can be considered as the weakest interface in terms of LD shear strength, with the GCL/SAND being the weakest interface at stresses higher than 300 kPa.

Table 4-4 Summary of peak and LD shear strength parameters of single interfaces.

Interface Configuration	Peak shear strength parameters		LD shear strength parameters	
	δ_p (°)	$c_{\alpha\text{-}p}$ (kPa)	δ_{LD} (°)	$c_{\alpha\text{-}LD}$ (kPa)
CLAY/GTX	31.5	11.1	23.5	15.7
GTX/GMB	28.4	13.0	13.8	12.8
GMB/GCL	21.8	63.0	9.8	34.4
GCL/SAND	22.9	25.9	9.5	37.2

* δ_p & δ_{LD} Peak and LD Interface friction angle respectively, $c_{\alpha\text{-}p}$ & $c_{\alpha\text{-}LD}$ Peak and LD apparent adhesion respectively.

4.3.3 Double Interfaces

This section discusses the peak and LD shear stress relationships against the normal stresses applied for the triple interface tests conducted. A comparison between the Mohr-Coulomb triple interface failure envelopes, which were plotted using data from **Table 4-2**, and the combination failure envelopes for single interface tests is shown in **Figure 4-6** to **Figure 4-8**. For a range of normal stresses applied, the combination of failure envelopes was constructed using segments of single interface strength envelopes representing the lowest peak or LD strength. The summary of the results obtained from **Figure 4-6** to **Figure 4-8** is presented quantitatively in **Table 4-5** to **Table 4-7**, followed by a comparative analysis and a summary of the discussions.

4.3.3.1 CLAY/GTX/GMB Interface

For the CLAY/GTX/GMB interface, the values of peak and LD shear stress at failure were plotted against the normally applied stress in **Figure 4-6**, and the best-fit straight lines fitted through the respective results. Moreover, using segments of the CLAY/GTX and GTX/GMB single interface strength envelopes representing the lowest peak or LD strength for comparative purposes, the combination failure envelope was constructed and plotted. The inclination of the failure envelopes to the horizontal axis corresponds to the interface friction angle (δ), whereas the intercept on the vertical axis gives the apparent adhesion, denoted by (c_α). For the different failure envelopes, the peak and LD shear strength parameters were obtained and are summarised in **Table 4-5**.

The peak combination strength envelope from the single interface tests is compared in **Figure 4-6**(a) with the corresponding peak strength envelope from the CLAY/GTX/GMB double interface test. It was observed that for single-interface tests, the peak strengths are slightly lower for the range of normal stresses considered, particularly at low normal stresses. This difference may be attributed to isolated single-interface tests that are not affected by surrounding geosynthetics.

Figure 4-6(b) presents comparisons of LD strength envelopes from the single and double interface tests. For the single and CLAY/GTX/GMB double interface test results, this figure shows a bigger difference in the LD envelopes than the peak envelopes. The double interface test resulted in higher LD envelopes than the single test interface. In the double interface tests, the higher LD strengths are consistent with higher peak strengths in the double interface tests shown in **Figure 4-6** (a) and may be due to differences in shear displacement between single and double interface tests on the critical interface. The peak and LD failure envelopes for single and double interfaces were determined in terms of strength parameters from **Figure 4-6** and summarized in **Table 4-5**.

It was evident from **Table 4-5** that there was a difference in the interface friction angle between the two failure envelopes. In comparison to the CLAY/GTX/GMB envelope, the combination envelope showed a higher peak and LD interface friction angle. The peak and LD interface friction angles obtained were 24.7º and 11.7º for the combination envelope and 28.5° and 13.8° for the CLAY/GTX/GMB envelope, respectively. For the two investigated failure envelopes, this represented a percentage difference of about 13 % and 15 % in peak and LD friction angles, respectively. This implied that the double interface test produced more conservative shear strength parameters as compared to single interfaces.

Table 4-5 Summary of peak and LD shear strength parameters of CLAY/GTX/GMB interface.

Interface Configuration	Peak shear strength parameters		LD shear strength parameters	
	δ_p (°)	$c_{\alpha\text{-}p}$ (kPa)	δ_{LD} (°)	$c_{\alpha\text{-}LD}$ (kPa)
CLAY/GTX/GMB Envelope	24.7	32.5	11.7	47.7
CLAY/GTX/GMB Combination Envelope	28.5	12.9	13.8	12.8

* δ_p & δ_{LD} Peak and LD Interface friction angle respectively, $c_{\alpha\text{-}p}$ & $c_{\alpha\text{-}LD}$ Peak and LD apparent adhesion respectively.

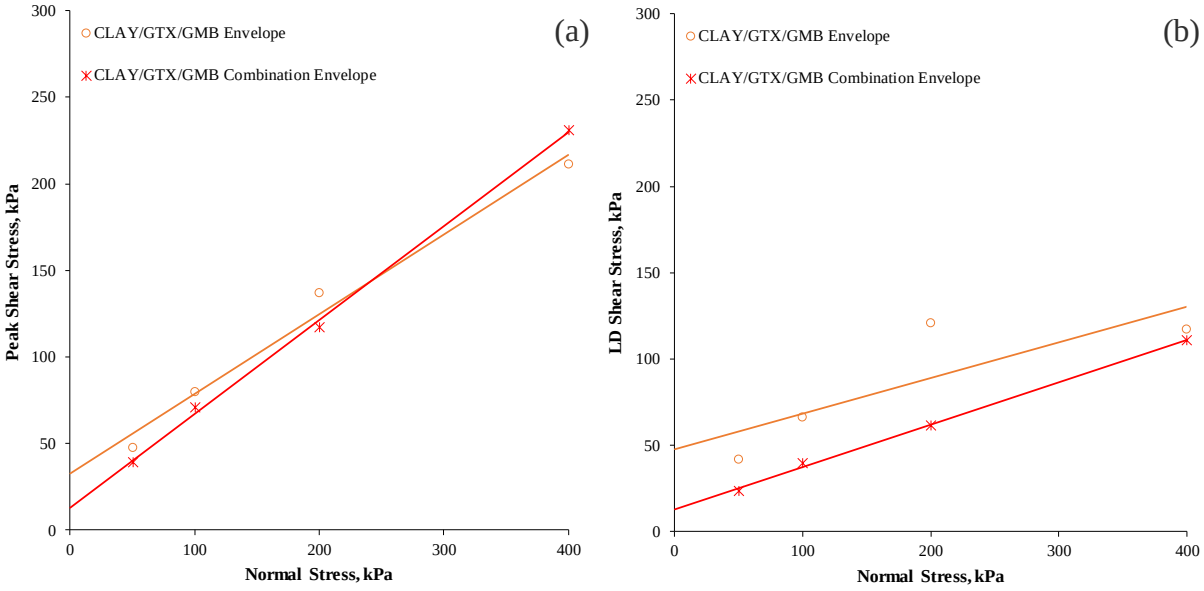

Figure 4-6 Shear stress versus normal stress for CLAY/GTX/GMB interface: (a) peak and (b) LD.

In **Table 4-5**, the apparent adhesion values of two failure envelopes were also presented. It was noted that the peak apparent adhesion value of the CLAY/GTX/GMB envelope was 32.5 kPa, which is 60 % greater than the value obtained from the combination envelope. In addition, a higher adhesion value was mobilized by the CLAY/GTX/GMB envelope at LD strength compared to the combination envelope (see **Table 4-5**). Based on these results, it is therefore safe to conclude that the double interface yielded a conservative estimate of the peak and LD shear strength, as compared to the single interface.

4.3.3.2 GTX/GMB/GCL Interface

The values of peak and LD shear stress at failure were plotted against the normal applied stress in **Figure 4-7** for the GTX/GMB/GCL interface, and the best-fit straight lines fitted through the respective results. Similarly, the interface friction angle (δ) corresponds to the inclination of the failure envelopes to the horizontal axis, whereas the intercept on the vertical axis gives an apparent adhesion, denoted by (c_a).

The peak combination strength envelope from two single interface tests, i.e. GTX/GMB and GMB/GCL, is compared in **Figure 4-7**(a) with the corresponding peak strength envelope from the GTX/GMB/GCL double interface test. For the double interface test, the peak strengths were observed to be slightly lower for the range of normal stresses considered, especially at low normal stresses. However, the peak shear stress of the double interface increased, as the applied stress increased beyond 300 kPa.

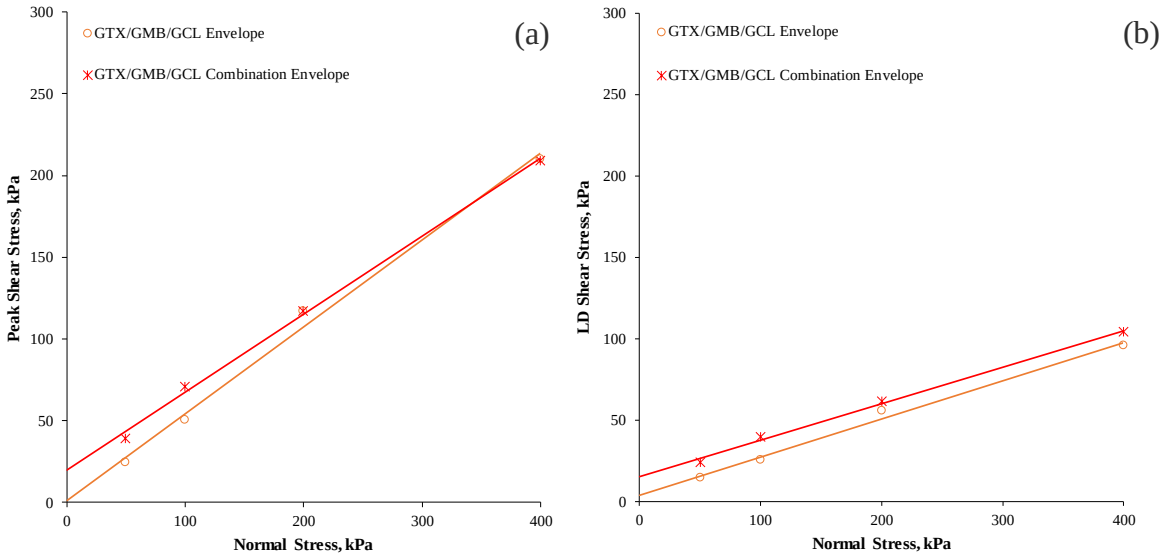

Figure 4-7 Shear stress versus normal stress for GTX/GMB/GCL interface: (a) peak and (b) LD.

Comparisons of LD strength envelopes from the single and double interface tests are presented in **Figure 4-7**(b). This figure shows a similar difference in the LD envelopes as in the peak envelopes for the single and double interface test results, which remains the same as the increase in normal stress. The single interface test combination envelope resulted in higher LD envelopes than the double interface test. The higher LD strengths are consistent with higher peak strengths in the combination envelope from single interface tests, as was shown in **Figure 4-7**(a). For further comparison and discussion, the parameters of peak and LD shear strength for the different failure envelopes were obtained and are summarized in **Table 4-6**.

The results, as detailed in **Table 4-6**, show that from the GTX/GMB/GCL interface envelope, the measured peak and LD interface friction angles were higher than that of the combination envelope. A peak friction angle of 28.0° was achieved by the GTX/GMB/GCL interface envelope, whereas the combination envelope achieved a peak friction angle of 25.5°. Also as compared to the 12.7° achieved with the combination envelope, the GTX/GMB/GCL interface envelope had a slightly larger LD interface friction angle of 13.2°. The percentage difference in both the peak and LD interface friction angle for the GTX/GMB/GCL interface envelope and combination envelope was 9.0% and 4.0%, respectively.

Table 4-6 Summary of peak and LD shear strength parameters of GTX/GMB/GCL interface.

Interface Configuration	Peak shear strength parameters		LD shear strength parameters	
	δ_p (°)	$c_{\alpha\text{-}p}$ (kPa)	δ_{LD} (°)	$c_{\alpha\text{-}LD}$ (kPa)
GTX/GMB/GCL Envelope	28.0	0.8	13.2	3.8
GTX/GMB/GCL Combination Envelope	25.5	19.7	12.7	14.9

* δ_p & δ_{LD} Peak and LD Interface friction angle respectively, $c_{\alpha\text{-}p}$ & $c_{\alpha\text{-}LD}$ Peak and LD apparent adhesion respectively.

Table 4-6 also included the obtained apparent adhesion values from the plotted failure envelopes. The comparison of the results presented shows that the peak adhesion values of the combination envelope were greater than those of the GTX/GMB/GCL envelope. The combination and the GTX/GMB/GCL envelope, respectively, had peak adhesion values of 19.7 kPa and 0.8 kPa, a difference of about 96 %. The very low adhesion value obtained by the GTX/GMB/GCL envelope implies that during shear testing, the interface experienced no adhesion. Also, from the combination envelope, the LD apparent adhesion value of 14.9 kPa was measured, while from the GTX/GMB/GCL envelope, 3.8 kPa was obtained.

4.3.3.3 GMB/GCL/Sand Interface

Figure 4-8 shows the peak and LD failure envelope derived from the direct shear tests on the GMB/GCL/SAND interface and the combination envelope derived from the minimum peak and LD shear stress values of the GMB/GCL and GCL/SAND single interface tests. Similarly, through the respective results, best-fit straight lines were fitted and the corresponding interface angle of friction (δ) and apparent adhesion (c_α) values were determined.

In **Figure 4-8**, similar peak strength envelopes were observed at lower normal stresses. However, the peak strength of the GMB/GCL/SAND envelope became slightly higher than that of the combination envelope beyond normal stresses of 100 kPa. On the other hand, compared to the GMB/GCL/SAND envelope, the combination envelope exhibited lower LD strength at lower applied stresses. Nevertheless, since the normal stresses increased beyond 150 kPa, the GMB/GCL/SAND envelope tends to show lower LD shear strength, indicating that the GMB/GCL/SAND interface generates more conservative LD strength at higher stresses. As shown in **Table 4-7**, the LD interface friction angles and adhesions were determined similarly to the peak shear strength characteristics.

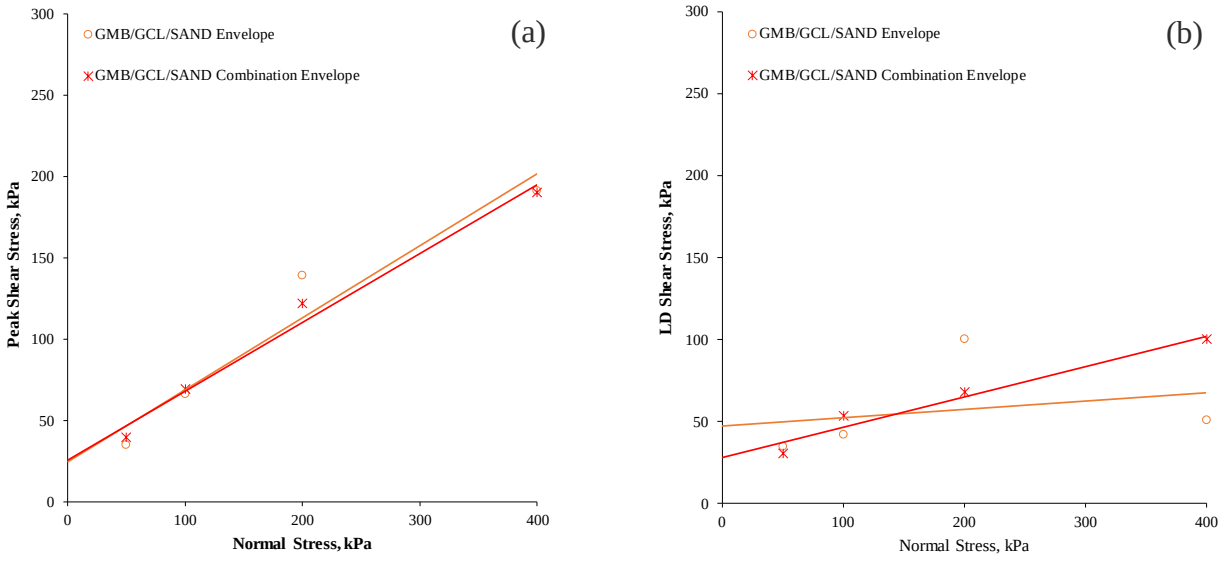

Figure 4-8 Shear stress versus normal stress for GMB/GCL/SAND interface: (a) peak and (b) LD.

Comparable peak angles of friction were observed between the envelopes of failure in **Table 4-7**. A higher peak friction angle than the combination envelope has been achieved by the GMB/GCL/SAND envelope. The respective peak friction angles were 23.9° and 22.9° from the GMB/GCL/SAND envelope and combination envelope, which is a percentage difference of around 4 %. It is therefore safe to conclude that the double interface tests essentially yielded the same maximum strength envelope as the single interface tests, which is consistent with similar findings in Stark et al. (2015). The LD friction angle for the GMB/GCL/SAND envelope was found to be significantly smaller compared with the combination envelope, unlike the friction angles obtained at the peak. An LD friction angle of 2.9° was obtained from the GMB/GCL/SAND envelope, which is 72 % lower than the 10.5° mobilized by the combination envelope. The adhesion results were also presented in **Table 4-7** and similar to the peak friction angles, the peak adhesion values were also comparable. The GMB/GCL/SAND envelope yielded a slightly lower adhesion (24.7 kPa) than the combination envelope which had an adhesion of 25.9 kPa. On the other hand, based on the observation, an apparent difference in the LD adhesion between the GMB/GCL/SAND envelope and the combination envelope was noticed. At LD strength, the GMB/GCL/SAND envelope produced high adhesion values compared to the combination envelope values.

Table 4-7 Summary of peak and LD shear strength parameters of GTX/GMB/GCL interface.

Interface Configuration	Peak shear strength parameters		LD shear strength parameters	
	δ_p (°)	$c_{\alpha\text{-}p}$ (kPa)	δ_{LD} (°)	$c_{\alpha\text{-}LD}$ (kPa)
GMB/GCL/SAND Envelope	23.9	24.7	2.9	47.2
GMB/GCL/SAND Combination Envelope	22.9	25.9	10.5	28.1

* δ_p & δ_{LD} Peak and LD Interface friction angle respectively, $c_{\alpha\text{-}p}$ & $c_{\alpha\text{-}LD}$ Peak and LD apparent adhesion respectively.

4.3.4 Triple Interfaces

Similarly, in this section the peak and LD shear stress relationships against the normal stresses applied of the triple interface tests conducted were discussed. A comparison between the Mohr-Coulomb failure envelope of the triple interface tests, which were plotted using data from **Table 4-3**, and the combination failure envelopes of the corresponding single interface tests is shown in **Figure 4-9** to **Figure 4-10**. For a range of normal stresses applied, the combination failure envelopes were constructed using segments of single interface strength envelopes representing the lowest peak or LD strength values. The summary of the results obtained from **Figure 4-9** to **Figure 4-10** is presented quantitatively from **Table 4-8** to **Table 4-9**, followed by a comparative analysis and a summary of the discussions.

4.3.4.1 CLAY/GTX/GMB/GCL Interface

In **Figure 4-9**, the failure envelopes of the CLAY/GTX/GMB/GCL triple interface in terms of peak interface shear strength parameters and LD strength parameters are shown. For further comparison, the combination failure envelope was plotted using the minimum peak and LD shear stress values of the CLAY/GTX, GTX/GMB and GMB/GCL single interface tests generated

from the graphs in section 4.2.4. Best-fit lines were fitted through the respective results and their inclination to the horizontal axis corresponds to the interface friction angle, δ. The intercept on the vertical (shear stress) axis gives the apparent adhesion, c_a.

The peak combination strength envelope from the single interface tests is compared in **Figure 4-9**(a) with the corresponding peak strength envelope from the CLAY/GTX/GMB/GCL triple interface test. It was observed that for the triple interface, the peak strengths are slightly lower particularly at normal stresses below 100 kPa. However, as the normal stresses increase beyond 100 kPa, the peak strengths from the combination envelope from the single interfaces becomes lower. Hence, at higher stresses the triple interface exhibits higher peak shear strength.

In **Figure 4-9**(b), a comparison of LD strength envelopes from the single and triple interface tests is shown. The triple interface test shows slightly higher LD envelopes than the single test interface at lower stresses. As the applied normal stress increases, the LD strength of the triple interface increases as well. This demonstrates that the CLAY/GTX/GMB/GCL envelope exhibits higher LD strength than the combination envelope. The peak and LD failure envelopes for the single and triple interface were determined in terms of strength parameters from **Figure 4-9** and summarized in **Table 4-8**.

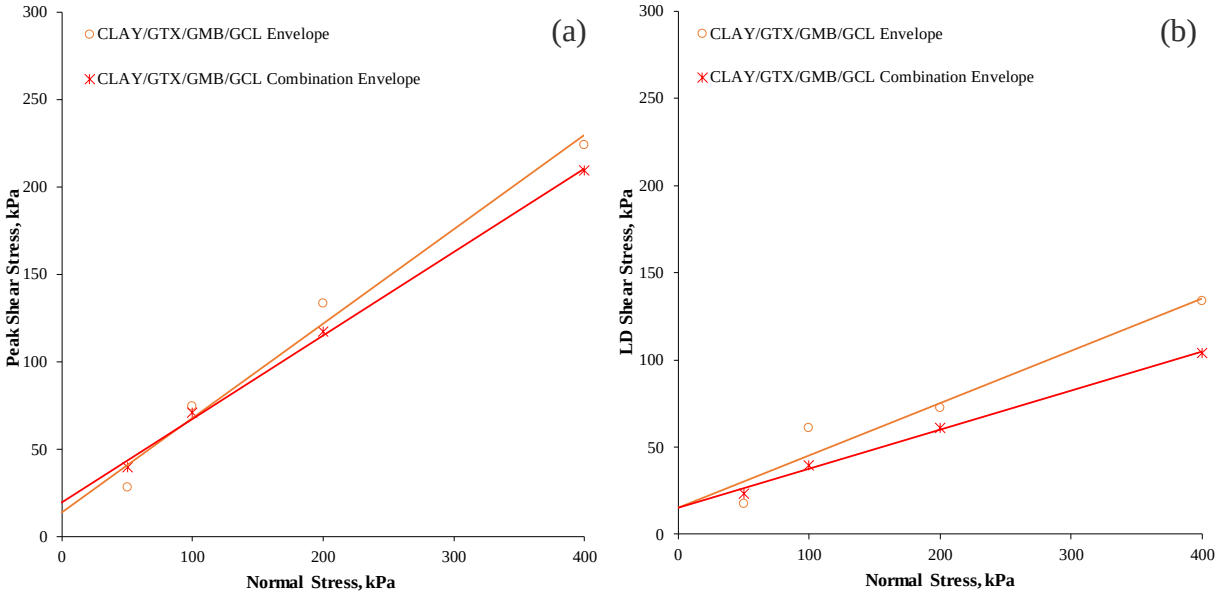

Figure 4-9 Shear stress versus normal stress for CLAY/GTX/GMB/GCL interface: (a) peak and (b) LD shear stress

From **Table 4-8**, it was observed that a higher peak friction angle than the combination envelope was attained by the CLAY/GTX/GMB/GCL envelope. The respective peak friction angles from the triple interface were 28.4 °, which is about 10.2 % higher than the combination envelope. Similarly, the LD friction angle for the CLAY/GTX/GMB/GCL envelope was found to be slightly higher compared to the combination envelope. An LD friction angle of 16.7° was obtained from the CLAY/GTX/GMB/GCL envelope, which is 24 % higher than the 12.7° mobilized by the combination envelope.

Table 4-8 also included the obtained apparent adhesion values from the plotted failure envelopes. The comparison of the results shows that the peak adhesion values of the combination envelope were greater than those of the CLAY/GTX/GMB/GCL envelope. The combination and the CLAY/GTX/GMB/GCL envelope, respectively, had peak apparent adhesion values of 19.6 kPa and 13.4 kPa, a difference of about 32 %. On the other hand, similar LD apparent adhesion was observed between the CLAY/GTX/GMB/GCL and combination failure envelopes. An LD apparent adhesion value of 14.9 kPa was exhibited.

Based on these observations, it can be said that the combination envelope yielded a conservative estimate of the peak and LD interface shear strength values, as compared to the triple interface.

Table 4-8 Summary of peak and LD shear strength parameters of CLAY/GTX/GMB/GCL interface

Interface Configuration	Peak shear strength parameters		LD shear strength parameters	
	δ_p (°)	$c_{\alpha\text{-}p}$ (kPa)	δ_{LD} (°)	$c_{\alpha\text{-}LD}$ (kPa)
CLAY/GTX/GMB/GCL Envelope	28.4	13.4	16.7	14.9
CLAY/GTX/GMB/GCL Combination Envelope	25.5	19.6	12.7	14.9

* δ_p & δ_{LD} Peak and LD Interface friction angle respectively, $c_{\alpha\text{-}p}$ & $c_{\alpha\text{-}LD}$ Peak and LD apparent adhesion respectively.

4.3.4.2 GTX/GMB/GCL/SAND Interface

Figure 4-10 shows the peak and LD failure envelope derived from the direct shear tests on the GTX/GMB/GCL/SAND interface and the combination envelope derived from the minimum peak and LD shear stress values of the GTX/GMB, GMB/GCL and GCL/SAND single interface tests. Similarly, through the respective results, best-fit straight lines were fitted and the corresponding interface angle of friction (δ) and apparent adhesion (c_α) values were determined.

In **Figure 4-10**(a), a similar difference in the peak strength failure envelopes was observed for both the GTX/GMB/GCL/SAND and the single interfaces. The combination failure envelope for the single interfaces consisted of the minimum values from the GTX/GMB and GCL/SAND interfaces. The peak strength of the GTX/GMB/GCL/SAND envelope was higher than that of the combination envelope at all normal stresses observed. On the other hand, in **Figure 4-10**(b), compared to the GTX/GMB/GCL/SAND envelope, the combination envelope exhibited lower LD strength at applied normal stresses below 300 kPa. However, once the normal stresses increased beyond 300 kPa, the GTX/GMB/GCL/SAND envelope tends to exhibit lower LD shear strength, indicating that the GTX/GMB/GCL/SAND interface generates more conservative LD strength at higher stresses. The GTX/GMB was considered to be the weakest interface amongst all the three single interfaces involved in the multi-layer interface test for the LD combination failure envelope.

For further comparison and discussion, the parameters of peak and LD shear strength for the different failure envelopes were obtained and are summarized in **Table 4-9**.

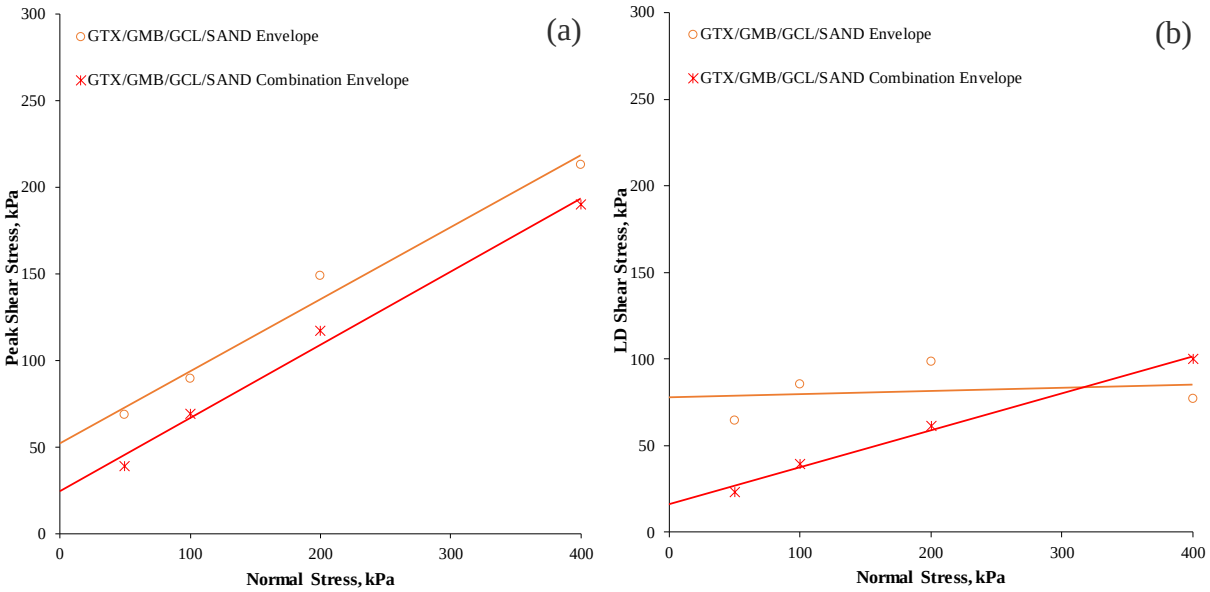

Figure 4-10 Shear stress versus normal stress for GTX/GMB/GCL/SAND interface: (a) peak and (b) LD shear stress.

Table 4-9 Summary of peak and LD shear strength parameters of GTX/GMB/GCL/SAND interface.

Interface Configuration	Peak shear strength parameters		LD shear strength parameters	
	δ_p (°)	$c_{\alpha\text{-}p}$ (kPa)	δ_{LD} (°)	$c_{\alpha\text{-}LD}$ (kPa)
GTX/GMB/GCL/SAND Envelope	22.5	52.3	1.0	78.2
GTX/GMB/GCL/SAND Combination Envelope	22.9	24.7	12.0	16.1

* δ_p & δ_{LD} Peak and LD Interface friction angle respectively, $c_{\alpha\text{-}p}$ & $c_{\alpha\text{-}LD}$ Peak and LD apparent adhesion respectively.

It was evident from **Table 4-9** that the interface peak friction angles between the two failure envelopes were comparable. In comparison to the GTX/GMB/GCL/SAND envelope, the combination envelope showed a higher peak and LD interface friction angle. The peak and LD interface friction angles obtained were 22.9º and 12.0º for the combination strength envelope and 22.5° and 1.0° for the GTX/GMB/GCL/SAND envelope, respectively. For the two investigated failure envelopes, this represented a percentage difference of about 2 % and 92 % in peak and LD friction angles, respectively. This implied that the triple interface test produced more conservative peak and LD shear strength parameters as compared to single interfaces.

Similarly, in **Table 4-9**, the apparent adhesion values of the two failure envelopes were also presented. It was noted that the peak apparent adhesion value of the GTX/GMB/GCL/SAND envelope was 52.3 kPa, which is 53 % greater than the value obtained from the combination envelope (24.7 kPa). In addition, a higher adhesion value was mobilized by the GTX/GMB/GCL/SAND envelope at LD strength compared to the combination envelope, as can be observed in **Table 4-9**.

4.3.5 Quadruple Interface

This section discusses the peak and LD shear stress relationships against the normal stresses applied of the quadruple interface test conducted. A comparison between the Mohr-Coulomb failure envelope, which was plotted using data from **Table 4-3**, and the combination failure envelopes for single interface tests is shown in **Figure 4-11**. For a range of normal stresses applied, the combination failure envelopes were constructed using segments of single interface strength envelopes representing the minimum peak or LD shear stress values. The summary of the results obtained from **Figure 4-11** is presented quantitatively in **Table 4-10**, followed by a comparative analysis and a summary of the discussions.

4.3.5.1 CLAY/GTX/GMB/GCL/SAND Interface

For the CLAY/GTX/GMB/SAND interface, the values of peak and LD shear stress at failure were plotted against the normally applied stress as shown in **Figure 4-11**, and the best-fit straight lines fitted through the respective results. Moreover, the combination failure envelope from the minimum peak and LD shear stress values of all the four single interfaces was constructed and plotted for comparison purposes. Best-fit straight lines were fitted through the respective results, and the corresponding interface angle of friction (δ) and apparent adhesion (c_a) values were determined.

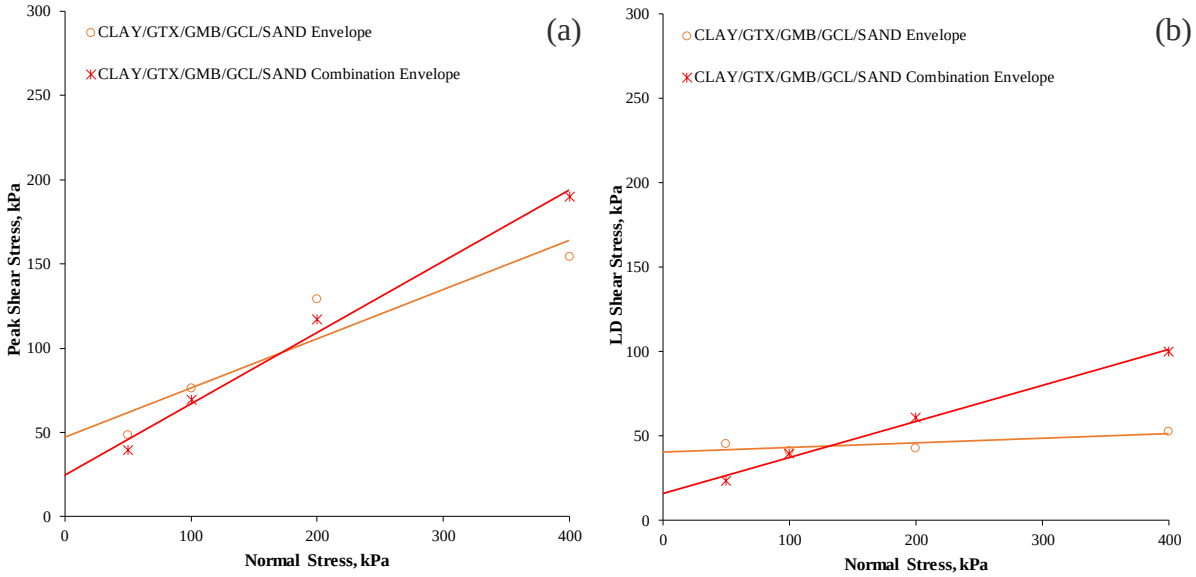

Figure 4-11 Shear stress versus normal stress for CLAY/GTX/GMB/GCL/SAND interface: (a) peak and (b) LD shear stress.

The peak combination strength envelope from the single interface tests is compared in **Figure 4-11**(a) with the corresponding peak strength envelope from the CLAY/GTX/GMB/GCL/SAND multi-layer interface test. It was observed that for single-interface tests, the peak strengths are slightly lower for the range of normal stresses considered, particularly at low normal stresses. This difference may be attributed to isolated single-interface tests that are not affected by

surrounding geosynthetics. On the other hand, compared to the CLAY/GTX/GMB/GCL/SAND envelope, the combination envelope (**Figure 4-11**(b)) exhibited lower LD strength at lower applied stresses. However, once the normal stresses increased beyond 150 kPa, the CLAY/GTX/GMB/GCL/SAND envelope tends to show lower LD shear strength, indicating that the CLAY/GTX/GMB/GCL/SAND interface generates more conservative LD shear strength at higher stresses. The parameters of peak and LD shear strength for the various failure envelopes were obtained for further comparison and discussion and are summarized in **Table 4-10**.

The results, as detailed in **Table 4-10**, show that from the CLAY/GTX/GMB/GCL/SAND multi-layer interface envelope, the measured peak and LD interface friction angles were lower than that of the combination envelope. A peak friction angle of 16.3° was achieved by the CLAY/GTX/GMB/GCL/SAND interface envelope, whereas the combination envelope achieved a peak friction angle of 22.9°. Also as compared to the 12.7° achieved with the combination envelope, the GTX/GMB/GCL interface envelope had a largely lesser LD interface friction angle of 1.5°. The percentage difference in both the peak and LD interface friction angle for the CLAY/GTX/GMB/GCL/SAND interface envelope and combination envelope was 29.0 % and 88.0 %, respectively. Based on these observations, it can be said that the multi-layer interface test produced more conservative peak shear strength parameters as compared to single interfaces.

Table 4-10 Summary of peak and LD shear strength parameters of CLAYGTX/GMB/GCL/SAND multi-layer interface.

Interface Configuration	Peak shear strength parameters		LD shear strength parameters	
	δ_p (°)	$c_{\alpha\text{-}p}$ (kPa)	δ_{LD} (°)	$c_{\alpha\text{-}LD}$ (kPa)
CLAY/GTX/GMB/GCL/SAND Envelope	16.3	47.0	1.5	40.7
CLAY/GTX/GMB/GCL/SAND Combination Envelope	22.9	24.7	12.0	16.1

* δ_p & δ_{LD} Peak and LD Interface friction angle respectively, $c_{\alpha\text{-}p}$ & $c_{\alpha\text{-}LD}$ Peak and LD apparent adhesion respectively.

Similarly, **Table 4-6** also included the obtained apparent adhesion values from the plotted failure envelopes. The comparison of the results presented shows that the peak adhesion values of the combination envelope were lesser than those of the CLAY/GTX/GMB/GCL/SAND envelope. The combination and the CLAY/GTX/GMB/GCL/SAND envelope, respectively, had peak adhesion values of 24.7 kPa and 47.0 kPa, a difference of about 47 %. Also, from the combination envelope, the LD apparent adhesion value of 16.1 kPa was measured, while from the CLAY/GTX/GMB/GCL/SAND envelope, 40.7 kPa was obtained.

4.3.6 Summary of Shear versus Normal Stress

Generally, the shear versus normal stress graphs of the geosynthetic interface shear strength is as good as the corresponding shear stress versus horizontal displacement relationships. When observing the interface friction angles and apparent adhesion values obtained from shear versus normal stress curves in **Table 4-4** to **Table 4-10**, it was evident that there existed a difference in the determined shear strength characteristics. This dissimilarity was attributed to the variation in the characteristics of the geosynthetics used during the experiments as all the respective testing conditions, i.e. procedures, standards, etc. were kept the same (refer to chapter 3).

4.4 Failure Envelope

4.4.1 Introduction

In this study, the failure envelopes were approximated using a straight fitted line which was analysed using Equation 3-1 for linear Mohr-Coulomb. However, it was recognized after further observation of **Figure 4-5** to **Figure 4-11** that multi-linear (i.e. bilinear) or non-linear (i.e. curvilinear) models could more appropriately represent the failure envelopes. The normal stress range over which tests are performed often dictates the degree of nonlinearity in the resulting data and the appropriate relationship that should be used, according to Fox & Stark (2015). Although linear envelopes are the simplest relationships, multi-linear envelopes consisting of two or more line segments or non-linear envelopes provide an abrupt change in the angle of interface friction at the intersection point(s) and may in some cases reflect the true behaviour of shear strength, (Fox & Stark, 2015). Therefore, this section attempted to evaluate the non-linearity of the shear strengths of both single and multi-layer interfaces tested, to report suitable normal stress ranges with parameters of interface strength obtained using linear equations.

4.4.2 Characterization of Nonlinear Envelopes

The coefficient of regression (R^2) was presented and examined to determine the type of strength envelopes (multi-linear or non-linear) most described by a given soil/geosynthetic or geosynthetic/geosynthetic interface shear characteristics. All best-fit lines with R^2 values below 0.98 were replaced with bilinear/curvilinear failure envelopes to ensure consistency of the R^2 values and the precise representation of the shear versus normal stress curves. The closer the R^2 values were to 1.0, the better the fit of the regression line (i.e. line or curves passed through most points).

The interface friction angle varies proportionally according to the confining stress for a multi-linear and curvilinear failure envelope. Equation 3-1 was used to obtain the multi-linear (i.e. bilinear) strength envelope, fitted to two separate smaller shear stress ranges. On the other hand, the curvilinear plots were obtained in form of Equation 3-2. Thus, by drawing a tangent to the best-fit curve, the shear characteristics (friction angle and adhesion) at each stress level were obtained in curvilinear envelopes. The inclination of this line/slope corresponded to the friction angle of the interface being tested, whereas the apparent adhesion was represented by the vertical intercept. Thiel (2001) and Fox & Stark (2004, 2015) recommended this method of determining shear parameters for curvilinear failure envelopes.

The figures in the next sections present linear (dashed lines), bilinear and curvilinear (continuous lines) failure envelopes of single and multi-layer interfaces. The best-fit straight lines (dashed line) were included in the graphs for comparison purposes. The summary of peak and large displacement shear strength parameters obtained from single and multi-layer interfaces were quantitatively summarized in **Table 4-11** to **Table 4-12** and **Table 4-13** to **Table 4-14** respectively.

4.4.3 Single Interface Envelopes

In single-interface tests, as seen in **Figure 4-12**, only 37.5 % of the tests were best-fitted ($0.98 \leq R^2 \leq 1$) using linear failure envelopes. On the other hand, curvilinear failure envelopes were best represented in about 50 % of the tests, while only 12.5 % best-exhibited bilinear envelopes.

It can be observed from **Figure 4-12** that curvilinear failure envelopes showed that the shear strength increased with the application of increased normal stress, but only up to a certain point of shear stress, after which the rate of shear strength gradually changed in the downward direction of the concave with normal stress. This was particularly observed for the peak failure envelope of the GMB/GCL interface, (see **Figure 4-12** (a)). This curvilinear failure envelope indicated that the interface friction angle at any point on the curve of the failure envelope was unique to any normal stress applied, depending on the interface test carried out. Thus, by drawing a tangent to the best-fit curve, the shear strength parameters (i.e. friction angle and adhesion) at each stress level were obtained in curvilinear envelopes, as can be seen in **Table 4-11**.

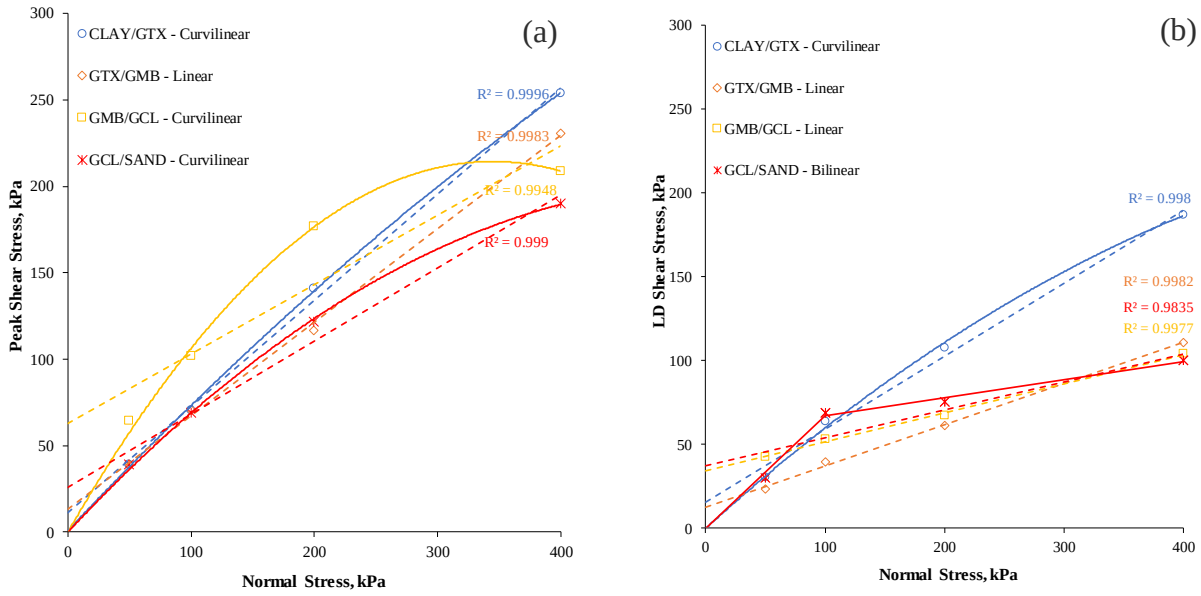

Figure 4-12 Failure Envelopes for single interfaces: (a) Peak and (b) LD shear stress.

Alternatively, the GCL/SAND interface exhibited a bilinear failure envelope for the LD shear strength plot. As seen in **Figure 4-12**(b), the bilinear failure envelope, similar to curvilinear curves, showed that the shear strengths increased with increasing normal stress until a certain critical normal stress (i.e. 100 kPa) was achieved. The rate of shear strength suddenly changed beyond this critical normal stress, and the slope became less steep and became much flatter, resulting in a bilinear curve. As a result, after the critical stress was experienced, a change in the interface friction angle and apparent adhesion occurred. Therefore, Equation 3-1 was used but fitted twice on separate smaller shear stress ranges, i.e. 0 - 100 kPa and 100 - 400 kPa, to determine the shear strength parameters. Consequently, as can be seen in **Table 4-12**, two interface friction angles and apparent adhesion values were obtained.

4.4.4 Multi-layer Interface Envelopes

This section demonstrated the peak and LD failure envelopes for the multi-layer interface tests conducted. A comparison between the multi-layer interface Mohr-Coulomb failure envelopes and the combination failure envelopes for single interface tests were plotted and are shown in **Figure 4-13** and **Figure 4-14**.

4.4.4.1 Double Interface Envelopes

For double interface tests, as seen in **Figure 4-13**, about 50 % of the tests were best fitted using linear failure envelopes. On the other hand, curvilinear failure envelopes accounted for about 33 % of the tests, while only 17 % best-exhibited bilinear envelopes.

Observation in **Figure 4-13** shows that two types of curves (i.e. bilinear and curvilinear) were generated. The selection of which non-linearity curve to use was based on how close the respective graph is to the data points, i.e. a non-linearity curve with a higher R^2 was preferred to represent the failure envelope. Curvilinear envelopes were exhibited by the CLAY/GTX/GMB interface for both the peak and LD failure envelopes, whereas the combination envelopes displayed linear curves. On the other hand, both the GTX/GMB/GCL envelope and combination envelope were best fitted linearly. This was mainly due to the GTX/GMB interface being the weakest interface. Bilinear plots were only exhibited by the LD failure envelope for both the GMB/GCL/SAND envelope and the combination envelope. The shear strength parameters obtained for all the respective linear, multi-linear and nonlinear failure envelopes for the peak and LD shear strength are summarized in **Table 4-13** and **Table 4-14**.

4.4.4.2 Triple Interface Envelopes

For triple interface tests, as seen in **Figure 4-14**, about 25 % of the tests were best fitted using linear failure envelopes. On the other hand, curvilinear failure envelopes accounted for about 62.5 % of the tests, while only 12.5 % best exhibited bilinear envelopes.

From **Figure 4-14**, it can be seen that the peak failure envelopes for both the CLAY/GTX/GMB/GCL and GTX/GMB/GCL/SAND interfaces were best fitted on curvilinear envelopes, including the combination envelope. This could be as a result of shearing occurring between the interfaces that involved sand and GCL, as soil/geosynthetic interfaces are known to exhibit multi-linear or non-linear failure envelopes, (Fox & Stark, 2015). Alternatively, the LD shear strength envelope for the CLAY/GTX/GMB/GCL interface was best fitted using bilinear failure envelopes. The shear strength parameters obtained for all the respective linear, multi-linear and non-linear double interface failure envelopes for the peak and LD shear strength are summarized in **Table 4-13** and **Table 4-14** respectively.

4.4.4.3 Quadruple Interface Envelopes

For quadruple interface tests, as seen in **Figure 4-14**, about 25 % of the tests were best fitted using linear failure envelopes. On the other hand, curvilinear failure envelopes accounted for about 75 % of the tests, while only 12.5 % best-exhibited bilinear envelopes.

It was observed from **Figure 4-14** that curvilinear envelopes were the best fit for the peak failure envelopes. The non-linearity of the geosynthetic failure envelopes was observed by other

researchers and was attributed to the change in interaction mechanisms of the material tested, (Adeleke, 2020; Buthelezi, 2017; Sikwanda, 2018). For consistency, the intercept of both curvilinear and bilinear failure envelopes was set to zero. Only the LD shear strength combination envelope exhibited a bilinear. In **Table 4-13** and **Table 4-14**, the shear strength parameters obtained for all the respective linear, multi-linear and non-linear multi-layer interface failure envelopes for the peak and LD shear strength are summarized.

Table 4-11 Summary of the peak interface friction angle and apparent adhesion obtained from Figure 4-12(a).

Interface Configuration	Peak Friction Angle (°)							Peak Adhesion (kPa)						
	Linear	Bilinear		Curvilinear				Linear	Bilinear		Curvilinear			
	δ_p	$\delta_{p,b1}$	$\delta_{p,b2}$	$\delta_{p,50}$	$\delta_{p,100}$	$\delta_{p,200}$	$\delta_{p,400}$	$c_{a\text{-}p}$	$c_{a\text{-}p,b1}$	$c_{a\text{-}p,b2}$	$c_{a\text{-}p,50}$	$c_{a\text{-}p,100}$	$c_{a\text{-}p,200}$	$c_{a\text{-}p,400}$
CLAY/GTX	31.5	-	-	35.8	35.2	31.8	26.5	11.1	-	-	2.2	4.7	17.0	55.0
GTX/GMB	28.4	-	-	-	-	-	-	13.0	-	-	-	-	-	-
GMB/GCL	21.8	-	-	46.1	42.2	27.5	11.3	63.0	-	-	6.4	17.7	74.0	290.0
GCL/SAND	22.9	-	-	34.1	31.8	25.6	10.2	25.9	-	-	4.4	9.3	29.0	119.0

Table 4-12 Summary of the LD interface friction angle and apparent adhesion obtained from Figure 4-12(b).

Interface Configuration	LD Friction Angle (°)							LD Adhesion (kPa)						
	Linear	Bilinear		Curvilinear				Linear	Bilinear		Curvilinear			
	δ_{ld}	$\delta_{ld,b1}$	$\delta_{ld,b2}$	$\delta_{ld,50}$	$\delta_{ld,100}$	$\delta_{ld,200}$	$\delta_{ld,400}$	$c_{a\text{-}ld}$	$c_{a\text{-}ld,b1}$	$c_{a\text{-}ld,b2}$	$c_{a\text{-}ld,50}$	$c_{a\text{-}ld,100}$	$c_{a\text{-}ld,200}$	$c_{a\text{-}ld,400}$
CLAY/GTX	23.5	-	-	31.1	28.8	25.2	18.8	15.7	-	-	2.7	6.5	17.5	53
GTX/GMB	13.8	-	-	-	-	-	-	12.8	-	-	-	-	-	-
GMB/GCL	9.8	-	-	-	-	-	-	34.4	-	-	-	-	-	-
GCL/SAND	9.5	33.8	0.6	-	-	-	-	37.2	0	56.4	-	-	-	-

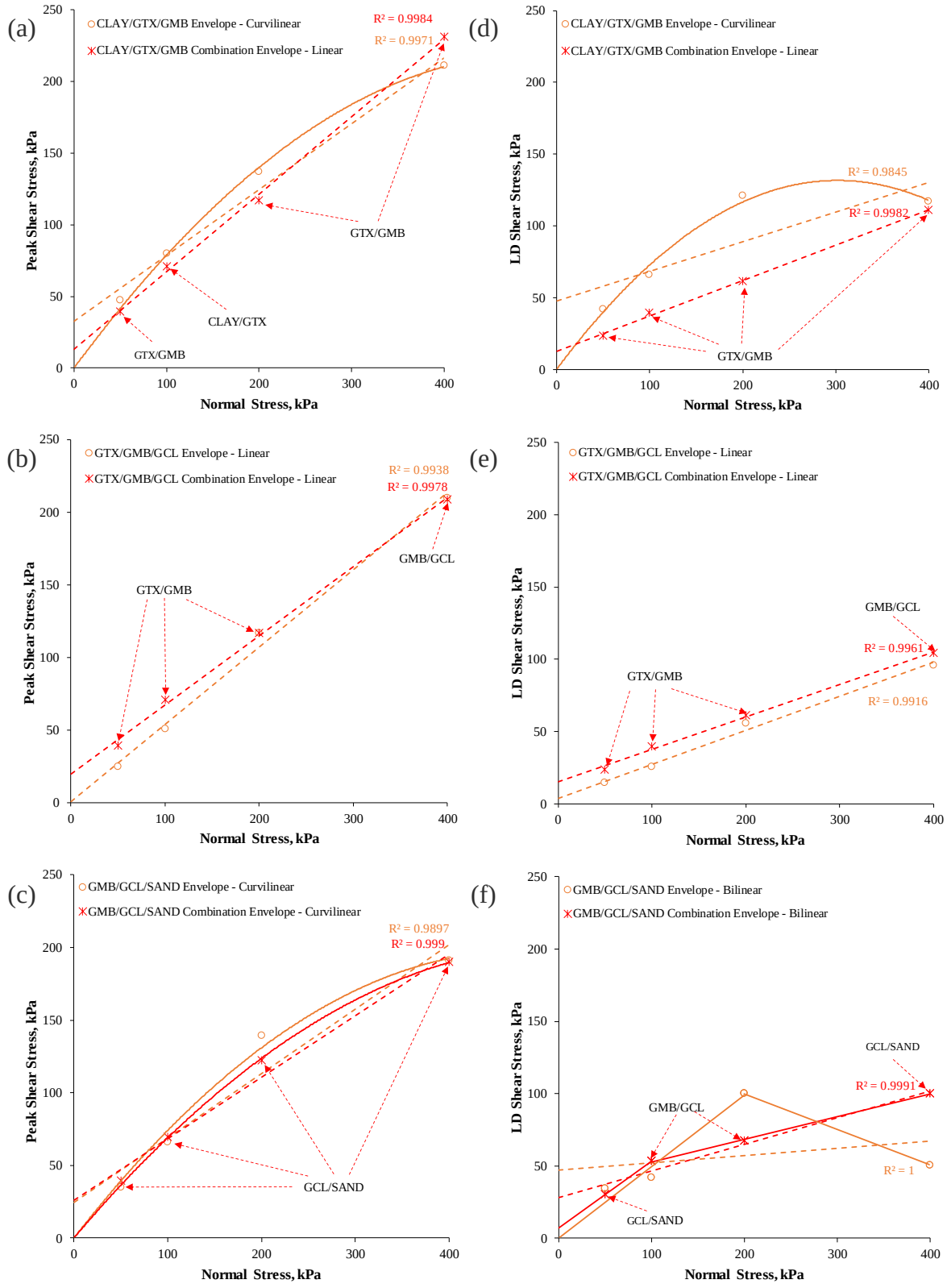

Figure 4-13 Failure Envelopes for double interfaces: (a) – (c) Peak vs normal stress and (d) – (f) LD vs normal stress.

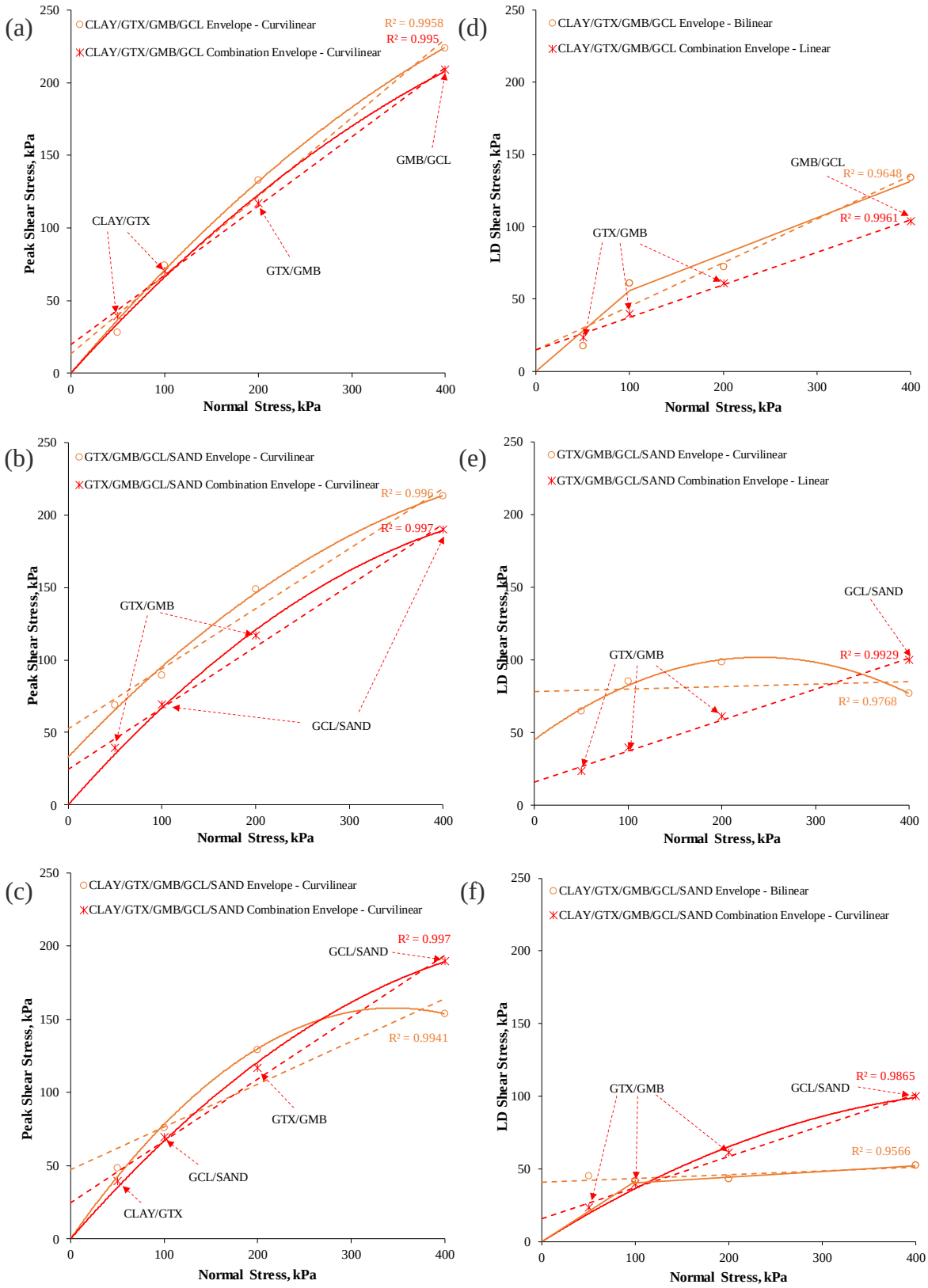

Figure 4-14 Failure Envelopes for triple and quadruple interfaces: (a) – (c) peak vs normal stress and (d) – (f) LD vs normal stress.

Table 4-13 Summary of the peak interface friction angle and apparent adhesion obtained from Figure 4 13 to Figure 4-14 (a) - (c).

Interface Configuration		Peak Friction Angle (°)							Peak Adhesion (kPa)						
		Linear	Bilinear		Curvilinear				Linear	Bilinear		Curvilinear			
		δ_p	$\delta_{p,b1}$	$\delta_{p,b2}$	$\delta_{p,50}$	$\delta_{p,100}$	$\delta_{p,200}$	$\delta_{p,400}$	$c_{a\text{-}p}$	$c_{a\text{-}p,b1}$	$c_{a\text{-}p,b2}$	$c_{a\text{-}p,50}$	$c_{a\text{-}p,100}$	$c_{a\text{-}p,200}$	$c_{a\text{-}p,400}$
CLAY/GTX/GMB	Envelope	24.7	-	-	37.8	35.2	27.9	11.7	32.5	-	-	1.9	8.2	35.5	128.0
	Combination Envelope	28.5	-	-	-	-	-	-	12.9	-	-	-	-	-	-
GTX/GMB/GCL	Envelope	28.0	-	-	-	-	-	-	0.8	-	-	-	-	-	-
	Combination Envelope	25.5	-	-	-	-	-	-	19.7	-	-	-	-	-	-
GMB/GCL/SAND	Envelope	23.9	-	-	37.8	32.8	25.2	9.5	24.7	-	-	1.8	11.0	37.5	126.0
	Combination Envelope	22.9	-	-	35.1	31.0	25.6	11.1	25.9	-	-	2.4	10.0	28.0	112.0
CLAY/GTX/GMB/GCL	Envelope	28.4	-	-	35.0	32.8	28.8	20.8	13.4	-	-	2.4	6.0	22.5	73.0
	Combination Envelope	25.5	-	-	32.7	30.6	27.6	19.8	19.6	-	-	2.9	8.4	19.6	65.0
GTX/GMB/GCL/SAND	Envelope	22.5	-	-	31.8	29.5	24.8	14.6	52.3	-	-	35.0	39.7	54.3	110.0
	Combination Envelope	22.9	-	-	33.9	31.1	25.6	13.3	24.7	-	-	2.6	7.9	25.4	96.0
CLAY/GTX/GMB/GCL/SAND	Envelope	16.3	-	-	36.5	33.5	21.8	4.8	47.0	-	-	7.1	13.6	50.0	189.0
	Combination Envelope	22.9	-	-	33.9	31.1	26.0	13.3	24.7	-	-	2.6	7.9	24.3	96.0

Table 4-14 Summary of the peak interface friction angle and apparent adhesion obtained from Figure 4 13 to Figure 4-14 (d) - (f).

Interface Configuration		LD Friction Angle (°)							LD Adhesion (kPa)						
		Linear	Bilinear		Curvilinear				Linear	Bilinear		Curvilinear			
		δ_{ld}	$\delta_{ld,b1}$	$\delta_{ld,b2}$	$\delta_{ld,50}$	$\delta_{ld,100}$	$\delta_{ld,200}$	$\delta_{ld,400}$	$c_{a\text{-}ld}$	$c_{a\text{-}ld,b1}$	$c_{a\text{-}ld,b2}$	$c_{a\text{-}ld,50}$	$c_{a\text{-}ld,100}$	$c_{a\text{-}ld,200}$	$c_{a\text{-}ld,400}$
CLAY/GTX/GMB	Envelope	11.7	-	-	36.3	30.7	16.4	14.8	47.7	-	-	4.1	14.3	57.4	224.0
	Combination Envelope	13.8	-	-	-	-	-	-	12.8	-	-	-	-	-	-
GTX/GMB/GCL	Envelope	13.2	-	-	-	-	-	-	3.8	-	-	-	-	-	-
	Combination Envelope	12.7	-	-	-	-	-	-	14.9	-	-	-	-	-	-
GMB/GCL/SAND	Envelope	2.9	26.2	13.9	-	-	-	-	47.2	0.0	149.0	-	-	-	-
	Combination Envelope	10.5	24.8	8.9	-	-	-	-	28.1	7.1	37.1	-	-	-	-
CLAY/GTX/GMB/GCL	Envelope	16.7	29.2	14.1	-	-	-	-	14.9	0.0	30.5	-	-	-	-
	Combination Envelope	12.7	-	-	-	-	-	-	14.9	-	-	-	-	-	-
GTX/GMB/GCL/SAND	Envelope	1.0	-	-	19.7	16.2	4.4	17.3	78.2	-	-	49.1	55.5	85.6	203.0
	Combination Envelope	12.0	-	-	-	-	-	-	16.1	-	-	-	-	-	-
CLAY/GTX/GMB/GCL/SAND	Envelope	1.5	29.2	14.1	-	-	-	-	40.7	0.0	30.5	-	-	-	-
	Combination Envelope	12.0	-	-	19.2	17.9	13.2	5.7	16.1	-	-	3.2	5.5	19.6	60.0

4.5 Critical Interface

4.5.1 Introduction

For both single and multi-layer interfaces, the main objective of the shear stress versus normal stress graphs was primarily to determine the critical/weakest interface of the materials tested, i.e. soils and geosynthetics. In structures with multi-layered geosynthetic liners such as landfills, finding the critical interface is key in the analysis of the stability of that structure, (Xuede, 2008). According to Sikwanda (2018), a critical interface can be defined as the surface having the minimum shear resistance and is likely to cause the failure of a structure if its interface friction is exceeded. As a result, it is very imperative to locate this interface in multi-layered geosynthetic liners, as it governs the stability design analysis, (Sikwanda, 2018).

Stark et al. (2011) have previously reported that there is stress-dependent shear resistance on geosynthetic interfaces and as a result, the critical interface varies with the normal stress applied. It can therefore be beneficial to determine the weakest interface by assessing each interface component of a multi-layered liner as a single interface test. The weakest interface in landfills was primarily determined using single interface tests and little has been reported compared to multi-interface shear tests. Consequently, a comparative discussion and analysis of the peak and LD failure strength envelopes presented in **Figure 4-12** (single interfaces) and **Figure 4-13** to **Figure 4-14** (multi-layer interfaces) was considered in this section. These findings were particularly preferred since, as mentioned in section 4.4, they provided the best fit ($0.98 \leq R^2 \leq 1$) of the failure envelopes.

4.5.2 Peak Strength

This section discusses the strongest and critical/weakest interfaces from the peak shear strength failure envelopes for both single and multi-layer interface tests. Firstly, a comparison was done on the single interfaces to determine the strongest and the weakest interface. Then, from the failure envelopes that were generated from the minimum peak values of all respective single interface tests representing the multi-layer interfaces, the critical interface was as well determined as compared to the failure planes of the multi-layer interfaces.

4.5.2.1 Single interfaces

Figure 4-12(a) displayed the strongest and critical/weakest single interface shear plane tested. The strongest and critical interface was the interface plotted above and below on the shear stress versus normal stress graph, respectively. It was evident from **Figure 4-12**(a) that the strongest and the weakest interface varied with an increase in the normal stresses. At normal stresses of 0 to 300 kPa, the strongest interface was the GMB/GCL interface. However, beyond the 300 kPa, there was a change in the strongest interface, with the CLAY/GTX becoming the strongest interface. On the other hand, the critical interface was found to be the GCL/SAND interface at all the range normal stresses except between the ranges of 0 to 100 kPa, as can be seen in **Figure 4-12**(a). Between normal stresses of 100 and 200 kPa, the GTX/GMB interface exhibited the lowest peak strength, and as such was the critical interface.

4.5.2.2 Double interfaces

In **Figure 4-13**(a) - (c), the peak failure combination strength envelopes generated from segments of single interface strength envelopes representing the critical peak strength values were shown for all the double interface tests. It was necessary to construct these failure combination strength envelopes to represent the critical interface for the normal stresses considered and compare them to the respective double interface failure envelopes.

4.5.2.2.1 CLAY/GTX/GMB interface

For the CLAY/GTX/GMB interface, it was clear from **Figure 4-13** a) that the critical interface was exhibited at low (i.e. below 50 kPa) and high normal stresses (i.e. above 300 kPa). According to Stark & Choi (2004), if there was a change in the critical interface multi-layer interface with increasing normal stress, then the combination strength envelope would also change interfaces. Similarly, in the case of the combination failure envelope for the CLAY/GMB/GTX interface, it was observed that the critical interface transferred for much of the normal stresses considered in the investigation. Initially, the critical interface at 50 kPa was the GTX/GMB interface and this switched to the CLAY/GTX interface. Eventually, at normal stresses beyond 200 kPa, the critical interface reverted to the GTX/GMB interface.

4.5.2.2.2 GTX/GMB/GCL interface

From **Figure 4-13**(b), the peak failure envelopes for the GTX/GMB/GCL interface, as well as the combination failure envelopes, are presented. It can be seen that the GTX/GMB was the critical interface at stresses between 0 kPa and 300 kPa. However, as the normal stresses increased beyond 300 kPa, there was a switch in the critical interface from the GTX/GMB to the GMB/GCL interface. Also, the GTX/GMB/GCL interface was observed to be the weaker of the two failure envelopes at low stresses between 0 kPa and 300 kPa. Nevertheless, this changed as the normal stress increased beyond 300 kPa, with the combination failure envelope becoming the weakest interface. This is in accordance with Stark & Choi (2004), who described that if the critical interface for multi-layer interface changes with increasing normal stress, the combination strength envelope would also change interfaces.

4.5.2.2.3 GMB/GCL/SAND interface

Figure 4-13(c) presents the shear stress versus normal stress for the GMB/GCL/SAND peak strength envelope and the combination peak strength envelope. As previously mentioned, if the critical interface for multi-layer interface changes with increasing normal stress, the combination strength envelope would also change interfaces, as described by Stark & Choi (2004) but this is not the case for this testing. It was observed from **Figure 4-13**(c) that the critical interface through the entire range of normal stresses was the GCL/SAND interface. This critical interface did not change with an increase in normal stresses, thus making it the weakest interface in the GMB/GCL/SAND interface test. Moreover, the combination failure envelope was found to be the weakest interface at all normal stress ranges as compared to the GMB/GCL/SAND failure envelope. It was therefore safe to conclude that single interface tests yielded more conservative peak strength as compared to multi-layer interfaces.

4.5.2.3 Triple interfaces

In **Figure 4-14**(a) - (b), the peak failure combination strength envelopes generated from segments of single interface strength envelopes representing the critical peak strength values was shown for all the triple interface tests.

4.5.2.3.1 CLAY/GTX/GMB/GCL interface

It can be seen from **Figure 4-14(**a) that the lowest interface displayed a stress-dependent shear resistance with the increase in the applied normal stresses. For instance, from the combination envelope, the CLAY/GTX was the critical interface at normal stresses between 0 kPa and 100 kPa, whereas the GTX/GMB interface was the weakest interface for normal stresses exceeding 200 kPa. At normal stresses of 400 kPa, however, the critical interface was observed to have switched to the GMB/GCL interface. Lastly, as can be seen in **Figure 4-14**(a), the CLAY/GTX/GMB/GCL combination failure envelope displayed the weakest peak strength at all the ranges of normal stresses. As a result, the single interface tests yielded conservative peak strength values as compared to the multi-layer interface.

4.5.2.3.2 GTX/GMB/GCL/SAND interface

Comparing the weakest interface failure envelope obtained from the CLAY/GTX/GMB/GCL to the GTX/GMB/GCL/SAND, similar trend as seen in **Figure 4-14**(a) was observed in **Figure 4-14**(b). However, for the GTX/GMB/GCL/SAND combination failure envelope, there was a change in the critical interface with increasing normal stress. Initially, at 50 kPa the critical interface was found to be the GTX/GMB. At 100 kPa, however, the critical interface shifted from the GTX/GMB to the GCL/SAND, and then eventually changed back to the GTX/GMB at normal stress of 200 kPa. Ultimately, the weakest interface became the GCL/SAND interface at the highest normal stress of 400 kPa.

4.5.2.4 Quadruple interfaces

In **Figure 4-14**(c), the peak failure combination strength envelope generated from segments of single interface strength envelopes representing the critical peak strength values was shown for the quadruple interface test.

4.5.2.4.1 CLAY/GTX/GMB/GCL/SAND interface

The combination peak strength failure envelope displayed in **Figure 4-14**(c) yielded lower peak strength values and was considered to be more conservative as compared to the multi-layer interface. Beyond normal stress of about 270 kPa, however, the combination envelope began to exhibit higher peak strength values. On the other hand, it can be observed that the CLAY/GTX interface was the critical interface in the combination envelope at stresses of 50 kPa. The weakest interface however changes at 100 kPa to the GCL/SAND interface. As the normal stress was increased to 200 kPa, there was again a switch in the critical interface to the GTX/GMB interface. Ultimately, at the highest normal stress of 400 kPa the critical interface switched back to the GCL/SAND interface. Thus, it can be concluded that at higher normal stresses, the GCL/SAND interface tends to be the weakest in the entire multi-layer interface.

4.5.3 LD Strength

This section discusses the strongest and critical/weakest interface from the LD shear strength failure envelopes for both single and multi-layer interface tests.

4.5.3.1 Single interface

The LD failure combination strengths envelopes determined from the single interface tests are presented in **Figure 4-12**(b). It was evident from **Figure 4-12**(b) that the strongest and the critical/weakest interface varied with an increase in the normal stresses. From **Figure 4-12**(b), it was observed that the CLAY/GTX interface yielded the highest LD strength envelope in all single interface tests considered at normal stresses higher than 80 kPa. The critical interface was observed to be the GTX/GMB interface from normal stresses of 0 kPa to 300 kPa. Beyond 300 kPa, however, the critical interface switched to the GCL/SAND interface.

4.5.3.2 Double interfaces

In **Figure 4-13**(d) - (f), the LD failure combination strength envelopes generated from segments of single interface strength envelopes representing the critical LD strength values were shown for all the double interface tests.

4.5.3.2.1 CLAY/GTX/GMB interface

In **Figure 4-13**(d), the LD failure strength envelopes obtained for the CLAY/GTX/GMB interface are displayed. The combination failure envelope was observed to be exhibiting the lowest LD strength values from the two failure envelopes. Thus, indicating that LD strength values from the single interface tests were more conservative compared to the LD strength values for the CLAY/GTX/GMB multi-layer interface. Additionally, the GTX/GMB interface was found to be the weakest interface through the range of normal stresses for the combination LD strength envelope. It is therefore safe to conclude that the GTX/GMB interface was the critical interface n this double interface test.

4.5.3.2.2 GTX/GMB/GCL interface

From **Figure 4-13**(e), the LD failure strengths envelopes determined from the GTX/GMB/GCL interface test are presented. It can be seen that the GTX/GMB interface was observed to be the critical interface at normal stresses between 0 kPa and 200 kPa. At 400 kPa, however, the weakest interface switched from the GTX/GMB to the GMB/GCL interface. The GTX/GMB/GCL envelope was found to be exhibiting lower LD strength values as compared to the combination failure envelope. As a result, the GTX/GMB/GCL double interface test was said to be producing more conservative LD strength values as compared to the single interface test.

4.5.3.2.3 GMB/GTX/SAND interface

As can be seen in **Figure 4-13**(f), the strongest interface was found to be a function of normal stress, thus, it changed with increasing normal stresses. The lowest interface interchanged between the GCL/SAND and GMB/GCL interfaces, as observed in **Figure 4-13**(f). At normal stresses between 0 kPa and 100 kPa, the GCL/SAND interface was observed to be the weakest

interface. Beyond the 100 kPa, the critical interface switched from the GCL/SAND to the GMB/GCL interface. Eventually, the critical interface reverts to be the GCL/SAND interface at higher stresses of 400 kPa.

4.5.3.3 Triple interfaces

In **Figure 4-14**(d) - (e), the LD failure strength envelopes generated from segments of single interface strength envelopes representing the critical LD strength values were shown for all the triple interface tests conducted.

4.5.3.3.1 CLAY/GTX/GMB/GCL interface

From **Figure 4-14**(d), the LD failure envelopes for the CLAY/GTX/GMB/GCL interface, as well as the combination failure envelopes are presented. Comparing the failure envelopes obtained from the CLAY/GTX/GMB/GCL interface test to the combination failure envelope from the single interface tests, it was found that the single interface tests yielded the weakest interface for all normal stresses considered, as observed in **Figure 4-14**(d). The GTX/GMB interface was found to the critical interface at normal stresses between 0 kPa and 200 kPa, while the GMB/GCL interface was observed to be the weakest interface at a normal stress of 400 kPa.

4.5.3.3.2 GTX/GMB/GCL/SAND interface

Figure 4-14(e) displayed the strongest and critical/weakest interface LD failure envelopes for the GTX/GMB/GCL/SAND interface tested. The lowest interface, in **Figure 4-14**(e), displayed a stress-dependent shear resistance with the increase in the applied normal stresses. For instance, the GTX/GMB interface was the lowest and critical interface for the normal stress between 0 kPa and 200 kPa, whereas the GCL/SAND interface was the weakest interface for normal stresses exceeding 300 kPa. Consequently, the combination failure envelope was found to be more conservative in terms of LD strength values as compared to the multi-layer interface.

4.5.3.4 Quadruple interfaces

In **Figure 4-14**(f), the LD failure strength envelope generated from segments of single interface strength envelopes representing the critical LD strength values was shown for the quadruple interface test.

4.5.3.4.1 CLAY/GTX/GMB/GCL/SAND interface

As can be seen in **Figure 4-14**(f), the LD strength envelope and the combination peak strength envelope for the CLAY/GTX/GMB/GCL/SAND interface are presented. It can be observed that the combination failure envelope exhibited lower LD strength values at normal stresses below 150 kPa as compared to the CLAY/GTX/GMB/GCL/SAND envelope. Beyond 150 kPa, the LD strength values obtained by the combination envelope become higher, thus making it the stronger interface. Furthermore, at normal stresses between 0 kPa and 200 kPa, the GTX/GMB interface was found to be the critical/weakest interface, whereas the GCL/SAND interface was the weakest interface at a normal stress of 400 kPa. It can therefore be concluded that the GTX/GMB interface is the critical interface within the CLAY/GTX/GMB/GCL/SAND interface.

5 CONCLUSIONS AND RECOMMENDATIONS

5.1 Introduction

To study the effects of using various test configurations, single and multi-layer interfaces, on the shear strength at soil/geosynthetic and geosynthetic/geosynthetic interfaces, the ShearTrac-III large direct shear apparatus of 305 mm x 305 mm box size was used. An interface test program was therefore implemented to include a series of single and multi-layer tests for different interfaces.

The test methods developed in this work made it possible to study responses such as shear stress against horizontal displacement, peak displacement against normal stress, shear stress versus normal stress, and determine the appropriate failure envelopes. Key information on the importance of using one test configuration (single interface), as opposed to the other (multi-layer interface), was provided by the analysis of the results in determining the geosynthetic shear strength characteristics of each respective interface. This chapter provides a summary of the main conclusions of this study, followed by some recommendations for further research work.

5.2 Conclusions

The following conclusions were drawn based on the results and interpretation presented in this study:

1. In all interface tests conducted, typical soil/geosynthetic and geosynthetic/geosynthetic shear stress versus shear displacement responses with nonlinear behaviour was exhibited in both the single and multi-layer interface tests, regardless of the normal stress applied. However, it was noted that with increasing normal stress, irrespective of the interface tested, the deviation in the mobilized shear stress between the two test configurations increased. Nevertheless, in relation to multi-layer interface tests, the exact percentage difference in shear strength parameters obtained when single interface tests are used was not established as it varied depending on the interface.

2. In single interface tests, the high shear strength obtained can be related to the clamping that confined each of the test specimens during shearing to one end of the shear block. This resulted in sufficient shear resistance being provided to avoid non-uniform displacement of the geosynthetics tested, thus transferring the normal stress applied within the pre-determined failure plan, which was not the case with multi-layer interface tests. Only the top and bottom test specimens were clamped in multi-layer interface tests, thereby leaving the middle test specimens unconfined. As a consequence, depending on which plane was the weakest, failure could have occurred at any of the interfaces available.

3. Regardless of the different multi-layer interface configuration used, the observations showed that there could have been a transfer of shear stresses within the system when

performing the multi-layer interface shear tests once the system started to shear (fail). This resulted in little to no tension within the different layers.

4. The linear Mohr-Coulomb failure envelope can underestimate or overestimate the shear strength to determine the interface shear strength characteristics between soil/geosynthetic and geosynthetic/geosynthetic interfaces. The nonlinearity analysis of the interface shear strength failure envelopes, which is bilinear and curvilinear, should therefore be highly considered particularly if the experiment is conducted over a wide range of normal stresses.

5. The peak and LD strengths used for the identification of the critical interface are dependent on the applied normal stress, geosynthetic type and test procedures. As such, site-specific testing should be performed. Peak strengths were generally 9 % lower for the single interface tests for the range of normal stresses considered, especially at low normal stresses between 50 and 200 kPa, as compared to the peak strength values for the multi-layer interface tests. Moreover, LD strengths were generally 24 % lower for the single interface tests as compared to the multi-layer interface tests, and these lower LD strengths observed were probably caused by the rigid clamping of the geosynthetics which resulted in some tensile strains in the geosynthetics.

6. Single interface tests yielded a conservative estimate of the peak and LD strength for the interfaces tested herein. As suggested by Stark et al. (2015), this may be attributed to the greater displacement along with the critical interface in single interface tests than those in the multi-layer interface tests.

5.3 Recommendations

The following recommendations are made for future studies:

1. As only one type of geosythentic speciment has been tested, the data from these results are limited to the scope of ths study. As such additional testing is required using other different types of geosynthetics to present a full comparison of single and multi-layer interface tests.

2. Additional tests should be performed using different recommended large direct shear devices, that is 1.0 m x 1.0 m, to reduce boundary effects and the findings be compared with respective results obtained in this study.

3. Real-time monitoring of displacement mobilization in multi-layer interface tests during shearing would be another viable area for further research. This would allow the investigator to observe the displacement during shearing of the different geosynthetic specimens to identify the most critical interface.

REFERENCES

Adeleke, D. (2020). *An Investigation into the Effects of Asperities on Geomembrane / Geotextile Interface Shear Characteristics*. MSc Thesis submitted to University of Cape Town.

Adeleke, D. D., Kalumba, D., & Hardie, P. (2019). Effects of asperities on the geotextile-geomembrane interface shear characteristics. *Proceedings of the 13th Australia New Zealand Conference on Geomechanics.*, 699–704. Pert, Western Australia: Australian Geomechanics Society: H.E. Acosta Martinez & B.M. Lahane, Eds.

Adeleke, D., Kalumba, D., Nolutshungu, L., Oriokot, J., & Martinez, A. (2021). The Influence of Asperities and Surface Roughness on Geomembrane/Geotextile Interface Friction Angle. *International Journal of Geosynthetics and Ground Engineering*, *7*(2), 1–12. https://doi.org/10.1007/s40891-021-00265-y

Adeleke, D., Kalumba, D., & Oriokot, J. (2019). Asperities effect on polypropylene & polyester geotextile-geomembrane interface shear behaviour. *7th International Symposium on Deformation Characteristics of Geomaterials, Glasgow, United Kingdom, 26-28 June 2019, In E3S Web of Conferences*, Vol. 92, pp. 1–5.

Akgün, H. (1997). *Lined waste containment systems : a method for design and performance evaluation*. *30*.

AKS Lining Systems (Pty) Ltd. (2019). *AKS Technical Data-Sheet Double Textured Geomembrane (HDPE)*.

Alzahrani, S. (2018). *Effect of Time on Soil-Geomembrane Interface Shear Strength* (MSc Thesis submitted to University of Dayton). https://doi.org/10.13140/RG.2.2.25743.28320

Anubhav, & Basudhar, P. K. (2010). Modeling of soil-woven geotextile interface behavior from direct shear test results. *Geotextiles and Geomembranes*, Vol. 28, pp. 403–408.

Anubhav, & Wu, H. (2015). Modelling of Non-linear Shear Displacement Behaviour of Soil–Geotextile Interface. *International Journal of Geosynthetics and Ground Engineering*, *1*(2), 1–10. https://doi.org/10.1007/s40891-015-0021-7

ASTM D2487. (2020). Standard Practice for Classification of Soils for Engineering Purposes (Unified Soil Classification System). *American Society for Testing and Materials (ASTM) International*, pp. 1–12. https://doi.org/10.1520/D2487-11.

ASTM D4439. (2017). Standard Terminology for Geosynthetics. *American Society for Testing and Materials (ASTM) International*, *i*(May), 1–4. https://doi.org/10.1520/D4439-17.2

ASTM D5321. (2017). Standard Test Method for Determining the Shear Strength of Soil-Geosynthetic and Geosynthetic-Geosynthetic Interfaces by Direct Shear. *American Society for Testing and Materials International*, pp. 1–11. https://doi.org/10.1520/D5321

ASTM D6243. (2018). Standard Test Method for Determining the Internal and Interface Shear Strength of Geosynthetic Clay Liner by the Direct Shear Method. *American Society for Testing and Materials (ASTM) International*, Vol. 1, pp. 1–12. https://doi.org/10.1520/D6243

ASTM D6706. (2013). Standard Test Method for Measuring Geosynthetic Pullout Resistance in Soil. *American Society for Testing and Materials (ASTM) International*, Vol. 1, pp. 1–8. https://doi.org/DOI: 10.1520/D6706-01R13.

Aza-Gnandji, R., Kalumba, D., & Gbaguidi, V. (2019). Modelling the geomembrane – fly ash interface behaviour. *Proceedings of the XVII European Conference on Soil Mechanics and Geotechnical Engineering (ECSMGE)-2019*, 1–8.

Bacas, B. M., Cañizal, J., & Konietzky, H. (2015). Shear strength behavior of geotextile/geomembrane interfaces. *Journal of Rock Mechanics and Geotechnical Engineering*, *7*(6), 638–645. https://doi.org/10.1016/j.jrmge.2015.08.001

Bacas, B. M., Konietzky, H., Berini, J. C., & Sagaseta, C. (2011). A new constitutive model for textured geomembrane/geotextile interfaces. *Geotextiles and Geomembranes*, *29*(2), 137–148. https://doi.org/10.1016/j.geotexmem.2010.10.014

Barlaz, M. (2016). Design and Operation of Landfills. *The Responsible Management of Waste Foams and Plastics Mixed with Flame Retardants*, 1–41. Berkeley, California.

Bouazza, A., Zornberg, J. G., & Adam, D. (2002). Geosynthetics in Waste Containment Facilities: Recent Advances. *7th International Conference on Geosynthetics*, 445–507.

Bouazza, Abdelmalek, & Bowders, J. (2009). Geosynthetic Clay Liners for Waste Containment Facilities. In *Geosynthetic Clay Liners for Waste Containment Facilities*. https://doi.org/10.1201/b10828

Buthelezi, S, Kalumba, D., & James, G. (2016). Comparison of interface shear strength characteristics of HDPE and LLDPE geomembrane interfaces. *Proceedings of the 6th EuroGeo Conference (EuroGeo6), Ljubljana Exhibition and Convention Centre, Ljubljana, Slovenia*, *1*(25-26 September 2016), 1067–1076.

Buthelezi, Sanelisiwe. (2017). *Comparison of Shear Strength Properties of Textured Polyethylene Geomembrane Interfaces in Landfill Liner Systems*. MSc Thesis submitted to University of Cape Town.

Chai, J. C., & Saito, A. (2016). Interface Shear Strengths Between Geosynthetics and Clayey Soils. *International Journal of Geosynthetics and Ground Engineering*, *2*(3), 1–9. https://doi.org/10.1007/s40891-016-0060-8

Chrysovergis, T. S. (2012). *Laboratory Investigation of the Effects of Temperature and Moisture on Interface Shear Strength of Textured Geomembrane and Geosynthetic Clay Liner*. MSc thesis submitted to California Polytechnic State University.

Deparment of Water Affairs and Forestry. (1998). Minimum requirements for waste disposal by landfill. In *Waste Management Series*.

Department of Environmental Affairs. (2013). Waste Classification and Management Regulations. *Government Gazette*, Vol. 578, pp. 1–48.

Eid, H. T., & Stark, T. D. (1997). Shear behavior of AN unreinforced geosynthetic clay liner. *Geosynthetics International*, *4*(6), 645–659. https://doi.org/10.1680/gein.4.0109

Eid, H. T., Stark, T. D., & Doerfler, C. K. (1999). Effect of Shear Displacement Rate on Internal Shear Strength of a Reinforced Geosynthetic Clay Liner. *Geosynthetics International*, *6*(3), 219–239. https://doi.org/10.1680/gein.6.0151

Esterhuizen, J. J. B., Filz, G. M., & Duncan, J. M. (2001). Constitutive Behavior of Geosynthetic Interfaces. *Journal of Geotechnical and Geoenvironmental Engineering*, *127*(10), 810–817.

Evangelou, I. N., & Markou, E. D. (2018). Shear Resistance Characteristics of Soil – Geomembrane Interfaces. *International Journal of Geosynthetics and Ground Engineering*, *4*(4), 1–16. https://doi.org/10.1007/s40891-018-0146-6

Feng, S.-J., & Cheng, D. (2014). *Shear Strength between Soil/Geomembrane and Geotextile/Geomembrane Interfaces*. (May), 558–569. https://doi.org/10.1061/9780784413449.054

Fowmes, G., Dixon, N., & Jones, D. R. V. (2007). Landfill stability and integrity: the UK design approach. *Proceedings of the Institution of Civil Engineers - Waste and Resource Management*, *160*(2), 51–61. https://doi.org/10.1680/warm.2007.160.2.51

Fowmes, G. J., Dixon, N., & Jones, D. R. V. (2008). Validation of a numerical modelling technique for multilayered geosynthetic landfill lining systems. *Geotextiles and Geomembranes*, *26*(2), 109–121. https://doi.org/10.1016/j.geotexmem.2007.09.003

Fox, P. J., & Stark, T. D. (2004). State-of-the-art report: GCL shear strength and its measurement. *Geosynthetics International*, *11*(3), 141–175. https://doi.org/10.1680/gein.14.00030

Fox, P. J., & Stark, T. D. (2015). State-of-the-art report: GCL shear strength and its measurement. *Geosynthetics International*, *22*(1), 1–47. https://doi.org/10.1680/gein.2004.11.3.141

Fox, Patrick J., & Kim, R. H. (2008). Effect of progressive failure on measured shear strength of geomembrane/GCL interface. *Journal of Geotechnical and Geoenvironmental Engineering*, *134*(4), 459–469. https://doi.org/10.1061/(ASCE)1090-0241(2008)134:4(459)

Geocomp. (2020). *ShearTrac-III - Technical Specifications*.

Gomez, J. E., Filz, G. M., & Ebeling, R. M. (2000). *Technical Report ITL-99-1: Development of an Improved Numerical Model for Concrete-to-Soil Interfaces in Soil-Structure Interaction Analyses*.

Gourc, J. P., Pitanga, H. N., Vilar, O. M., Paulo, S., Carlos, S., Paulo, S., … Americas, D. (2008). *Attempt of Interpreting Comprehensively the Inclined Plane Test for Geosynthetics Interfaces*. (March), 120–128.

Gourc, J., R.Reyes-Ramirez, & P.Villard. (2004). Assessment of geosynthetics interface friction for slope barriers of landfill. *Proceedings of 3rd Asian Regional Conference on Geosynthetics*, 116–149.

Guler, E. (2017). A material which started a new era in geotechnical engineering: geosynthetics. *Innovative Infrastructure Solutions*, *2*(1), 1–21. https://doi.org/10.1007/s41062-017-0090-7

Head, K. H. (2006). *Manual of Soil Laboratory Testing - Volume 1: Soil Classification and*

Compaction Tests (3rd ed.). Whittles Publishing.

Hegde, A., & Roy, R. (2018). A Comparative Numerical Study on Soil–Geosynthetic Interactions Using Large Scale Direct Shear Test and Pullout Test. *International Journal of Geosynthetics and Ground Engineering*, *4*(1), 1–11. https://doi.org/10.1007/s40891-017-0119-1

Jogi, M. (2005). *A Method for Measuring Smooth Geomembrane/Soil Interface Shear Behaviour Under Unsaturated Conditions*. MSc Thesis submitted to University of Saskatchewan.

Jones, D. R. V., & Dixon, N. (1998). Shear strength properties of geomembrane/geotextile interfaces. *Geotextiles and Geomembranes*, *16*(1), 45–71. https://doi.org/10.1016/S0266-1144(97)10022-X

Kalumba, D. (1998). *Effect of grading and grain size on the friction characteristics of a sand/geotextile interface*. MSc Thesis submitted to University of Cape Town.

Kalumba, D., & Scheele, F. (1999). Friction Characteristics of Sand/Geotextile Interfaces for Three Selected Sand Materials. *12th African Regional Conference: Conference Proceedings, Durban, South Africa.*, 201–206.

Karademir, T. (2011). *Elevated Tempreature Effects on Interface Shear Behavior*. PhD Thesis submitted to Georgia Institue of Technology.

Kaytech Engineered Fabrics Ltd. (2015a). *Envirofix Brochure: Needlepunched & Thermally Locked Geosynthetic Clay Liner*.

Kaytech Engineered Fabrics Ltd. (2015b). *EnviroFix X2000 Technical Data Sheet*.

Kaytech Engineered Fabrics Ltd. (2017). *Bidim: General Civil Engineering Applications*.

Kaytech Engineered Fabrics Ltd. (2019). *Bidim A10 Technical data sheet with MARV values*.

Khilnani, K., Stark, T. D., & Bahadori, T. M. (2017). Comparison of Single and Multi-Layer Interface Strengths for Geosynthetic/Geosynthetic and Soil/Geosynthetic Interfaces. *Geotechnical Frontiers*, 42–51.

Kiptoo, D., Aschrafi, J., Kalumba, D., Lehn, J., Moormann, C., & Zannoni, E. (2018). Laboratory Investigation of a Geosynthetic Reinforced Pavement Under Static and Dynamic Loading. *Journal of Testing and Evaluation*, (May). https://doi.org/10.1520/JTE20160170

Koerner. (2003). A recommendation to use peak shear strengths for geosynthetic interface design. In *Geosynthetics Fabrics Report*.

Koerner, R. M. (2005). *Designing with Geoynthetics* (5th ed.). Pearson Prentice Hall.

Koffler, A., Choura, M., Bendriss, A., & Zengerink, E. (2008). Geosynthetics in protection against erosion for river and coastal banks and marine and hydraulic construction. *Journal of Coastal Conservation*, *12*(1), 11–17. https://doi.org/10.1007/s11852-008-0023-x

Li, D., Yin, K., Glade, T., & Leo, C. (2017). Effect of over-consolidation and shear rate on the residual strength of soils of silty sand in the Three Gorges Reservoir. *Scientific Reports*, *7*(1), 1–11. https://doi.org/10.1038/s41598-017-05749-4

Lings, M. L., & Dietz, M. S. (2004). An improved direct shear apparatus for sand. *Geotechnique*, *54*(4), 245–256.

Lopes, M. L., Ferreira, F., Carneiro, J. R., & Vieira, C. S. (2014). Soil - Geosynthetic inclined plane shear behavior: Influence of soil moisture content and geosynthetic type. *International Journal of Geotechnical Engineering*, *8*(3), 335–342. https://doi.org/10.1179/1939787914Y.0000000047

Markou, I. N. (2018). A Study on Geotextile—Sand Interface Behavior Based on Direct Shear and Triaxial Compression Tests. *International Journal of Geosynthetics and Ground Engineering*, *4*(1), 1–15. https://doi.org/10.1007/s40891-017-0121-7

McCartney, J. S., Zornberg, J., & Swan, R. (2002). Internal and Interface Shear Strength of Geosynthetic Clay Liners (GCLs). PhD Thesis submitted to University of Colorado.

Meegoda, J. N., Hettiarachchi, H., & Hettiaratchi, J. P. A. (2016). Chapter 18: Landfill Design and Operation. In *Sustainable Solid Waste Management* (pp. 577–604). https://doi.org/10.1061/9780784414101.ch18

Moraci, N., Cardile, G., Gioffrè, D., Mandaglio, M. C., Calvarano, L. S., & Carbone, L. (2014). Soil Geosynthetic Interaction: Design Parameters from Experimental and Theoretical Analysis. *Transportation Infrastructure Geotechnology*, *1*(2), 165–227. https://doi.org/10.1007/s40515-014-0007-2

Ng, H. B., & Ramsey, B. (2012). Geosynthetic lining system for modern waste facilities - Experiences in developing Asia. *Geotechnical Engineering*, *43*(3), 62–67.

Orebowale, P. B. (2006). *Investigating the Stability of Geosynthetic Landfill Capping Systems*. PhD thesis submitted to Loughborough University.

Oriokot, J. (2014). *Reinforcement of Pavement Subgrade uisng Granula Fill and a Geosynthetic layer*. MSc Thesis submitted to University of Cape Town.

Othman, M. (2016). *Interface Behaviour and Stability of Geocomposite drain/soil systems* (PhD thesis submitted to Loughborough University). https://doi.org/10.13140/RG.2.2.22646.91204

Palmeira, E., Tatsuoka, F., Bathurst, R., Stevenson, P., & Zornberg, J. (2008). Advances in geosynthetics materials and applications for soil reinforcement and environmental protection works. *Electron J Geotech Eng, Spec Issue State of the Art in Geotech Eng*, *13*, 1–38.

Park, J. B., Kim, D., Yang, S. B., & Kim, J. H. (2017). Pullout Characteristics of Geosynthetics Reinforced Earth Using Multilayer Spreading Pullout Test. *Advances in Materials Science and Engineering*, *2017*(1991). https://doi.org/10.1155/2017/9485826

Perkins, S. W. (2007). Chapter 2: The material properties of geosynthetics. In R. W. Sarsby (Ed.), *Geosynthetics in Civil Engneering* (p. 308). Woodhead Publishing Series in Textiles.

Pitanga, H. N., Gourc, J. P., & Vilar, O. M. (2009). Interface shear strength of geosynthetics: Evaluation and analysis of inclined plane tests. *Geotextiles and Geomembranes*, *27*(6), 435–446. https://doi.org/10.1016/j.geotexmem.2009.05.003

Prashanth, V., Murali Krishna, A., & Dash, S. K. (2016). Pullout Tests Using Modified Direct Shear Test Setup for Measuring Soil–Geosynthetic Interaction Parameters. *International Journal of Geosynthetics and Ground Engineering*, *2*(2), 1–10. https://doi.org/10.1007/s40891-016-0050-x

Rouncivell, W. (2007). *Experimental Investigation of the Shear Strength Characteristics of a Geosynthetic Clay Liner and its application in a local Landfill Lining System*. MSc Thesis submitted to University of Cape Town.

Rowe, R. K. (1998). Geosynthetics and the minimization of containment migration through barrier systems beneath solid waste. *Geotechnical Research Centre Report, GEOT-2-98*, (1), 76.

Seo, M.-W., Park, J.-B., Park, I.-J., & Chung, M.-K. (2003). Modeling of interface shear behavior between geosynthetics. *KSCE Journal of Civil Engineering*, *7*(1), 9–16. https://doi.org/10.1007/bf02841987

Shenthan, T., Khilnani, K., Tark, T. D., & .. (2019). *Case Histories of Multi-Layer Interface Tests for Composite Liners and Comparison to Single Interface Tests*. *1*, 1–17.

Shukla, S. K. (2016). An Introduction to Geosynthetic Engineering. In *An Introduction to Geosynthetic Engineering*. https://doi.org/10.1201/9781315378930

Shukla, S. K., & Yin, J.-H. (2006). Fundamentals of Geosynthetic Engineering. In *Taylor & Fancis Group*.

Sikwanda, C. (2018). *An Investigation of the Effects of Specimen Gripping Systems on Shear Stress at the Geosynthetic-Geosynthetic Interface in Landfill Applications*. MSc Thesis submitted to University of Cape Town.

Sikwanda, C., Buthelezi, S., & Kalumba, D. (2018). Review of Effects of Poor Gripping Systems in Geosynthetics Shear Strength Testing. *Proceedings of GeoShanghai 2018 International Conference: Ground Improvement and Geosynthetics*, 420–429. https://doi.org/10.1007/978-981-13-0122-3

Sikwanda, C., Kalumba, D., & Nolutshungu, L. (2018). An Investigation of the Effects of Specimen Gripping Systems on Shear Stress at the Geosynthetic-Geosynthetic Interface. *Proceedings of Indian Geotechnical Conference: Sustainability and Geoenvironmental Engineering, Bangalore, India*, (13-15 December 2018).

Sikwanda, C., Kalumba, D., & Nolutshungu, L. (2019). A comparison of single and multi-interface shear strengths at geosynthetic/geosynthetic interface. *Proceedings of the 17th African Regional Conference on Soil Mechanics and Geotechnical Engineering.*, (October), 77–81.

Sikwanda, C., Kalumba, D., & Nolutshungu, L. (2020). An Investigation of the Effects of Specimen Gripping Systems on Shear Stress at the Geosynthetic – Geosynthetic Interface. *Geotechnical Characterization and Modelling*, *85*, 397–412.

Soleimanian, M. R. (2016). *A Novel Direct Shear Apparatus to Evaluate Internal Shear Strenght of Geosynthetic Clay Liner for Mining Applications*. MSc Thesis submitted to Colorado

State University.

South African National Standard. (2008). SANS 10234: 2008 Globally Harmonized System of classification and labelling of chemicals (GHS). In *South African Burea of Standards* (Vol. 10234).

Stark, Niazi, F. S., Keuscher, T. C., & . (2011). Comparison of Single and Multi Geosynthetic and Soil Interface Tests. In *Geosynthetics International Journal* (Vol. 1).

Stark, T.D., & Poeppel, A. R. (1994). Landfill Liner Interface Strengths from Torsional-Ring-Shear Tests. *Journal of Geotechnical Engineering*, *120*(3), 597–615. https://doi.org/10.1061/(asce)0733-9410(1995)121:6(510.x)

Stark, Timothy D., & Choi, H. (2004). Peak versus Residual Inteface Strengths for Landfill Liner and Cover Design. *Geosynthetics International*, *11*(6), 491–498.

Stark, Timothy D., Niazi, F. S., & Keuscher, T. C. (2015). Strength Envelopes from Single and Multi Geosynthetic Interface Tests. *Geotechnical and Geological Engineering*, *33*(5), 1351–1367. https://doi.org/10.1007/s10706-015-9906-4

Stark, Timothy D. (1999). Stability of Waste Containment Facilities. *Municipal and Industrial Solid Waste Disposal Technology, WasteTech'99*, p. 22. New Orleans, Louisiana.

Swan, R. H., & Stark, T. D. (2019). *Webinar: Multi-Layer Interface Shear Testing* (p. 51). p. 51. Fabricated Geomembrane Institute (FGI).

Taylor, J. R. (2002). Experimental Errors and Uncertainty. *Measurement*, 2000–2002.

Thiel, R. (2001). Peak vs. residual shear strength for landfill bottom liner stability analyses. *Proceedings of the 15th GRI Conference*, 31.

Triplett, E. J., & Fox, P. J. (2001). Shear Strength of HDPE Geomembrane/Geosynthetic Clay Liner Interfaces. *Journal of Geotechnical and Geoenvironmental Engineering*, (June), 543–552.

Wu, H. M., Shu, Y. M., & Zhu, J. G. (2011). Implementation and verification of interface constitutive model in FLAC3D. *Water Science and Engineering*, *4*(3), 305–316. https://doi.org/10.3882/j.issn.1674-2370.2011.03.007

Wu, W., Wick, H., Ferstl, F., & Aschauer, F. (2008). A tilt table device for testing geosynthetic interfaces in centrifuge. *Geotextiles and Geomembranes*, *26*(1), 31–38. https://doi.org/10.1016/j.geotexmem.2007.03.002

Xuede, Q. (2008). *Critical interfaces in geosynthetic multilayer liner system of a landfill*. *1*(4), 22–35. https://doi.org/10.3882/j.issn.1674-2370.2008.04.003

Zhao, L., & Karim, M. (2018). Use of Geosynthetic materials in solid waste landfill design: A review of geosynthetic related stability issues. *Annals of Civil and Environmental Engineering*, 006–015. https://doi.org/10.29328/journal.acee.1001010

APPENDICES

Appendix A: Characterization of Soils

The following results are presented in Appendix A;

A.1 Determination of specific gravity

A.2 Determination of particle size distribution

A.2.1 Determination of grading size of sand (dry sieving)

A.2.2 Determination of grading size of clay (sieving + atterberg limits)

A.3 Standard compaction test

A.3.1 Determination of MDD & OMC for sand

A.3.2 Determination of MDD & OMC for clay

A.4 Small direct shear test

A.4.1 Determination of c & ϕ for sand

A.4.2 Determination of c & ϕ for clay

APPENDIX A: CHARACTERIZATION OF SOILS

A.1 DETERMINATION OF SPECIFIC GRAVITY

	DATA SHEET **Particle Density** **Pyknometer Method**		
Project	Thesis/Dissertation	**Location**	UCT
Test Number	One (1)	**Lab**	Geotech Laboratory
Tested By	Shade Muluti	**Date**	21/08/2020

TEST METHOD	**BS 1377: Part 2: 1990**

Specimen Reference			RED CLAY			RIVER SAND		
Pyknometer number			10	21	25	1	2	4
Mass of bottle + soil + water	m_3	g	94.215	94.394	94.603	96.789	97.87	96.641
Mass of bottle + soil	m_2	g	49.772	49.758	50.119	50.049	52.441	50.411
Mass of bottle full of water	m_4	g	84.578	84.746	84.934	87.477	88.552	87.309
Mass of density bottle	m_1	g	34.728	34.717	35.047	34.993	37.376	35.354
Mass of soil	$m_2 - m_1$	g	15.044	15.041	15.072	15.056	15.065	15.057
Mass of water in full bottle	$m_4 - m_1$	g	49.85	50.029	49.887	52.484	51.176	51.955
Mass of water used	$m_3 - m_2$	g	44.443	44.636	44.484	46.74	45.429	46.23
Volume of soil particles	$(m_4 - m_1) - (m_3 - m_2)$	mL	5.407	5.393	5.403	5.744	5.747	5.725
Particle Density	$\rho_s = 1000 \times \frac{(m_2 - m_1)}{(m_4 - m_1) - (m_3 - m_2)}$	**kg/m^3**	2.78	2.79	2.79	2.62	2.62	2.63
Average	**ρ_s**	**kg/m^3**	**2.79**			**2.62**		

Remarks: _____

_____

_____

_____

A.2 DETERMINATION OF GRADING SIZE

A.2.1 DETERMINATION OF GRADING SIZE OF SAND

DATA SHEET

Particle Size Distribution
Sieve Analysis

Project	Thesis/Dissertation	**Location**	University of Cape Town
Test Number	One (1)	**Lab**	Geotech Laboratory
Tested By	Shade Muluti	**Date**	15/03/2020

TEST METHOD **BS 1377: Part 2: 1990**

Soil Sample		
Mass of Container (M_c)	410	g
Mass of Container + dry soil	1410	g
Initial Mass of dry soil	**1000**	**g**

Shape Parameters/Grading characteristics					
D_{10}	=	**0.231**			
D_{30}	=	**0.385**	C_u	=	**2.41**
D_{60}	=	**0.556**	C_c	=	**1.15**

Standard Sieve Number (U.S)	Sieve Opening size (mm)	Mass of Empty Sieve (g)	Mass of Sieve + Soil retained (g)	Mass of soil retained (g)	Percentage Retained (%)	Cumulative % Retained (%)	Percentage Passing (%)
	3.350	591.6	610.4	18.8	1.88	1.88	98.12
	2.000	573.8	599.3	25.5	2.56	4.44	95.56
	1.180	351.8	407.5	55.7	5.58	10.02	89.98
	0.600	533.1	747.6	214.5	21.50	31.52	68.48
	0.425	505.8	840.5	334.7	33.54	65.06	34.94
	0.300	487.6	639.9	152.3	15.26	80.33	19.67
	0.212	278.3	383.4	105.1	10.53	90.86	9.14
	0.150	469.6	519.2	49.6	4.97	95.83	4.17
	0.075	457.6	491.6	34	3.41	99.24	0.76
	Pan	459.8	467.4	7.6	0.76	100.00	0.00
			Total Mass =	**997.8**			

Grain Size Boundaries

Soil Type	USCS Symbol	Grain size range
Gravel	G	76.2 to 4.75
Sand	S	4.75 to 0.075
Silt	M	Fines < 0.075
Clay	C	

Soil grading

Grading type	Symbol
Well-Graded	W
Poorly Graded	P

% Gravel	=	0.00
% Sand	=	99.24
% Fines	=	0.76

A soil is said to be well-graded if the coefficient of curvature C_c lies between 1 and 3, with C_u greater than 4 for gravels and greater than 6 for sands.

Classification of Soil
SP - Poorly Graded Sand

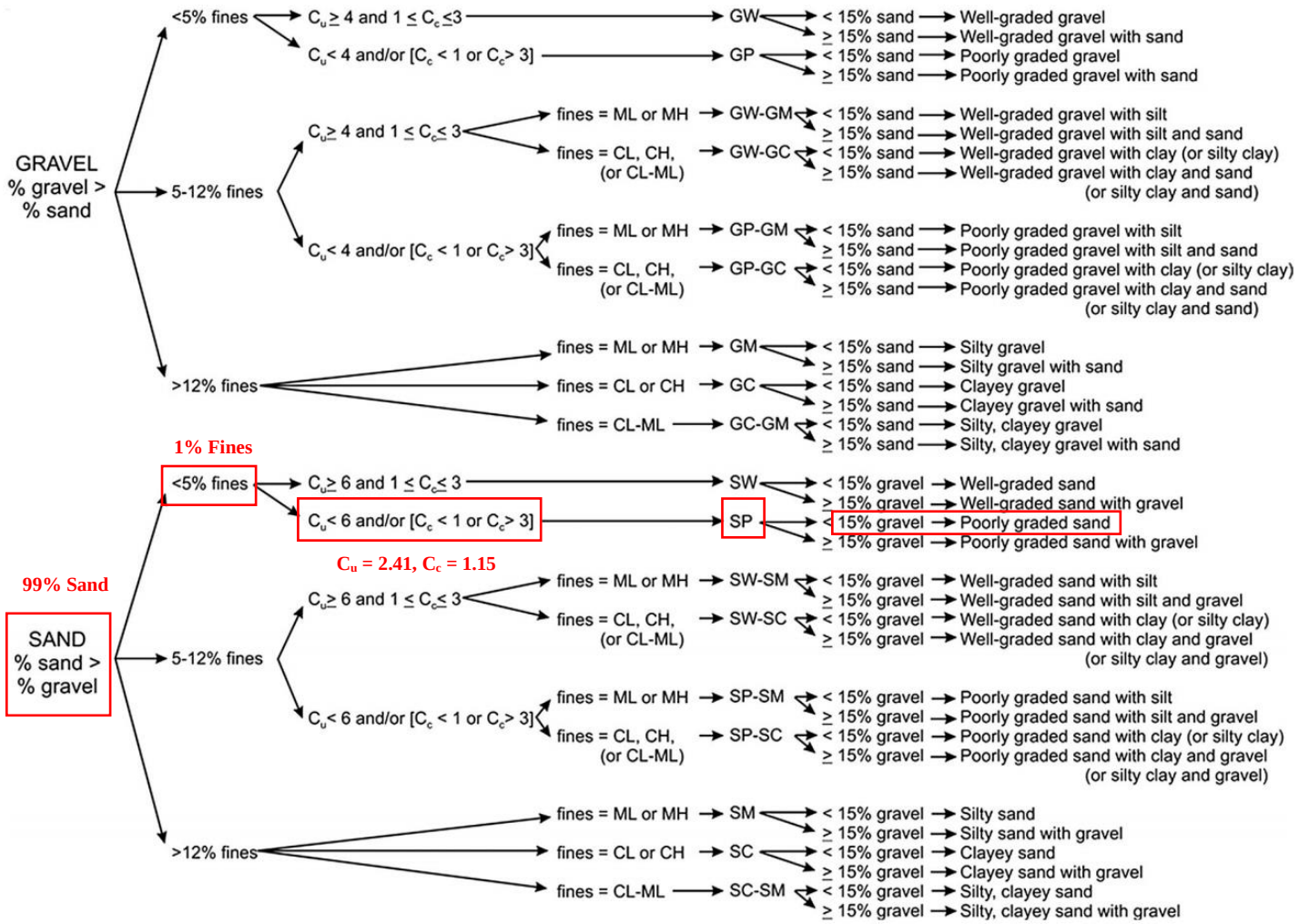

Unified Soil Classification System (USCS) of coarse-grained soils (ASTM D2487, 2020)

A.2.2 DETERMINATION OF GRADING SIZE OF CLAY

DATA SHEET

Particle Size Distribution + Atterberg Limits

Project	Thesis/Dissertation	**Location**	UCT
Test Number		**Lab**	Geotech Laboratory
Tested By	Shade Muluti	**Date**	19-03-2020

TEST METHOD **BS 1377: Part 2: 1990**

Sieve Size (mm)	% Passing
4.750	86.24
1.180	80.47
0.850	79.59
0.600	79.14
0.425	78.55
0.212	77.44
0.150	76.44
0.075	74.78
0.046	70.56
0.036	67.75
0.029	64.42
0.021	57.47
0.013	44.01
0.010	32.84
0.008	23.15
0.006	15.09
0.004	9.10
0.003	4.36
0.002	3.25
0.001	2.44
0.001	1.26
0.000	0.96
0.000	0.96
0.000	0.96
0.000	0.89

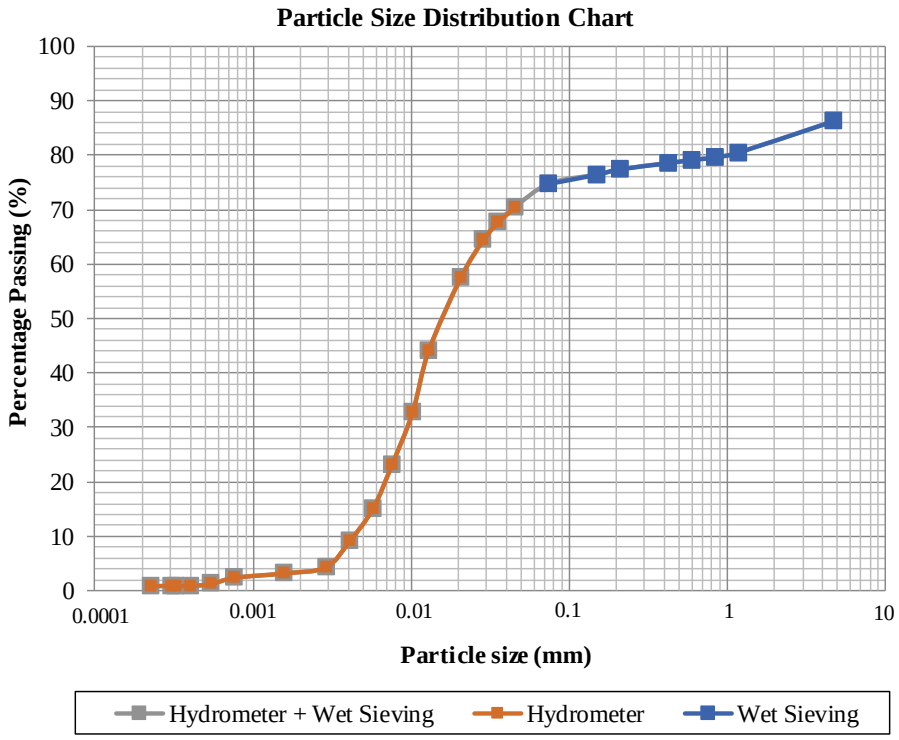

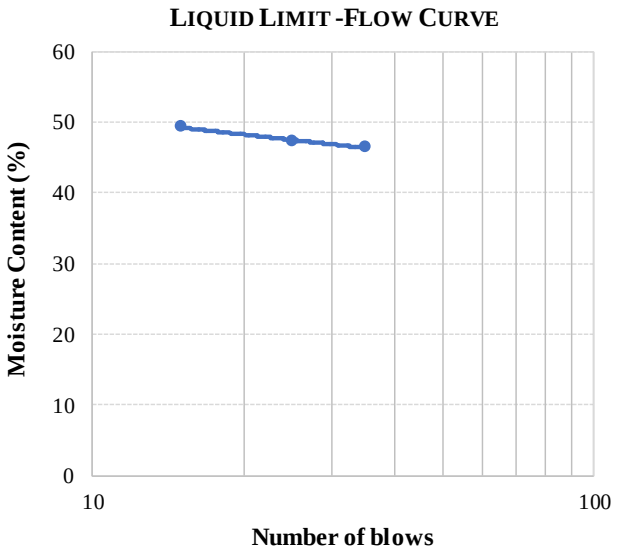

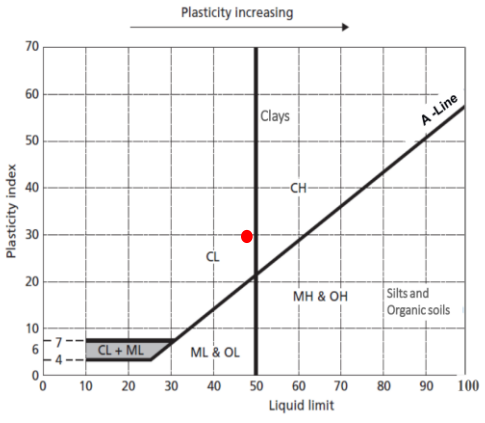

Summary

LIQUID LIMIT (LL)	=	**47.7** %
PLASTIC LIMIT (PL)	=	**17.5** %
PLASTICITY INDEX (PI)	=	**30.2** %

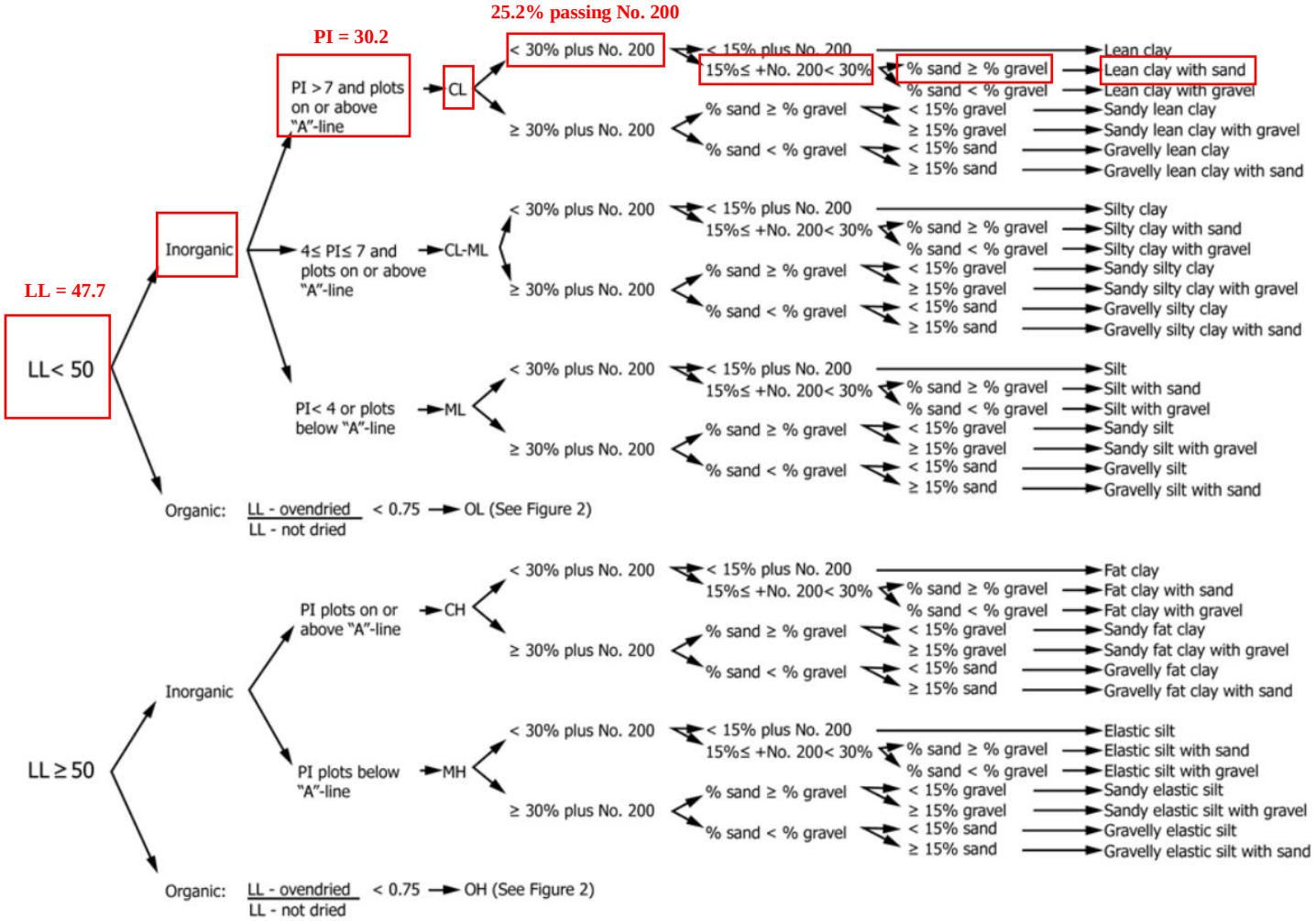

Unified Soil Classification System (USCS) of fine-grained soils (ASTM D2487, 2020)

A.3 STANDARD COMPACTION TEST

A.3.1 DETERMINATION OF MDD & OMC FOR SAND

DATA SHEET

Compaction Test
Dry Density - Moisture Content Relationship

Project	Thesis/Dissertation	**Location**	UCT
Test Number	One (1)	**Lab**	Geotech Laboratory)
Tested By	Shade Muluti	**Date**	25/3/2020

TEST METHOD	**BS 1377: Part 4: 1990**

Maximum Dry Density (MDD)	$\rho_{d(\max)}$	1.683	Mg/m^3
Optimum Moisture Content (OMC)	W_{opt}	11.5	%

Test no.		**1**	**2**	**3**	**4**	**5**	**6**
Moisture Content (w)	%	6.6	7.4	8.7	10.9	11.6	12.6
Dry Density	Mg/m^3	1.65	1.66	1.65	1.67	1.68	1.66

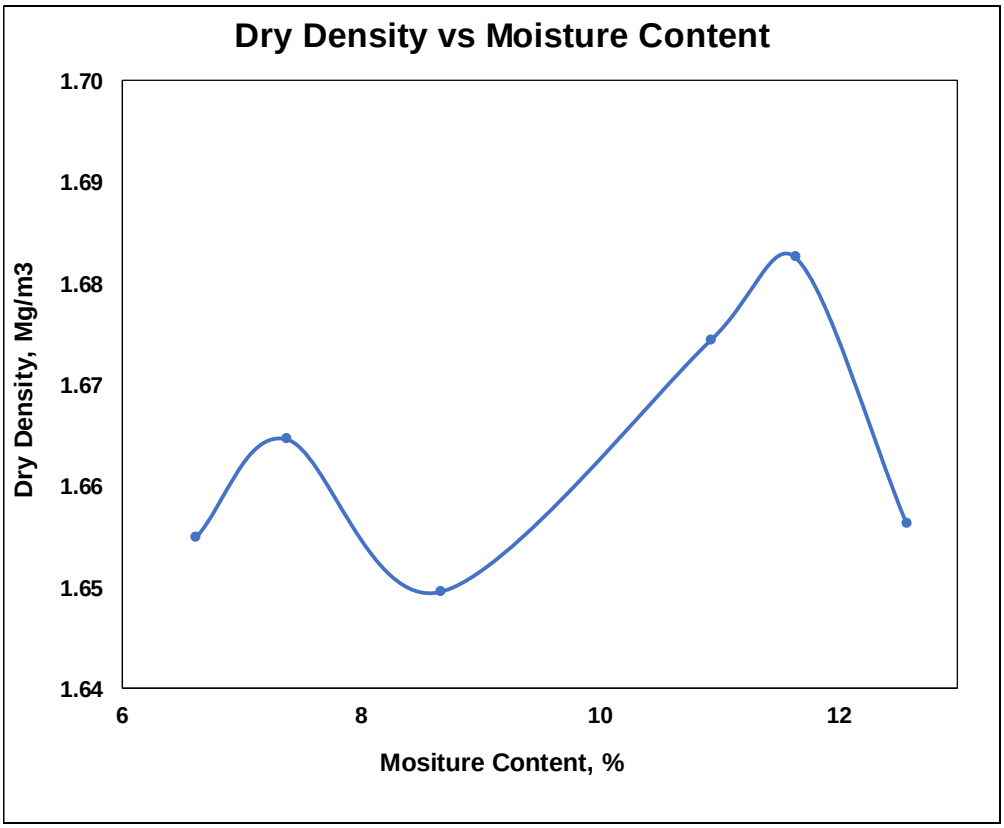

A.3.2 DETERMINATION OF MDD & OMC FOR CLAY

	DATA SHEET **Compaction Test** **Dry Density - Moisture Content Relationship**		
Project	Thesis/Dissertation	**Location**	UCT
Test Number	One (1)	**Lab**	Geotech Laboratory)
Tested By	Shade Muluti	**Date**	23/3/2020

TEST METHOD	**BS 1377: Part 4: 1990**

Maximum Dry Density (MDD)	$\rho_{d(\max)}$	1.590	Mg/m^3
Optimum Moisture Content (OMC)	W_{opt}	24.3	%

Test no.		**1**	**2**	**3**	**4**	**5**
Moisture Content (w)	%	20.4	21.6	22.8	24.4	26.1
Dry Density	Mg/m^3	1.524	1.545	1.565	1.589	1.571

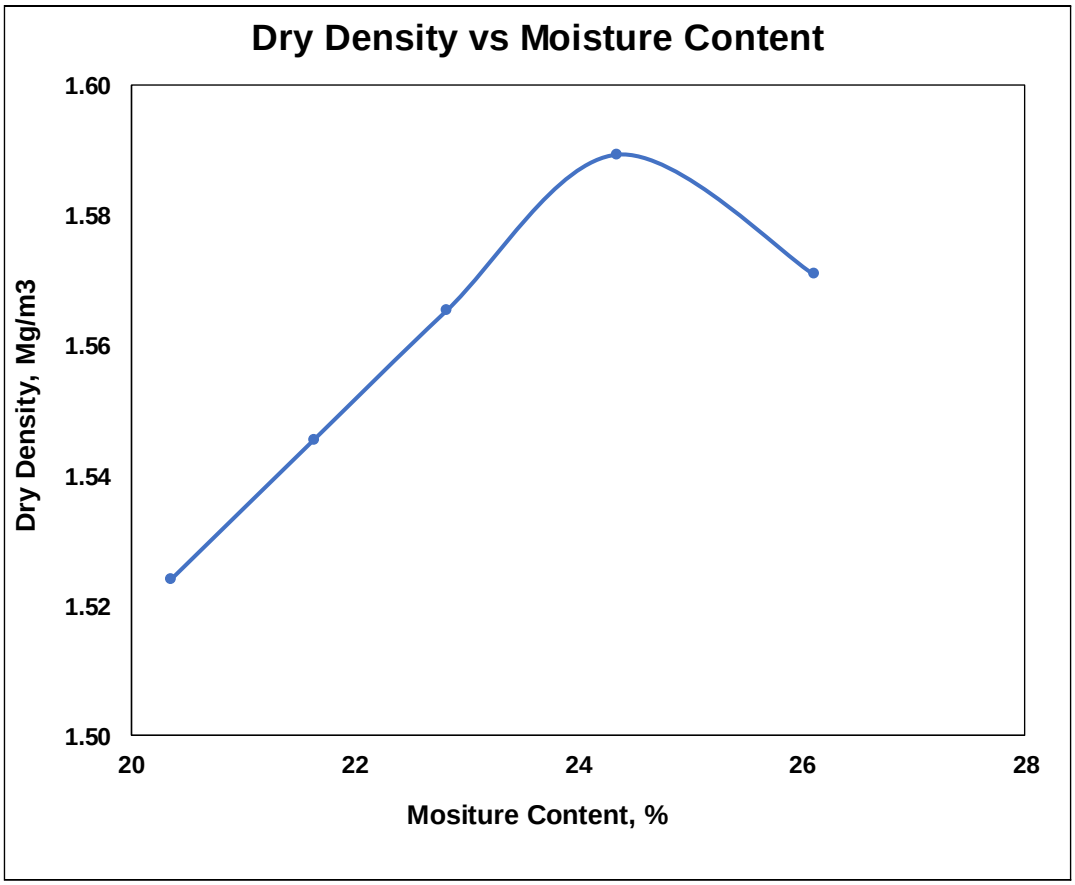

A.4 SMALL DIRECT SHEAR TEST

A.4.1. DETERMINATION OF C & ϕ FOR SAND

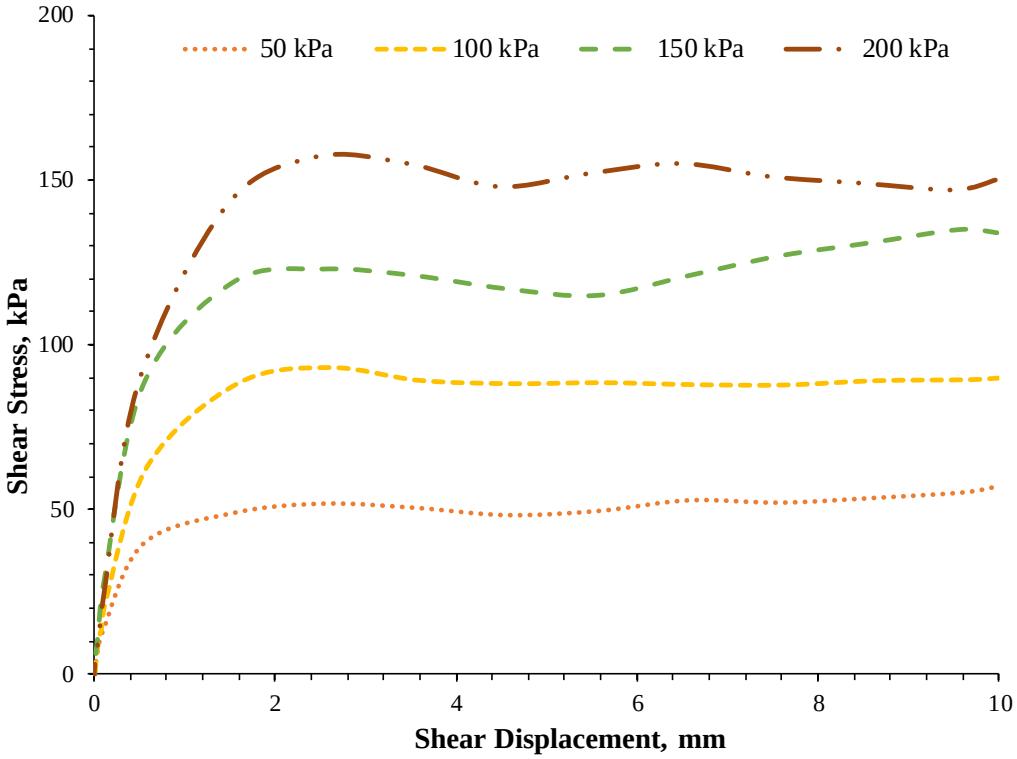

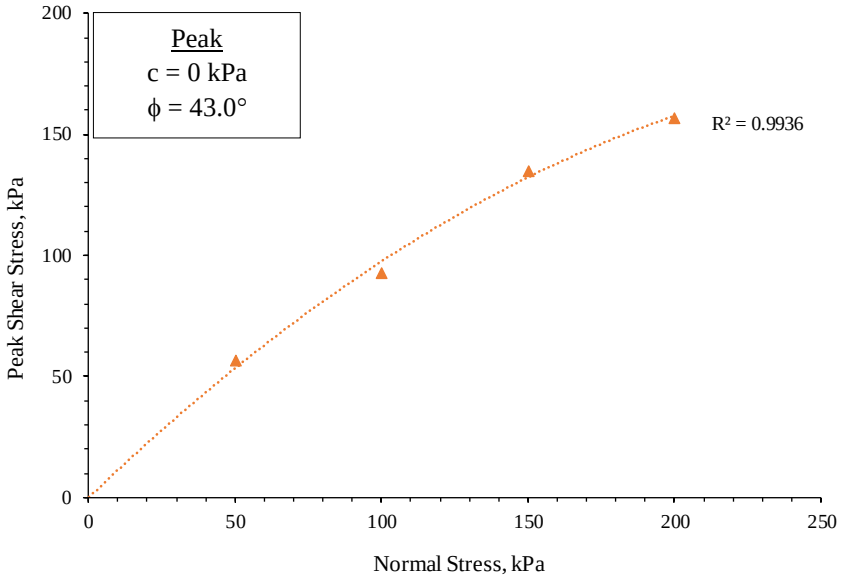

A.4.1. DETERMINATION OF C & ϕ FOR CLAY